

Politecnico di Torino

Department of Environmental, Land and Infrastructure Engineering

Master of Science in Georesources and Geoenergy Engineering

Analysis of rock failure in underbalanced drilling

Supervisor: Candidate:

Prof. Chiara Deangeli Himawan Ichwana

October 2025

List of Contents

1.	Prin	ciples and Fundamentals	6
1	l. 1 .	Introduction	6
1	l. 2 .	Overview of Drilling Methods	7
	1.2.		
	1.2.2	2. Managed Pressure Drilling	8
	1.2.3	3. Underbalanced Drilling	8
1	l. 3.	Advantages and Disadvantages of UBD	9
1	L. 4.	In Situ Stress State and Stress Redistribution	
	1.4.		
	1.4.2		
	1.4.3		
	l.5.	Stress Concentration around a Wellbore : Kirsch Solution	
	l.6.	Geomechanical Implications of Underbalanced Drilling (UBD)	
2 .	Con	stitutive Modelling for Wellbore Stability Analysis	
2	2.1.	The Role of Constitutive Model	
	2.1.		
	2.1.2		
	2.1.3		
2	2.2.	Mud Weight Window	22
<i>3</i> .		Influence of Pore Pressure Conditions on Wellbore Stability	
	3.1.	,	
	3.1.2		
	3.1.3	3. Undrained Conditions	25
3	3.2.	Objective of the Study	27
4.	Con	nparative Numerical Simulations with Different Constitutive Models	27
4	l.1.	Wellbore Stability Analysis with Elastic Model	29
	4.1.	1. Elastic Model: Dry Condition	
	4.1.2		
	4.1.3	3. Elastic Model: Undrained Condition	36
4	1.2.	Wellbore Stability Analysis with Mohr-Coulomb Model	
	4.2.		
	4.2.2	2. Mohr-Coulomb Model : Undrained Condition	50
4	1.3.	Wellbore Stability Analysis with Hoek-Brown Model	
	4.3.		
	4.3.2		
5.	Con	clusion	78
5	5.1.	Insights on Constitutive Model Performance	78
5	5.2.	Geomechanical Implications for Underbalanced Drilling	79
Rei	fereni	res	80

LIST OF FIGURES

Figure 1 Drilling Windows for Various Types of Drilling Techniques (Alawad, 2016)	7
Figure 2 OBD vs UBD (Jaf, 2017)	 9
Figure 3 Underground Stresses in Fault Regimes [37]	 10
Figure 4 Horizontal Stresses in a Borehole Related to Borehole Breakout and Drilling Induced Tensile Fractu	res
(Zoback, 2011)	_ 13
Figure 5 (A) Representation of stress concentration around a wellbore (after Kirsch, 1898), (B) stress	
distribution around a wellbore (Alliance, n.d.)	_ 14
Figure 6 Mohr-Coloumb Criterion (Wei et al., 2020)	_ 18
Figure 7 Mohr-Coloumb with a Tension Cutoff [33]	_ 19
Figure 8 Distribution of the Compressive to Tensile Strength Ratio in Sandstones (Cai, 2010)	_ 20
Figure 9 Hoek-Brown Failure Criterion [38]	_ 21
Figure 10 Distribution of Drilling-Induced Pore Pressure Around a Wellbore in an Anisotropic Stress Field	_ 25
Figure 11 Hoop and Radial Stresses at $\theta=90^\circ$ Elastic Model Dry Condition	_ 30
Figure 12 Hoop and Radial Stresses at $ heta=0^\circ$ Elastic Model Dry Condition	_ 30
Figure 13 Eff. Hoop and Eff. Radial Stresses at $\theta=90^\circ$ Elastic Model Drained Condition	_ 32
Figure 14 Eff. Hoop and Eff. Radial Stresses at $ heta=0^\circ$ Elastic Model Drained Condition	_ 33
Figure 15 Tension/Compression Region (Elastic Drained Model), Pw = 18 MPa	_ 34
Figure 16 Tension/Compression Region (Elastic Drained Model), Pw = 15 Mpa	_ 34
Figure 17 Tension/Compression Region (Elastic Drained Model), Pw=0 MPa (LIMIT CASE)	_ 35
Figure 18 Pore Pressure Undrained Scenario (Elastic Model)	_ 37
Figure 19 Pore Pressure Undrained Scenario (Elastic Model) FLAC2D	_ 37
Figure 20 Effective Stress Drained vs Undrained Condition at $\theta=90^\circ$ (Elastic Model), Pw=15MPa	_ 38
Figure 21 Effective Stress Drained vs Undrained Condition at $ heta=0^\circ$ (Elastic Model), Pw=15MPa	_ 38
Figure 22 Tension/Compression Region (Elastic Undrained Model), Pw = 18 MPa	_ 42
Figure 23 Tension/Compression Region (Elastic Undrained Model), Pw=15 MPa	_ 43
Figure 24 Tension/Compression Region (Elastic Undrained Model), Pw=0 MPa	_ 43
Figure 25 Eff. Hoop and Eff. Radial Stresses at $\theta=90^\circ$ MC Model Drained Condition	_ 46
Figure 26 Eff. Hoop and Eff. Radial Stresses at $ heta=0^\circ$ MC Model Drained Condition	_ 46
Figure 27 Tension/Compression Region (MC Drained Model), Pw=17.5 MPa	_ 48
Figure 28 Tension/Compression Region (MC Drained Model), Pw=16MPa	_ 48
Figure 29 Tension/Compression Region (MC Drained Model), Pw=15MPa	_ 49
Figure 30 Tension/Compression Region (MC Undrained Model), Pw=17.5MPa	_ 52
Figure 31 Tension/Compression Region (MC Undrained Model), Pw=18MPa	_ 53
Figure 32 Tension/Compression Region (MC Undrained Model), Pw=19MPa	_ 54
Figure 33 Tension/Compression Region (MC Undrained Model), Pw=21MPa	_ 55
Figure 34 Tension/Compression Region (MC Undrained Model), Pw=17.5MPa, $\sigma t = 2.91MPa$	
Figure 35 Eff. Hoop and Eff. Radial Stresses at $\theta=90^\circ$ HB Model Drained ConditionGSI=100	
Figure 36 Eff. Hoop and Eff. Radial Stresses at $ heta=0^\circ$ HB Model Drained Condition, GSI=100	
Figure 37 Tension/Compression Region (HB Drained Model) Pw=17.5MPa, GSI=100MPa	_ 59
Figure 38 Tension/Compression Region (HB Drained Model) Pw=18MPa, GSI=100MPa	
Figure 39 Tension/Compression Region (HB Drained Model) Pw=19MPa, GSI=100MPa	
Figure 40 Eff. Hoop and Eff. Radial Stresses at $\theta=90^\circ$ HB Model Drained Condition, GSI=96	
Figure 41 Eff. Hoop and Eff. Radial Stresses at $\theta=0^\circ$ HB Model Drained Condition, GSI=96	
Figure 42 Tension/Compression Region (HB Drained Model) Pw=17.5MPa, GSI=96MPa	
Figure 43 Tension/Compression Region (HB Drained Model) Pw=18MPa, GSI=96MPa	
Figure 44 Tension/Compression Region (HB Drained Model) Pw=19MPa, GSI=96MPa	
Figure 40 Eff. Hoop and Eff. Radial Stresses at $\theta=90^\circ$ HB Model Undrained Condition, GSI=100	
Figure 40 Eff. Hoop and Eff. Radial Stresses at $ heta=0^\circ$ HB Model Undrained Condition, GSI=100	
Figure 47 Tension/Compression Region (HB Undrained Model) Pw=17.5MPa, GSI=100MPa	_ 69

Figure 48 Tension/Compression Region (HB Undrained Model) Pw=18MPa, GSI=100MPa	70
Figure 49 Tension/Compression Region (HB Undrained Model) Pw=19MPa, GSI=100MPa	71
Figure 50 Eff. Hoop and Eff. Radial Stresses at $ heta=90^\circ$ HB Model Undrained Condition, GSI=96	72
Figure 51 Eff. Hoop and Eff. Radial Stresses at $ heta=90^\circ$ HB Model Undrained Condition, GSI=96	72
Figure 52 Tension/Compression Region (HB Undrained Model) Pw=17.5MPa, GSI=96MPa	73
Figure 53 Tension/Compression Region (HB Undrained Model) Pw=18MPa, GSI=96MPa	74
Figure 54 Tension/Compression Region (HB Undrained Model) Pw=19MPa, GSI=96MPa	75
Figure 55 Tension/Compression Region (HB Undrained Model) Pw=21MPa, GSI=100MPa	76
Figure 56 Tension/Compression Region (HB Undrained Model) Pw=21MPa, GSI=96MPa	77

LIST OF TABLES

Table 1 Data for Elastic Dry Simulation	28
Table 2 Comparison of Effective Stresses and Pore Pressure at θ =90° and θ =0° for Varying Wellbore Pressure	ıres
(Pw) under Undrained Conditions	42
Table 3 Mohr-Coulomb Parameters for Sandstone Formation	45
Table 4 Wellbore stability analysis with different well pressure (Pw) (MC Drained model)	47
Table 5 Wellbore Stress Distribution and Stability Analysis for Different Scenarios MC Undrained Model	51
Table 6 HB Parameters for Each GSI	57

1. Principles and Fundamentals

1.1.Introduction

The exploration and production of hydrocarbons are fundamentally dependent on the successful drilling of wellbores. One of the most important problems during this process is keeping the wellbore stable. This is necessary for safety, reducing non-productive time, and meeting economic goals. The stability of a wellbore depends on the complicated relationship between the in situ stresses of the rock formation, the rock's natural mechanical strength, and the pressure that the drilling fluid puts on the wellbore (Zoback, 2011). Drilling effectively removes a cylinder column of rock, disrupts the equilibrium, and forces the surrounding rock to bear the redistributed loads. As a result, stresses are concentrated around the newly formed hole. The controllable variables such as mud pressure is very essential to maintain the wellbore stability.

When the stresses concentration exceeds the strength of the rock formation, mechanical failure will occur and lead to wellbore instability in many forms. These include compressive shear failure which could lead to breakouts and borehole collapse, tensile failure which leads to inducing fractures, and time dependent deformation. Inability to mitigate wellbore stability issues can result in a significant operational and safety issue such as stuck pipe, drilling fluid loss, well pack off, drilling speed reduction, and so on (Bahrami et al., 2020). To avoid these risks, drilling operations are designed to maintain the wellbore pressure within a specific "mud weight window". This operational envelope is bounded by a lower limit, the collapse pressure, the minimum well pressure required to prevent compressive failure. The upper limit is the fracture pressure, the pressure at which the tensile strength of the rock is overcome, leading to fluid loss into induced fractures (Lake, 2006, P. 22).

In this study, a numerical simulation of wellbore stability in underbalanced drilling condition were performed. This study performs a systematic comparative analysis of three different constitutive models: the Linear Elastic model, the Mohr-Coulomb criterion, and the Generalized Hoek-Brown criterion. The models were tested and simulated by using FLAC 2D (Itasca Ltd.) in different pore pressure conditions of dry condition, drained condition, and undrained condition. The main aim is to understand the discrepancies in their instability

predictions and provide direct comparisons on between models and its condition for wellbore integrity assessment.

1.2. Overview of Drilling Methods

The choice of drilling technique primarily depends upon how it balances the wellbore pressure with respect to formation pressure. One of the primarily challenges is to keep within this safe mud weight window to maintain the wellbore stability. The operational window is a range from lower to upper bound. The lower bound is established by the formation pore pressure and the collapse pressure of the rock being drilled, the drilling fluid weight must be sufficient to prevent formation fluids from entering the wellbore (a "kick") and to stop the surrounding rock from failing under compressive stress and collapsing. On the other hand, the upper bound is controlled by formation fracture pressure. Drilling beyond this pressure would induce tensile fractures in the rock formation, allowing drilling fluids to enter the system, also known as "lost circulation". The exact position of this window results from a balance between the background natural conditions, such as in-situ stresses, pore pressure, rock strength, and controllable drilling parameters. Usually, in situ stress with high anisotropy makes the mud weight window become smaller (Aadnoy, 2019, P.178). Figure 1 shows how the window for each drilling technique. Each chosen to achieve specific drilling objectives while mitigating the associated risks of instability.

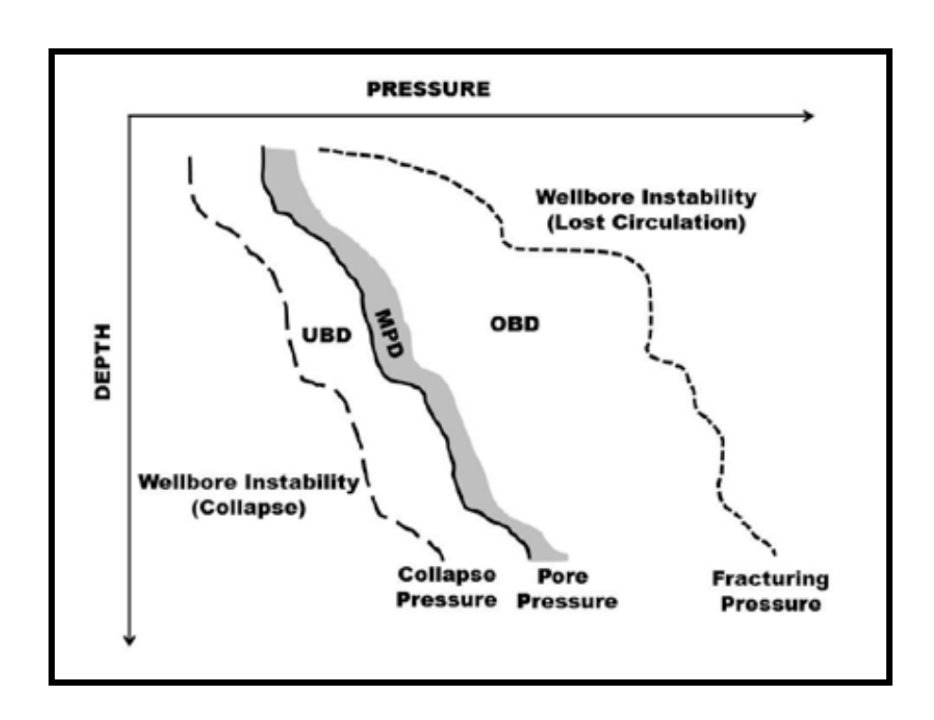


Figure 1 Drilling Windows for Various Types of Drilling Techniques (Alawad, 2016)

1.2.1. Overbalanced Drilling

This is the standard and the most common drilling technique where the hydrostatic mud pressure is greater than the formation pressure. To prevent formation fluids from entering the wellbore is one of the main benefits of this method. Thus, reducing the risk to have kicks and blowouts. However, an excessive overbalanced can damage the near wellbore formation by letting the mud entering into the formation which strengths the rocks. Another downside of OBD is that it can cause differential sticking problem when poor mud properties are not suitabale with the formation (Jaf, 2017, P. 3).

1.2.2. Managed Pressure Drilling

MPD (Managed Pressure Drilling) is an adaptable drilling practice used to more precisely control the annular pressure profile throughout the wellbore. MPD is designed to keep the wellbore pressure inside a narrow band, typically between pore pressure and fracture pressure, which in turn makes drilling safer. This is unlike the underbalanced drilling method, which only encourage inflows. These are of particular importance in the case of high pressure potential and for example for deep water drilling or subsurface condition with narrow pressure margins. MPD utilizes a closed-loop, pressurized fluid system, incorporating a rotating control device (RCD) and a choke manifold to apply surface backpressure, allowing for rapid and precise adjustments to the bottomhole pressure in real-time (Malloy, 2007).

1.2.3. Underbalanced Drilling

In mature or depleted reservoirs, with OBD, the positive differential pressure (Pw > PP) provides a supporting force on the wellbore wall, counteracting the in-situ stresses and helping to prevent collapse. But it also often creates problems such as formation damage and severe lost circulation (Salehi et al., 2010). To solve this problem, the underbalanced drilling (UBD) method has been recognized as an alternative technology.

Underbalanced drilling (UBD) is a method of drilling in which the hydrostatic pressure of the drilling fluid is lower than the pressure of the formations being drilled. The fluid hydrostatic pressure may naturally be lower than the formation pressure, or it can be achieved by adding air, nitrogen, or natural gas to the liquid phase of drilling mud. Underbalanced is either induced, the result may be an influx of formation fluids that must be circulated from the well

and controlled at surface (Jaf, 2017). Effective downhole circulating pressure of drilling fluid = hydrostatic head of the fluid column + back pressure + surface pressure (Nas, 2006).

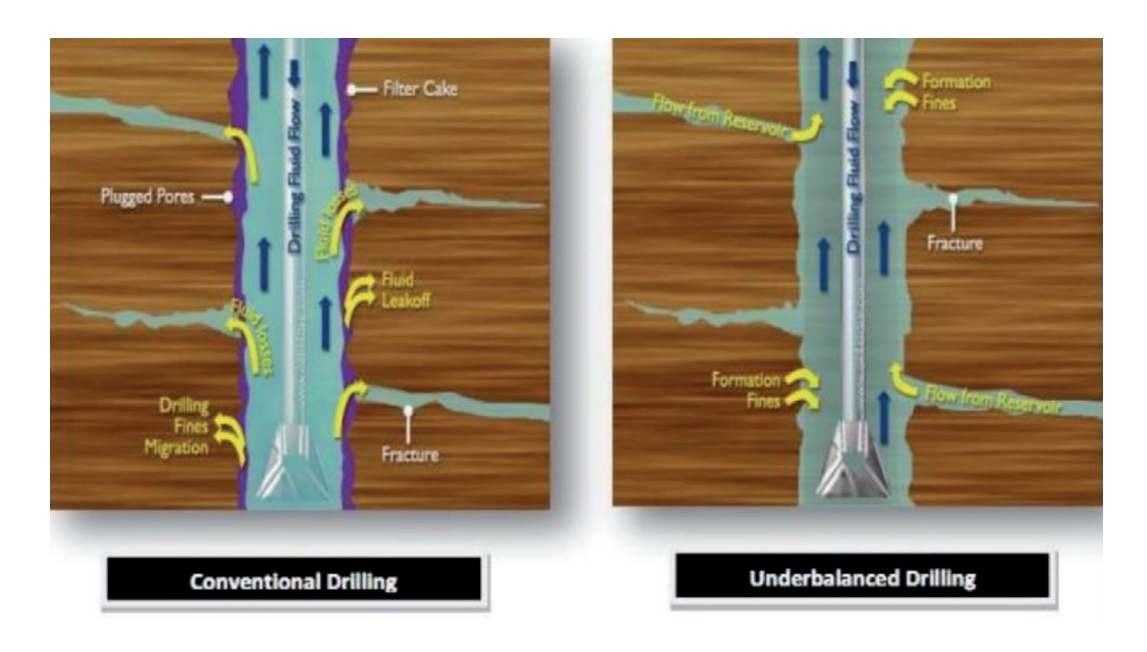


Figure 2 OBD vs UBD (Jaf, 2017)

1.3. Advantages and Disadvantages of UBD

There are some main advantages that can be obtained by implementing underbalance drilling. First, it can reduce formation damage. UBD is classified as a drilling procedure to protect the reservoir by eliminating formation damage during the operation. It reduces the problems associated with solid and fluid invasion into the formation. Then, UBD can also eliminate differential sticking and lost circulation problems. Differential sticking occurs when the toolstring sits in a thick filter cake within an overbalanced hole (Rehmet al., 2013, P. 114). In UBD the hydrostatic pressure is less than the formation pressure, and there is no filter cake built up. Therefore, it makes the differential sticking conditions low. Lost circulation is defined as loss of drilling fluid to the formation. It happens when the mud weight rises above the formation fracture pressure. Naturally fractured zones, low pressure, or high permeability reservoirs can be more costly to drill overbalanced when expensive drilling fluids are lost downhole (Qutob, 2004).

While UBD gives some advantages, it also has some disadvantages which related to the wellbore stability. UBD, by definition, means purposefully lowering the supportive pressure on the wellbore wall. This action moves the job of supporting the stresses in the surrounding

rock from the fluid column to the rock matrix itself. This greatly increases the differential stress on the rock. In formations that are naturally weak, like unconsolidated sands, naturally fractured carbonates, or reservoirs that are very depleted, this extra stress can easily be too much for the rock to handle. This causes mechanical failure, which can include breakouts, spalling, and maybe even a huge wellbore collapse due to lack of pressure support provided by mud pressure inside the wellbore, which leads to a higher concentration of stress transmitted on the surrounding rock (Salehi et al., 2010). A comprehensive geomechanical analysis is therefore essential to accurately define this window and ensure the wellbore remains stable throughout its operational life.

1.4. In Situ Stress State and Stress Redistribution

A complete analysis of wellbore stability commences with a quantitative understanding of the far field in situ stress state. Far field stresses can form in an isotropic (uniform stress in all directions) or anisotropic (varying stresses from distinct directions) manner. It is generally accepted that the vertical direction represents a principal stress direction, indicating that the vertical stress, (σ_v) , constitutes a principal stress. The maximum and minimum horizontal stresses $(\sigma_H$ and $\sigma_h)$ are the other two main stresses in the horizontal plane (Al-Ajmi, 2006). In this study also will assume the type of the fault is the normal fault.

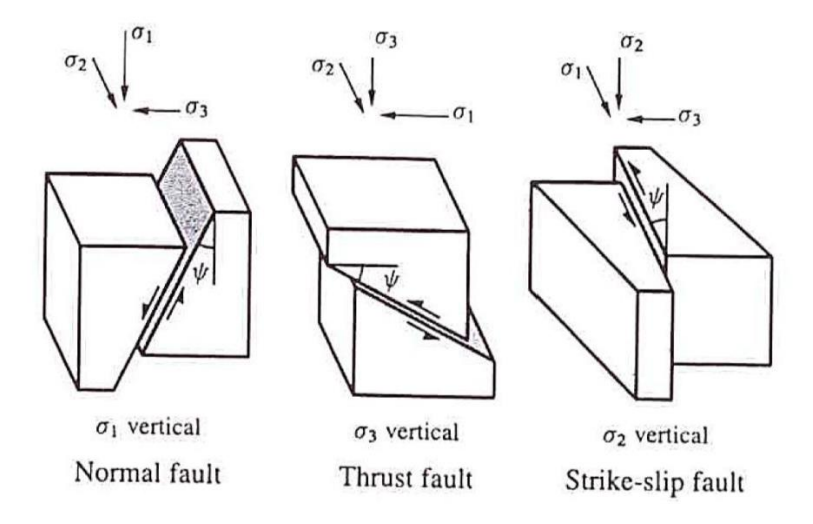


Figure 3 Underground Stresses in Fault Regimes (Fjaer. et al., 2008)

According to Anderson's theory of faulting, figure 3 shows the three main types of tectonic stress. These regimes dictate the characteristics of faulting within the Earth's crust and are

crucial for understanding the in-situ stress state for any geomechanical analysis. In a normally stressed formation, the vertical stress (σ_v) is the maximum principal stress. This is the same as the overburden stress.

While in the thrust fault (reverse fault) which is the type of fault happens when the crust is being pushed together. The vertical stress is the lowest principal stress ($\sigma_v = \sigma_3$), and the horizontal stresses are higher. And in the strike-slip fault, the intermediate principal stress ($\sigma_v = \sigma_2$) is the vertical stress. This condition leads to blocks of rock slide past each other horizontally.

1.4.1. Vertical Stress

The total vertical stress at any given depth is calculated by integrating the bulk density of the overlying rock column from the surface down to that depth (Zoback, 2011).

$$\sigma_{v} = \int_{0}^{z} \rho(z) g dz \tag{1.1}$$

Where:

- σ_v is the total vertical stress at depth z
- $\rho(z)$ is the density at depth z below the surface
- g is the acceleration due to gravity

1.4.2. Minimum Horizontal Stress

The most direct method to obtain the σ_h (minimum horizontal stress) is by direct measurement which can be done by leak of test (LOT) or controlled mini frac test. The idea behind this method is that a tensile fracture that happens when fluid is injected into a separate part of a wellbore will always open up against the path of least resistance, which is the plane that is perpendicular to the minimum principal stress. Once a small fracture is made and the injection stops, the fluid pressure goes down. The "fracture closure pressure" is the pressure at the exact moment the fracture walls close. This is thought to be the same as the minimum horizontal stress (Ye & Ghassemi, 2023).

While direct measurements provide accurate data at certain depths, but it's not practical to do them all the time. So, poroelastic models are used to make an estimate of σ_h (minimum

horizontal stress) continuous profile. These models, which are often based on Eaton's equation, use well log data to connect the horizontal stress to the vertical stress (σ_v), pore pressure, and the rock's elastic properties, like Poisson's ratio.

The assessment of the horizontal stresses is not a simple task since its actual value depends on the geologic stress history of the deposits. This formula (1.2) can be used to find the total horizontal minimum by assuming a relaxed area where the horizontal stress is caused only by the vertical stress:

$$\sigma_h = Ko * (\sigma_v - P_p) + P_p \tag{1.2}$$

Where:

- σ_h is the total minimum horizontal stress
- σ_v is the total vertical stress
- P_p is the pore pressure

The Ko is unknown coefficient of lateral stress at rest (means the σ_h when there is no lateral strain occurs) which depend on the depth coordinates. This Ko is also known as Effective Stress Ratio (ESR) in oil and gas industry. σ_h can become very large at shallow depth (0 - 150) m because of the residual stress, the stress which remains even after the force has been removed. The Ko has upper and lower limit which can be calculate with a formula below:

$$\frac{1-\sin\phi'}{1+\sin\phi'} \le Ko \le \frac{1+\sin\phi'}{1-\sin\phi'} \tag{1.3}$$

Where ϕ' is the friction angle of the rock. When the value of $Ko \leq 1$, the rock is in normally consolidated (NC) condition means the rock has undergone the same amount of consolidation in the past as it is currently experiencing. NC rocks is characterized by relatively low strength and stiffness. While for $Ko \geq 1$, the rock is in overconsolidated condition, which means the rock has experienced a higher effective state of stress in the past than its currently experiencing which makes it characterized by higher strength and stiffness so that it is more resistant to deformation.

1.4.3. Maximum Horizontal Stress

The maximum horizontal stress (σ_H), is the most challenging component of the stress tensor to determine due to its magnitude cannot be directly measured. On the other hand, its orientation is indirectly derived from wellbore data and its magnitude is constrained by integrating several different analyses. Orientation of the horizontal column is determined from failures induced by stress seen in caliper or borehole image logs (Tingay et al., 2008). Drilling induced tensile fractures form as small tensile cracks on opposite sides of the wellbore wall, aligned with the maximum horizontal stress (σ_H). The orientation of σ_H is therefore determined to be perpendicular to the azimuth of the breakouts or parallel to the azimuth of the drilling induced tensile fractures.

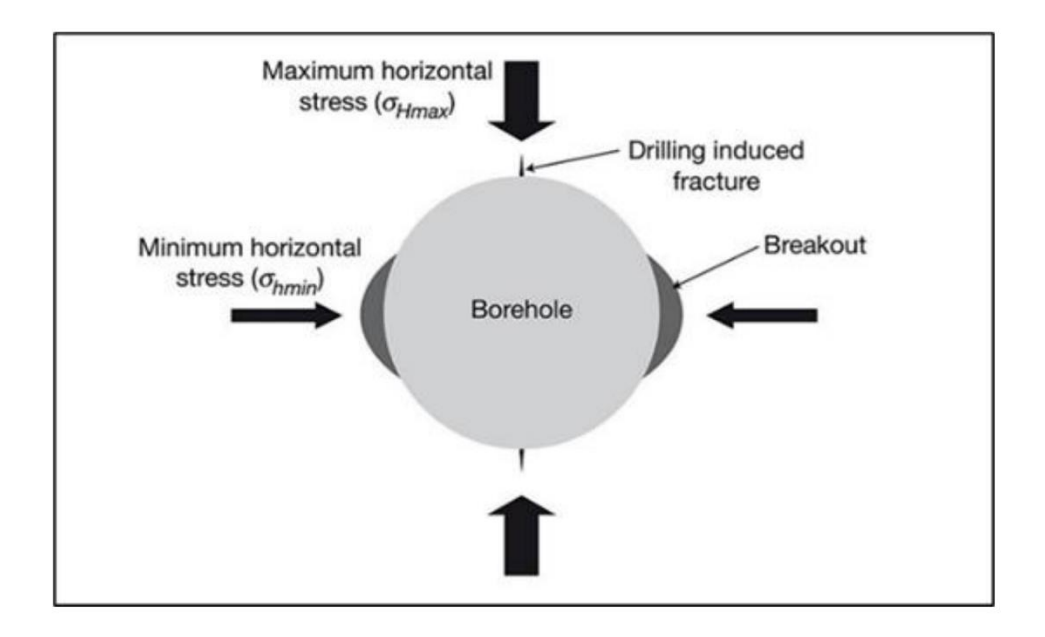


Figure 4 Horizontal Stresses in a Borehole Related to Borehole Breakout and Drilling Induced Tensile Fractures (Zoback, 2011)

A relationship between σ_h and σ_H can be expressed by a ratio R :

$$R = \frac{\sigma_H}{\sigma_h} \tag{1.4}$$

The higher the value of R means the higher the anisotropy. A higher anisotropy can cause challenges for wellbore stability, particularly in directional wells.

For the purposes of this study, synthetic generation of far field stress data will be employed. This method makes accessible to change the stress parameters in a controlled and systematic way, which is necessary for doing a thorough sensitivity analysis of how the model responds.

1.5. Stress Concentration around a Wellbore: Kirsch Solution

Drilling a wellbore fundamentally changes the local stress field. The Kirsch solution, which was first developed in 1898, is the basic analytical model that explains how this stress redistribution develops around a circular opening. This solution is based on material that is isotropic linear elastic, anisotropic far field stresses, circular hole in an infinite plate, and plane strain condition. These assumptions are not always true in real world condition, but the Kirsch equations are an important way to think about how stress concentration works (Zoback, 2011). For a vertical wellbore subjected to far field horizontal stresses (σ_H and σ_h) and an internal wellbore pressure (Pw), the general solution of Kirsch will be as follows:

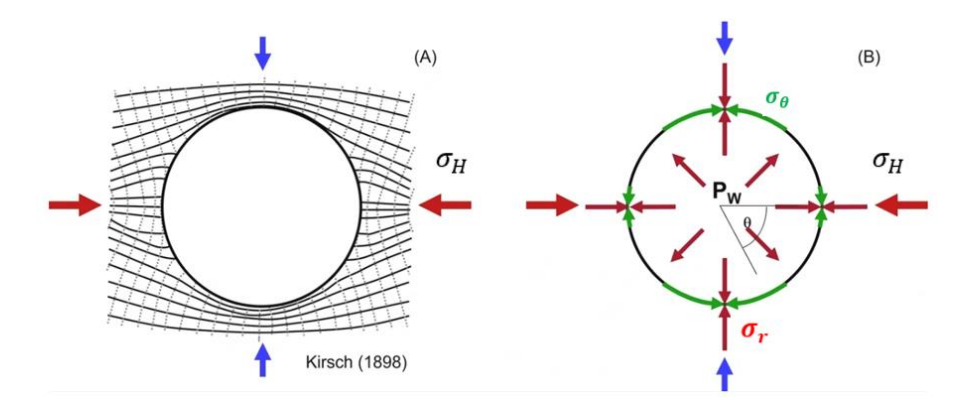


Figure 5 (A) Representation of stress concentration around a wellbore (after Kirsch, 1898), (B) stress distribution around a wellbore (Alliance, n.d.)

• Radial Stress (σ_r): The stress acting perpendicular to the borehole wall.

$$\sigma_r = \frac{1}{2} \left(\sigma_H + \sigma_h \right) \left(1 - \frac{R_W^2}{r^2} \right) + \frac{1}{2} \left(\sigma_H - \sigma_h \right) \left(1 + \frac{3R_W^4}{r^4} - \frac{4R_W^2}{r^2} \right) \cos 2\theta + p_W \frac{R_W^2}{r^2}$$
 (1.5)

At the borehole wall itself (r = Rw), it is simply equal to the pressure exerted by the drilling fluid:

$$\sigma_r = Pw \tag{1.6}$$

• Tangential or Hoop Stress (σ_{θ}): The stress acting tangent to the borehole wall. This is the most critical component for stability analysis, as it varies significantly around the circumference

$$\sigma_{\theta} = \frac{1}{2} \left(\sigma_{H} + \sigma_{h} \right) \left(1 + \frac{R_{w}^{2}}{r^{2}} \right) - \frac{1}{2} \left(\sigma_{H} - \sigma_{h} \right) \left(1 + \frac{3R_{w}^{4}}{r^{4}} \right) \cos 2\theta + p_{w} \frac{R_{w}^{2}}{r^{2}}$$
 (1.7)

At the borehole wall, the formula will become:

$$\sigma_{\theta} = \sigma_h + \sigma_H - 2(\sigma_H - \sigma_h)\cos 2\theta - P_w \tag{1.8}$$

• Axial Stress (σ_z): The stress component that acts parallel to the axis of the wellbore. For a vertical well, this stress is primarily governed by the weight of the overlying rock (σ_v) but is also modified by the concentration of horizontal stresses around the borehole due to the rock's elastic properties (Poisson's effect).

$$\sigma_z = \sigma_v - 2v(\sigma_H - \sigma_h) * \left(\frac{R_W^2}{r^2}\right) \cos 2\theta \tag{1.9}$$

At the borehole wall, the formula will become:

$$\sigma_z = \sigma_v - 2v(\sigma_H - \sigma_h)\cos 2\theta \tag{1.10}$$

• Shear Stresses $(\tau_{r\theta}, \tau_{\theta z}, \tau_{rz})$:

$$\tau_{r\theta} = -\frac{1}{2} \left(\sigma_H - \sigma_h \right) \left(1 - \frac{R_W^2}{r^2} \right) \left(1 - \frac{3R_W^4}{r^4} + \frac{4R_W^2}{r^2} \right) \sin 2\theta \tag{1.11}$$

$$\tau_{\theta z} = \tau_{rz} = 0 \tag{1.12}$$

At the borehole wall, the formula will become:

$$\tau_{\theta z} = \tau_{rz} = \tau_{r\theta} = 0 \tag{1.13}$$

In these equations, θ is the angle measured from the direction of the maximum horizontal stress, (σ_H) . From the hoop stress (σ_θ) equation, it can be seen the fundamental pattern of the stress concentration. The maximum value of hoop stress occurs when $\cos 2\theta = -1$, which corresponds to $\theta = 90^\circ$ or 270° . This is the azimuth aligned with the direction of the minimum horizontal stress (σ_h) . In contrast, the minimum compressive hoop stress (σ_θ) is a function of $\cos 2\theta$, when $\cos 2\theta = 0^\circ$ or 180° . This azimuth aligns with the maximum horizontal stress, σ_H . This non-uniform distribution of stress directly explains why wellbore failures are typically localized and oriented. Since the actual rocks are rarely perfectly elastic, isotropic and homogeneous, the real value of the Kirsch solution is not in its accuracy as a predictive tool.

Rather, it acts as a foundational concept. This thesis will quantify the error introduced by these idealizations and investigate their applicability by comparing simple elastic predictions to those obtained with more complex elasto plastic models such as Mohr Coulomb and Hoek Brown.

1.6. Geomechanical Implications of Underbalanced Drilling (UBD)

During drilling operations there is the occurrence of stress redistribution in the rock mass. This redistribution can cause stress concentration at some wellbore azimuth that can trigger rock shear failure. In order to counteract this effect, a wellbore pressure is selected. On the other hand in other azimuth the effect of the wellbore pressure can induce tensile failure. In overbalanced drilling (OBD) the wellbore pressure is higher than the pore pressure, thus the radial effective stress is positive. On the other hand, in underbalanced drilling (UBD) the wellbore pressure is lower than the pore pressure, thus, the radial effective stress becomes negative, resulting in tensile stress.

This phenomenon pushing UBD much closer to the failure envelope and creating a dual risk of instability. This represents the fundamental geomechanical trade off of UBD, which is that the operational and reservoir related benefits are purchased at the cost of a significantly elevated risk of mechanical wellbore instability. This risk is particularly high in formations that are inherently weak or mechanically compromised, such as unconsolidated sands, naturally fractured carbonates, or pressure depleted reservoirs where the rock strength has already been degraded.

2. Constitutive Modelling for Wellbore Stability Analysis

2.1. The Role of Constitutive Model

A constitutive model mathematically relates stress and strain for a material like rock. It includes a failure criterion to predict the conditions under which the rock will deform and break, which is essential for forecasting wellbore instability. One of the most important choices to make when doing a numerical simulation of wellbore stability is which constitutive model to use, since this decision directly affects how the rock mass is expected to behave. This study conducts a systematic comparison of three widely used constitutive models, covering from a straightforward idealization to a complex empirical formulation.

2.1.1. Model 1: Linear Elastic Model

The simplest constitutive model is the linear elastic model, which is based on Hooke's Law. It assumes that the material reacts to loading in a straight line, instantly, and completely reversibly, which means it goes back to its original shape when it is unloaded. When the model is isotropic, it has two main elastic constants which are the Young's Modulus (E), which measures how stiff the material is or how much it resists axial deformation, and Poisson's Ratio (v), which shows how much transverse strain is to axial strain. From these fundamental constants, other elastic parameters can be derived, such as the Bulk Modulus (K), representing resistance to volume change, and the Shear Modulus (G), representing resistance to shear distortion (Jaeger et al., 2009). The relationships are given by:

$$K = 3(1 - 2v) *E (2.1)$$

$$G = 2(1+v) *E$$
 (2.2)

The linear elastic model is based on a lot of strong assumptions. It assumes that the rock is a perfect continuum, that it is homogeneous and isotropic, and most importantly, that it does not change shape or fail permanently (plastic deformation). So, its main problem is that it can not predict what will happen after the stress exceeds the rock's strength limit. It is very useful for figuring out the initial stress distribution around a wellbore before it fails (as in the Kirsch solution), but it is not good enough for a full stability analysis because it can't model the process of failure, breakout formation, or behaviour after failure. In the context of this study,

it functions as the fundamental baseline model for comparison with more intricate, failure prone models.

2.1.2. Model 2: Mohr-Coulomb Criterion

The Mohr-Coulomb (M-C) criterion is a widely used model for predicting when materials will fail in soil and rock mechanics. It is an elasto-perfectly-plastic model, which means that it assumes the material acts elastically until it reaches a certain point of failure. After that, it deforms plastically.

A linear envelope in shear stress (τ) versus normal effective stress (σ n') space shows the failure criterion. This envelope is defined by two well known parameters: cohesion, c', and the angle of internal friction, ϕ' (Fjaer. et al., 2008).

$$\tau_S = c' + \sigma n' \tan \phi' \tag{2.3}$$

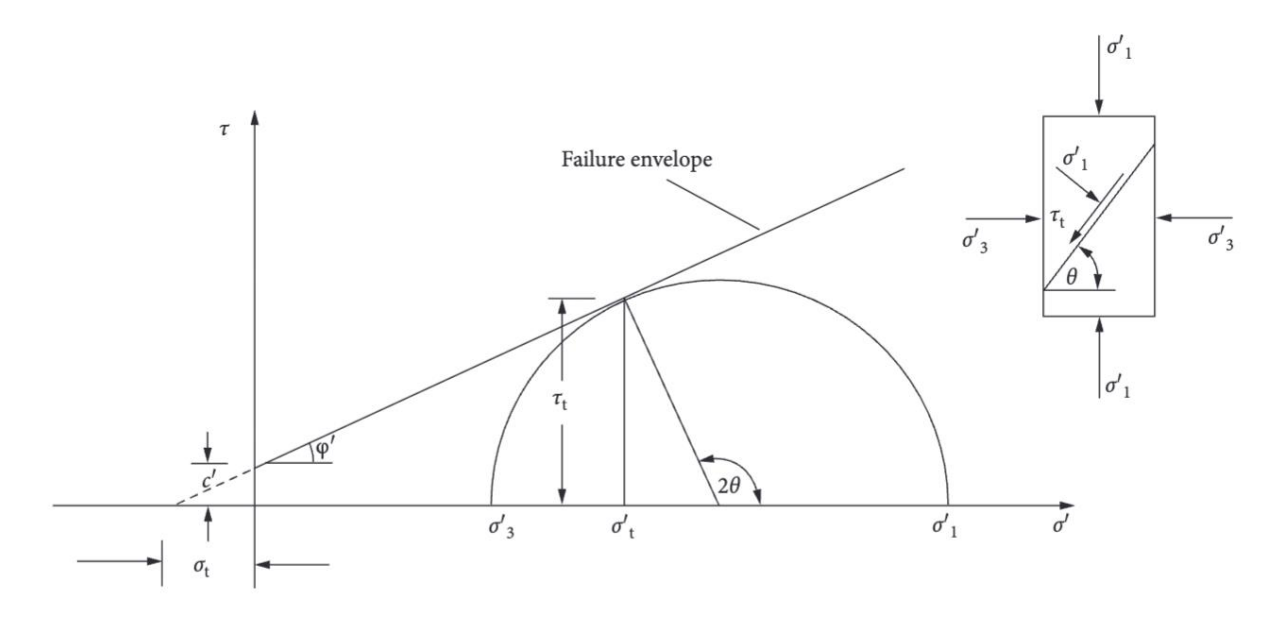


Figure 6 Mohr-Coloumb Criterion (Wei et al., 2020)

Figure 6 shows that the failure happens when the angle of 2θ touches the failure envelope line. This is the angle at which the sample fails. The Mohr-Coulomb criterion can be written as follow:

$$\sigma_{1s}' = \frac{2c'\cos\phi'}{(1-\sin\phi')} + \sigma_3' \frac{(1+\sin\phi')}{(1-\sin\phi')} = \sigma_c + \sigma_3' N_{\phi}$$
 (2.4)

Where σ'_{1s} represents the compressive stress that causes the rock to fail in shear under a specific confining pressure (σ'_{3}).

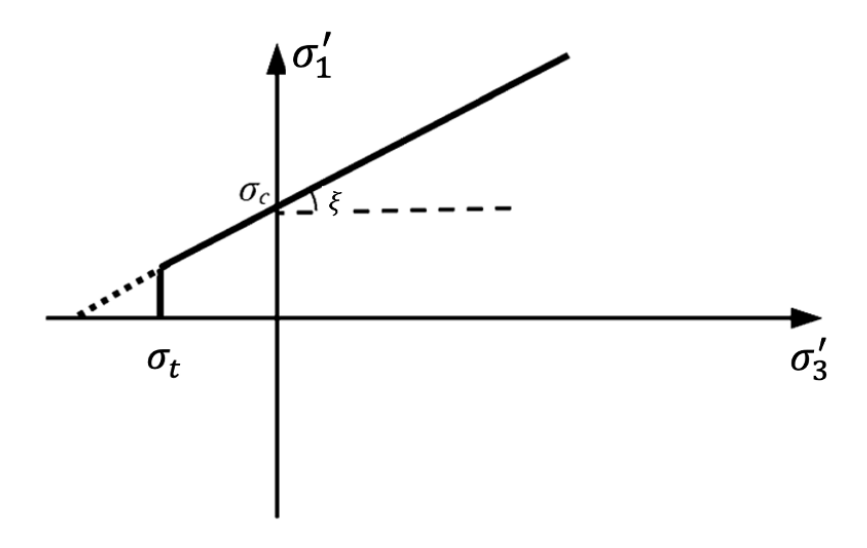


Figure 7 Mohr-Coloumb with a Tension Cutoff [33]

The Morh-Coulomb criterion can also predict the two strength parameters which are uniaxial compressive strength (σ_c) and the tensile strength (σ_t):

$$\sigma_c = \frac{2c'\cos\phi'}{(1-\sin\phi')} \tag{2.5}$$

$$\sigma_t = \frac{2c'\cos\phi'}{(1+\sin\phi')} \tag{2.6}$$

The standard Mohr-Coulomb criterion establishes a linear failure envelope determined by cohesion (c') and the angle of internal friction (ϕ '). This model works pretty well in the compressive stress range, but because it is linear, it greatly overestimates the rock's tensile strength when the failure envelope is moved into the tensile stress range. To address this problem and create more accurate model, a "tensile cut-off" is introduced. In practice, this means that the rock is set up to break in tension when the effective stress reaches this lower tensile strength value, even if the stress state is still below the main M-C failure line.

$$\sigma_t = \frac{1}{10} \ \sigma_c \tag{2.7}$$

Estimating rock tensile strength as 10% of its uniaxial compressive strength is a common practice, but it only gives a rough and often wrong value. The dataset in figure 8 shows that

the compressive to tensile strength ratio varies a lot, from 2.7 to 39. This distribution, with the average of 14.7, highlights the lack of applying a fixed ratio to estimate the tensile strength (Cai, 2010).

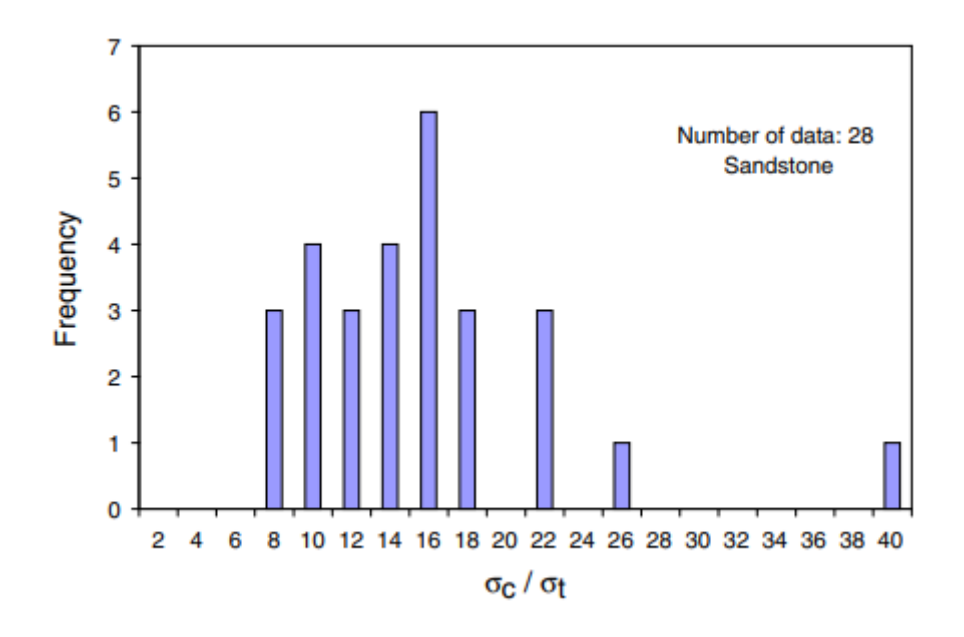


Figure 8 Distribution of the Compressive to Tensile Strength Ratio in Sandstones (Cai, 2010)

2.1.3. Model 3: The Generalized Hoek-Brown Failure Criterion

The Hoek Brown failure criterion is an empirical strength relationship that attempts to model the non-linear increase in peak strength of isotropic rock with increasing confining stress. Hoek Brown follows a non-linear parabolic form, in contrast to the linear Mohr—Coulomb failure criterion. The criterion comprises of companion processes aimed at providing a simple methodology to estimate the rock mass strength from the laboratory test values and field observations. Hoek Brown considers the intermediate principal stress to be independent (Eberhardt, 2012).

The Generalized Hoek-Brown criterion is defined by a relationship between the major ($\sigma'1$) and minor ($\sigma'3$) effective principal stresses at failure:

$$(\sigma'_{1} - \sigma'_{3}) = (m\sigma_{c}\sigma'_{3} + s\sigma_{c}^{2})^{a}$$
 (2.8)

Where:

• σ_c is the uniaxial compressive strength

- m and s are dimensionless strength parameters which depend on the type of rock and characteristic
- For hard intact rocks, the constant s is equal to 1, and the constant a is equal to 0.5.
 For highly fractured rocks, the constant s is equal to 0, and the constant a is equal to 0.65

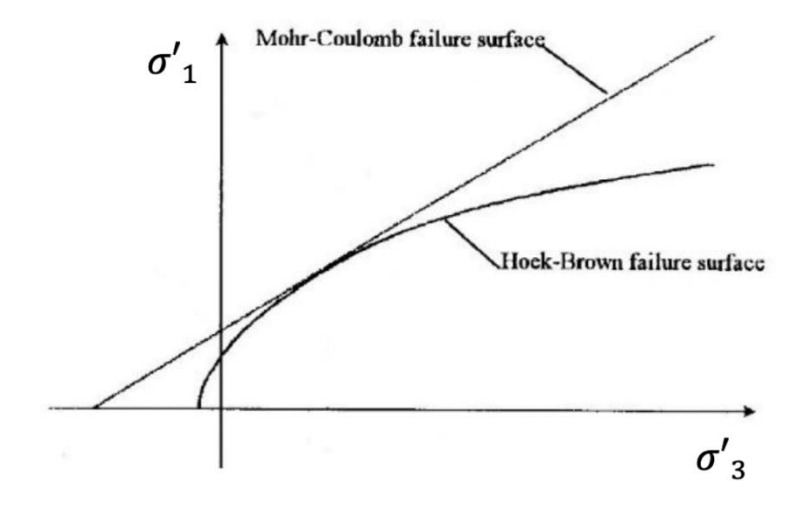


Figure 9 Hoek-Brown Failure Criterion [38]

The primary advantage of the Hoek-Brown criterion is that it can describe the non-linear failure behavior and the effects of discontinuities that are common in most rock masses. The GSI gives a systematic and widely accepted way to figure out how strong a jointed rock mass is, which is usually much weaker than the rock it came from. In particular, when dealing with low quality rock, this often gives more accurate and more cautious predictions of failure than the Mohr-Coulomb criterion, especially for the tensile strength (σ_t). However, it's important to say that the applicability of the H&B criterion has been questioned in certain stress regimes. According to Cai's study, the criterion works well for strong rock at high confining pressures, but not so well for low confining pressure and tension zones, which are the characteristics of underbalanced drilling. The study also showed that the material constant "m" isn't really a constant, it changes depending on the confining pressure (Deangeli, 2021).

The Geological Strength Index (GSI) is a system for classifying and characterizing rock masses based on their visual geological properties. The main goal is to give a number that illustrates the quality of a rock mass is. This number can then be used as a key input for the Hoek-Brown failure criterion (Eberhardt, 2012). In essence, GSI acts as the crucial bridge between the known properties of an intact rock sample which is tested in a lab and the much more complex

behavior of the in-situ rock mass which is affected by joints, fractures, and weathering. So that the constant s, mb, and a can be estimated with GSI as follows:

$$s = \exp(\frac{GSI - 100}{9 - 3D}) \tag{2.9}$$

$$mb = mi \exp(\frac{GSI - 100}{28 - 14D}) \tag{2.10}$$

$$a = \frac{1}{2} + \frac{1}{6} \left(exp \, \frac{-GSI}{15} - exp \, \frac{-20}{3} \right) \tag{2.11}$$

Where D is the disturbance factor and mi is the intact rock constant, which according to Cai (Davarpanah et al., 2021) varies from 13 to 21 for sandstone. The Hoek-Brown equation then can be written as follow:

$$(\sigma'_{1} - \sigma'_{3}) = (mb\sigma_{c}\sigma'_{3} + s\sigma_{c}^{2})^{a}$$
 (2.12)

Then the tensile strength can be estimated with this following formula (Hoek et al., 2022):

$$\sigma_t = -\frac{s\sigma_{ci}}{mb} \tag{2.13}$$

2.2. Mud Weight Window

The Kirsch equations, along with a failure criterion, make it possible to analytically define the boundaries of the mud weight window which is very important step to prevent shear failure and tensile failure. In UBD, the $P_{w|min}$ should be lower than pore pressure (Pp). The mud weight window should be meet this condition:

$$P_{w|min} < P_w < P_{w|max} \tag{2.14}$$

In order to obtain the appropriate minimum and maximum of the mud pressure, it is necessary to investigate the following cases: (for vertical well when $\sigma'_v > \sigma'_H > \sigma'_h$)

$$\sigma'_{\theta} > \sigma'_{z} > \sigma'_{r} \tag{2.15}$$

For $\theta = 90^{\circ}$

$$P_{w|min} = \frac{3(\sigma_H) - \sigma_h - \sigma_c + Pp(N_{\phi} - 1)}{(1 + N_{\phi})}$$
 (2.16)

and

$$\sigma'_{z} > \sigma'_{\theta} > \sigma'_{r} \tag{2.17}$$

$$P_{w|min} = \frac{\sigma'_{v} + 2v(\sigma_{H} - \sigma_{h}) - \sigma_{c} + Pp(N_{\phi} - 1)}{N_{\phi}}$$
(2.18)

From those 2 cases, the chosen $P_{w|min}$ will be the one that has the highest value.

For $\theta = 0^{\circ}$

$$P_{w|max} = 3(\sigma_h) - \sigma_H - Pp + \sigma_t \tag{2.19}$$

For the $P_{w|min}$, the value is not only limited by the criterion for shear failure, but need also accounts the condition for radial rensile failure:

$$\sigma'_r = -\sigma_t \tag{2.20}$$

$$Pw_{min}^{rad,tension} = Pp - \sigma_t \tag{2.21}$$

3. The Influence of Pore Pressure Conditions on Wellbore Stability

The mechanical behaviour of rock is closely related to the fluid pressure within its pore space. The presence and behaviour of pore fluids can greatly influence the stability of wellbore, and its consideration is the basis of contemporary geomechanics. This is carried out by using the principle of effective stress and setting appropriate pore pressure conditions for the simulation.

The fundamental principle which correlates fluid pressure with rock mechanics is the principle of effective stress, pioneered by Karl Terzaghi in the field of soil mechanics and subsequently generalized to rocks. The principle states that the deformation and failure of a porous material are not governed by the total stress (σ) applied to it, but by the portion of that stress supported by the solid grain to grain skeleton. This stress is the effective stress (σ '). The fluid pressure within the pore space (Pp) acts to counteract the total stress, effectively pushing the rock grains apart and reducing the contact forces between them. The relationship is generally given by the Terzaghi-Biot equation:

$$\sigma' = \sigma - \alpha P_n \tag{3.1}$$

$$\alpha = 1 - \frac{K'}{K_{S'}} \tag{3.2}$$

Where K' is drained bulk modulus of skeleton an K_s ' is the bulk modulus of solid grains, and α is the Biot effective stress coefficient, which is a measure of the efficiency of the pore pressure counteracting against the total stress. For the vast majority of applications in hard rocks, α is assumed to be close to 1, transforming back Terzaghi's original equation:

$$\sigma' = \sigma - P_p \tag{3.3}$$

The importance of this principle is that increasing the pore pressure decreases effective stress, which weakens the frictional strength of the rock, thereby making it weaker and more prone to failure. Instead, a reduction of pore pressure generally leads to an increase of the effective stress and strengthens the rock. Consequently, the estimation of wellbore stability in a fluid saturated formation is needed to be performed in the context of effective stresses.

The three scenarios of dry, drained, and undrained state considered in this study represent three physically different states, which facilitate a systematic investigation of pore pressure influences.

3.1.1. Dry Conditions

In dry condition, the pore pressure (Pp) is considered to be zero all over the rock mass. In this case, the effective stress is the same as the total stress ($\sigma'=\sigma$). A dry analysis is straightforward to carry out on a computer and serves as a theoretical baseline. It separates the rock matrix's purely mechanical response to the stresses caused by drilling, providing a standard against which the influence of pore fluids in the other cases can be quantitatively measured.

3.1.2. Drained Conditions

A drained analysis models the long term equilibrium state of the wellbore, assuming that the loading rate is slow relative to the fluid dissipation rate or in formations with high permeability, which allows for rapid pressure equilibration, so that the pore pressure remains constant $(\Delta P_p = 0)$. Under drained conditions, the stability assessment uses the final, steady-state pore pressure profile and the rock's intrinsic effective strength parameters which are the effective cohesion (c') and the effective angle of internal friction (θ') .

3.1.3. Undrained Conditions

An undrained analysis simulates the scenario when loading occurs so rapidly that the pore fluid is unable to drain from the rock matrix. This is a physical representation of drilling quickly in a formation with low permeability. In this case, the pore fluid pressure, which is almost impossible to compress compared to the rock skeleton, is trapped and has to carry some of the load change that was applied (Fjaer. et al., 2008). The drilling activity of the borehole leads to a re-distribution of the total stress in the rock mass. That change in the total stress causes an immediate change in the pore pressure, which ultimately controls the stability of the rock mass through the principle of effective stress. This response varies around the wellbore, as shown in Figure 10.

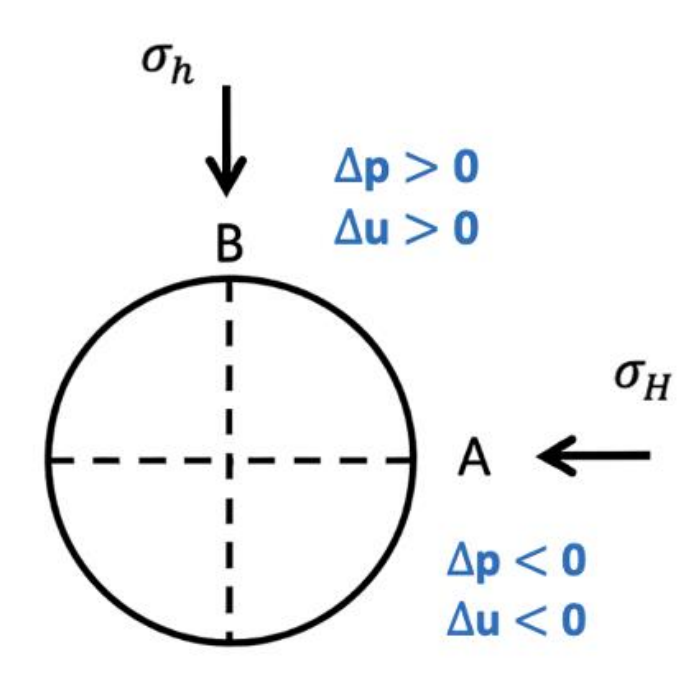


Figure 10 Distribution of Drilling-Induced Pore Pressure Around a Wellbore in an Anisotropic Stress Field

The condition immediately after drilling at point A ($\theta=0^\circ$) is more convenient than at the point B ($\theta=90^\circ$) due to the rock is unloaded. The pore pressure decreases ($\Delta u<0$) along the direction of the maximum horizontal stress. This drop of pore pressure increases the effective stress, making the rock locally stronger against shear failure. At point A, the mean stress also decreases which can be calculated from the Krisch's equations below:

$$P'_{Initial} = \frac{1}{3}(\sigma'_H + \sigma'_h + \sigma'_v) \tag{3.4}$$

$$P'_{Final} = \frac{1}{3} (\sigma'_r + \sigma'_\theta + \sigma'_z) = \frac{1}{3} (\sigma'_H + \sigma'_h + \sigma'_v - 2(1 - v)(\sigma'_H - \sigma'_h) \frac{Rw^2}{r^2} \cos 2\theta)$$
 (3.5)

Since at point A (θ =0), the value of $\cos 2\theta = 1$, the equation (3.5) at borehole wall becomes:

$$P'_{Final} = \frac{1}{3} \left(\sigma'_{H} + \sigma'_{h} + \sigma'_{v} - 2(1 - v)(\sigma'_{H} - \sigma'_{h}) \right)$$
(3.6)

$$\Delta P' = P'_{Final} - P'_{Initial} \tag{3.7}$$

It is also important to notice that at point A, the rock is more susceptible to tensile failure if the mud pressure is too high or if the far field stress anisotropy is too high. This phenomenon can be expressed from the equation below:

$$\sigma'_{\theta} = 3\sigma'_{h} - \sigma'_{H} - (Pw - Pp) \tag{3.8}$$

While in point B, the pore pressure ($\Delta u>0$) and the mean stress increases along the direction of the minimum horizontal stress. This rise in pore pressure reduces the effective stress, weakening the rock and pushing it closer to shear failure. This is the primary mechanism that initiates wellbore breakouts. The increase of mean stress and the effect of Pw at the borehole wall can be expressed from the equations below:

$$P'_{Final} = \frac{1}{3} \left(\sigma'_{H} + \sigma'_{h} + \sigma'_{v} + 2(1 - v)(\sigma'_{H} - \sigma'_{h}) \right)$$
(3.9)

$$\sigma'_{\theta} = 3\sigma'_{H} - \sigma'_{h} - (Pw - Pp) \tag{3.10}$$

3.2. Objective of the Study

The primary objective of this study is to conduct a systematic and comprehensive numerical investigation into the stability of a vertical wellbore drilled in a sandstone formation in underbalanced conditions. The underbalanced drilling (UBD) generates a tensile stresses in the rock mass that can result in tensile failure. To achieve this aim, the following specific objectives will be pursued:

- To develop a two dimensional numerical model of a vertical wellbore utilizing the finite difference software FLAC 2D (Itasca), incorporating synthetic yet realistic geomechanical and in-situ stress data that exemplify a sandstone formation at 2300m depth.
- 2. To simulate the geomechanical response of the wellbore using three distinct constitutive models: Linear Elastic, Mohr-Coulomb, and Hoek-Brown
- 3. To assess the impact of pore pressure behaviour on stability predictions by performing a comprehensive comparative analysis under three distinct and clearly defined conditions: dry, fully drained, and undrained.
- 4. To quantify, visualize and compare the extent of rock mass failure across all simulation cases using key stability indicators, including the stress fields and the size and shape of the plastic (yielded) zone.

4. Comparative Numerical Simulations with Different Constitutive Models

This chapter presents the principal numerical models of the study, methodically examining the geomechanical response of a vertical wellbore to drilling under underbalanced conditions. The analysis is organized to first find a baseline mechanical response in a dry rock mass, and then look at how pore pressure affects the response when it is drained and when it is in undrained condition. A comparative methodology is applied consistently, comparing the predictions of the Linear Elastic, Mohr-Coulomb, and Generalized Hoek-Brown constitutive models to highlight the essential significance of model selection in evaluating wellbore stability.

The analysis was performed using FLAC (Fast Langrangian Analysis of Continua, ver. 8.1, Itasca) 2D. A plane strain model was constructed to represent a transverse cross-section of a vertical wellbore. The model domain is sufficiently large relative to the wellbore diameter to ensure that the outer boundaries do not artificially influence the stress and displacement fields in the near-wellbore region. The simulation was configured using the synthetic, yet representative, parameters for a sandstone reservoir listed in table 1. A critical feature of this setup is the anisotropic horizontal stress field (σ_H =42 MPa > σ_h =37 MPa), as this anisotropy is the primary driver for non-uniform stress concentrations. This study also assume the normal fault scenario where the σ_v is the highest principal stress. But in this study, the axial stress (σ_z) is very high that affect the numerical simulation and gives a more complex scenario of the induced stresses and the type of failure.

Table 1 Data for Simulations

No	Description	Value	Unit
1	Well Radius	0.108	m
2	Formation Depth	2,300	m
3	Young Modulus, E	10	GPa
4	Bulk Modulus, K	9.8	GPa
5	Shear Modulus, G	3.76	GPa
6	Density	2,300	kg/m³
7	Poisson's Ratio	0.33	
8	Porosity	0.23	
9	σν	63	MPa
10	σΗ	42	Мра
11	σh	37	Мра
12	Pore Pressure for Drained/Undrained Case	20	Мра
13	Water Density	1000	Kg/m³
14	Bulk Modulus of Water (Drained Case)	0	MPa
15	Bulk Modulus of Water (Undrained Case)	2	GPa
16	Permeability (100mD)	9.8x10 ⁻¹¹	m²/(Pa.s)

4.1. Wellbore Stability Analysis with Elastic Model

In the first simulation, the Linear Elastic constitutive model is used. This model is based on the idea that the material can change shape without breaking, no matter how much stress is put on it. The results of this simulation, therefore, do not predict wellbore collapse but rather quantify the stress state that serves as the starting point for analyzing failure in more complex models.

4.1.1. Elastic Model: Dry Condition

This first simulation establishes a baseline for the geomechanical response of the wellbore. Utilizing a linear elastic model under dry conditions (Pp=0) allows for the observation of the solely mechanical effects of stress redistribution post drilling. In this idealized scenario, the total stress is the same as effective stress ($\sigma'=\sigma$), and any pressure from the wellbore (mud pressure) will cause the overbalanced drilling condition, thus, in dry condition it will not be possible to achieve underbalanced drilling condition. The main goal here is just to figure out how much stress is concentrated around the wellbore, providing a fundamental baseline against which the more complex effects of poroelasticity can be compared in subsequent sections. The simulation result must first be validated against the analytical Kirsch solution to confirm the model's reliability.

Figures 11 and figure 12 show the resulting effective stress contours around the wellbore from the FLAC simulation. The simulation results show the hoop stress at $\theta=90^\circ$, is ~89 MPa and the hoop stress at $\theta=0^\circ$ is ~69 MPa. The big difference in stress between the sides and the top and bottom of the wellbore is a direct and expected result of the anisotropic far field stresses acting on the rock.

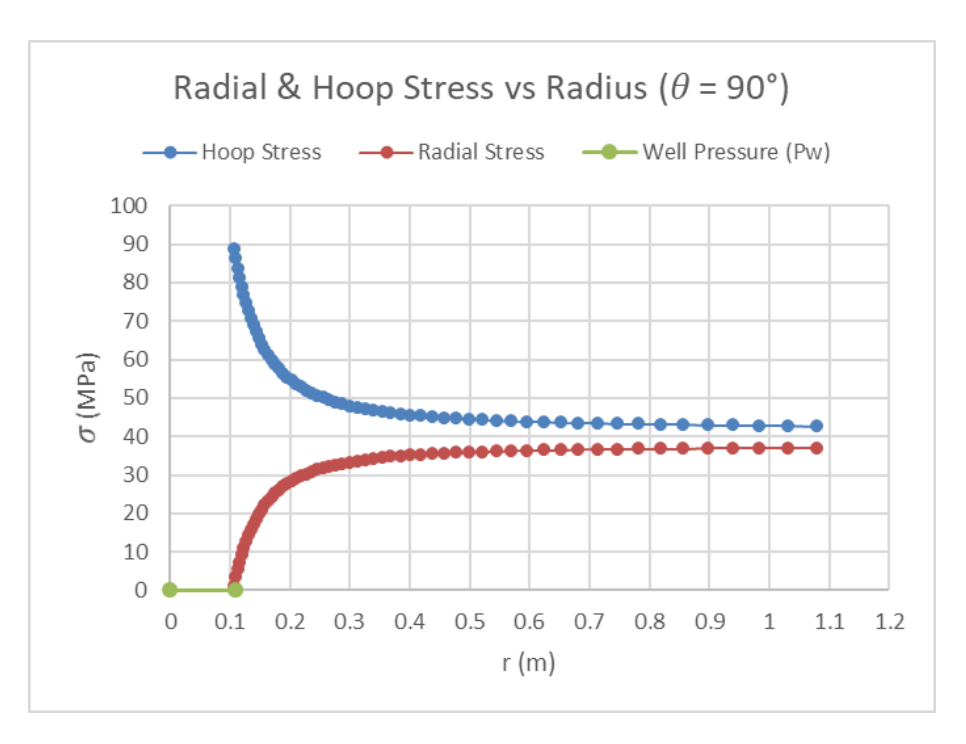


Figure 11 Hoop and Radial Stresses $at \theta = 90^{\circ}$ Elastic Model Dry Condition

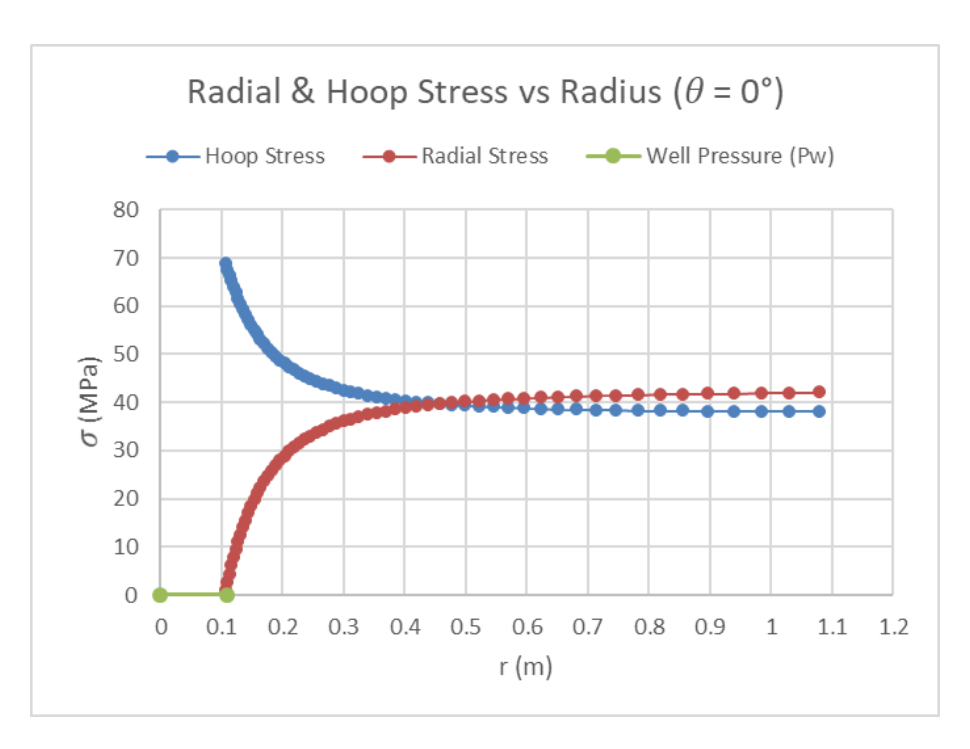


Figure 12 Hoop and Radial Stresses $at \theta = 0^\circ$ Elastic Model Dry Condition

Based on the Kirsch solution, the radial stress at the wellbore wall (r=Rw, Pp=0) is equal to the wellbore pressure, which is 0 MPa. As the distance from the wellbore increases, the influence of the drilling diminishes, and the radial stress goes back from the wellbore pressure to the magnitude of the far field stresses. To validate the numerical model's accuracy, these

results were compared with the analytical calculations from the Kirsch equations for stresses at the borehole wall.

The simulation correctly predicted a maximum hoop stress ($\theta = 90^{\circ}$) equals to 89 MPa which matches the analytical solution:

$$\sigma_{\theta \mid \theta = 90^{\circ}} = 3\sigma_{H} - \sigma_{h} - Pw = 3(42)MPa - 37MPa - 0MPa = 89 MPa$$

Similarly, the minimum hoop stress ($\theta=0^{\circ}$), was correctly calculated as 69 MPa also match the analytical solution:

$$\sigma_{\theta \mid \theta = 0^{\circ}} = 3\sigma_h - \sigma_H - Pw = 3(37)MPa - 42MPa - 0MPa = 69 MPa$$

The perfect match between the simulation results (89 MPa and 69 MPa) and the manual calculations validates that the model is set up correctly and performs as expected. This baseline proves that the model is reliable for more complex simulations with Mohr-Coulomb and Hoek-Brown models in both drained and undrained conditions. The results clearly demonstrate the fundamental principle of stress concentration which are the drilling activity causes the hoop stress to increase significantly, peaking in the direction of the minimum far field stress.

4.1.2. Elastic Model: Drained Condition

This section shifts from the theoretical dry rock mass to a more realistic scenario by integrating the influence of formation pore pressure in this scenario. In this simulation, the in-situ total stresses and elastic characteristics are the same as in the dry scenario. However, a constant formation pore pressure (Pp) of 20 MPa is now introduced. The wellbore pressure (Pw) now is established at 18 MPa which creates an underbalanced drilling condition, as the wellbore pressure is lower than the formation pore pressure.

To analyze the stress state, we must first convert the total in situ stresses to the effective stresses:

Effective Maximum Horizontal Stress :

$$\sigma'_H = \sigma_H - P_p = 42MPa - 20MPa = 22MPa$$

• Effective Minimum Horizontal Stress:

$$\sigma'_h = \sigma_h - P_p = 37MPa - 20 MPa = 17 MPa$$

To maintain consistency and validate the model under these new conditions, the analytical Kirsch solution is once again employed. The maximum and minimum effective hoop stresses at the wellbore wall are calculated as follows:

Maximum effective hoop stress:

$$\sigma'_{\theta|\theta=90^{\circ}} = 3\sigma'_{H} - \sigma'_{h} - (P_{w} - P_{p}) = 3(22)MPa - 17MPa - (18 - 20)MPa$$

$$\sigma'_{\theta|\theta=90^{\circ}} = 51MPa$$

• Minimum effective hoop stress:

$$\sigma'_{\theta|\theta=0^{\circ}} = 3\sigma'_{h} - \sigma'_{H} - (P_{w} - P_{p}) = 3(17)MPa - 22 MPa - (18 - 20) MPa$$

$$\sigma'_{\theta|\theta=0^{\circ}} = 31 MPa$$

Radial stress at borehole wall:

$$\sigma'_r = (P_w - P_p) = (18 - 20) MPa = -2 MPa$$

Figure 13 and figure 14 shows how the effective stresses distributed from the wellbore wall to 1.08m away from it. The data was obtained from the simulation with the elastic model in drained condition. As we can see the value of the effective hoop stress at $\theta=90^\circ$ is 51 MPa and the effective hoop stress $\theta=0^\circ$ is 31 MPa. These results align with the manual calculation with the Krisch equation.

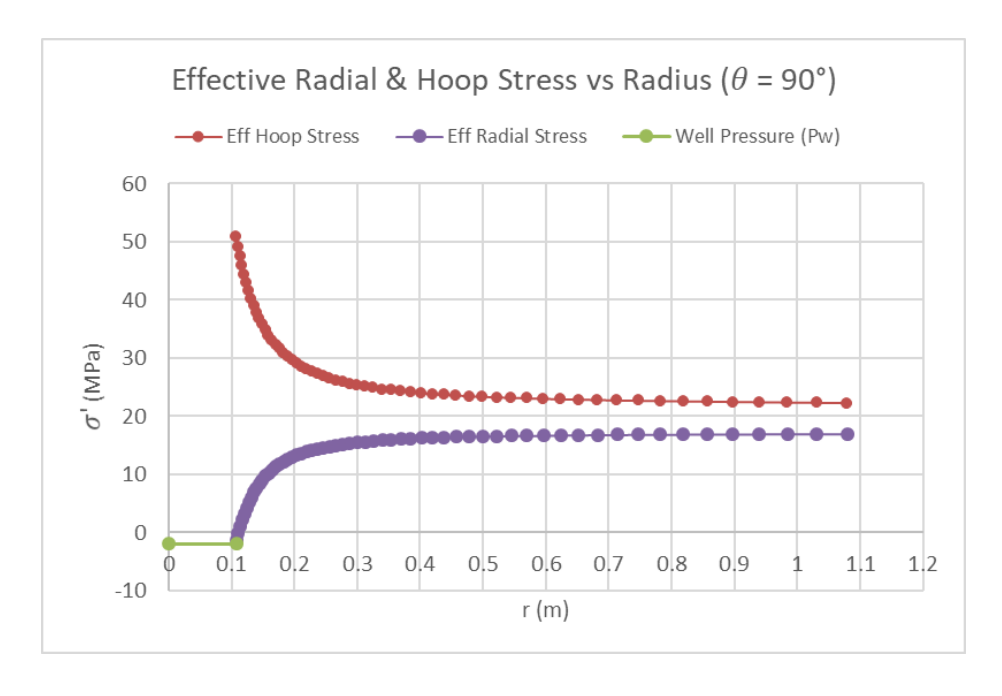


Figure 13 Eff. Hoop and Eff. Radial Stresses at $\theta = 90^{\circ}$ Elastic Model Drained Condition

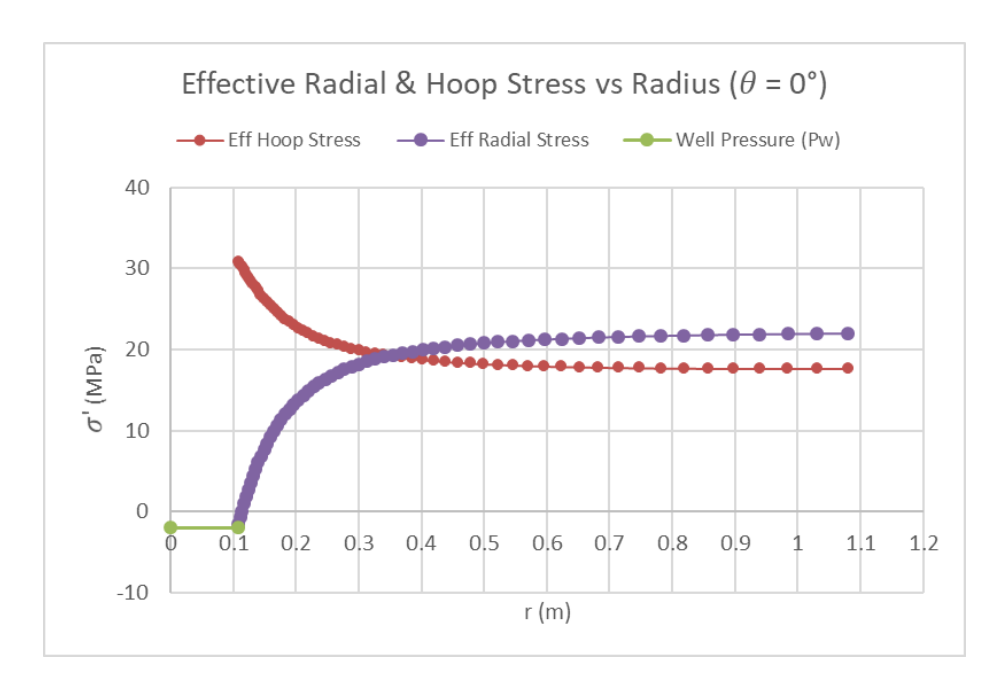


Figure 14 Eff. Hoop and Eff. Radial Stresses at $\theta=0^\circ$ Elastic Model Drained Condition

The negative sign of σ'_r indicates that the effective radial stress is in tensile and also indicates underbalanced drilling condition. A sensitivity study was performed to assess the effect of underbalance magnitude on wellbore stability by modifying the wellbore pressure (Pw). This analysis examines the impact of underbalance magnitude on the near wellbore effective stress field. Three scenarios were simulated, ranging from mild to the limit (Pw=0) underbalance:

Case A : Pw = 18 MPa,

• Effective radial stress:

$$\sigma'_r = (P_w - P_p) = (18 - 20) MPa = -2 MPa$$

Maximum effective hoop stress:

$$\sigma'_{\theta|\theta=90^{\circ}} = 51 MPa$$

• Minimum effective hoop stress:

$$\sigma'_{\theta|\theta=0^{\circ}} = 31 MPa$$

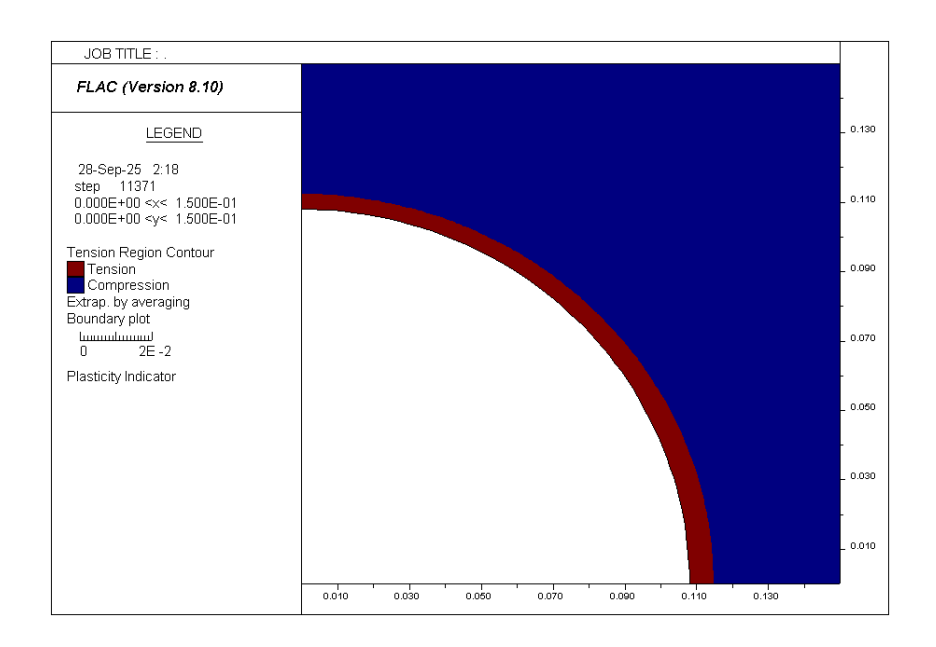


Figure 15 Tension/Compression Region (Elastic Drained Model), Pw = 18 MPa

Case B : Pw = 15 MPa

• Effective radial stress:

$$\sigma'_r = (P_w - P_p) = (18 - 20) MPa = -2 MPa$$

• Maximum effective hoop stress:

$$\sigma'_{\theta|\theta=90^{\circ}} = 54 MPa$$

• Minimum effective hoop stress :

$$\sigma'_{\theta|\theta=0^{\circ}} = 34 MPa$$

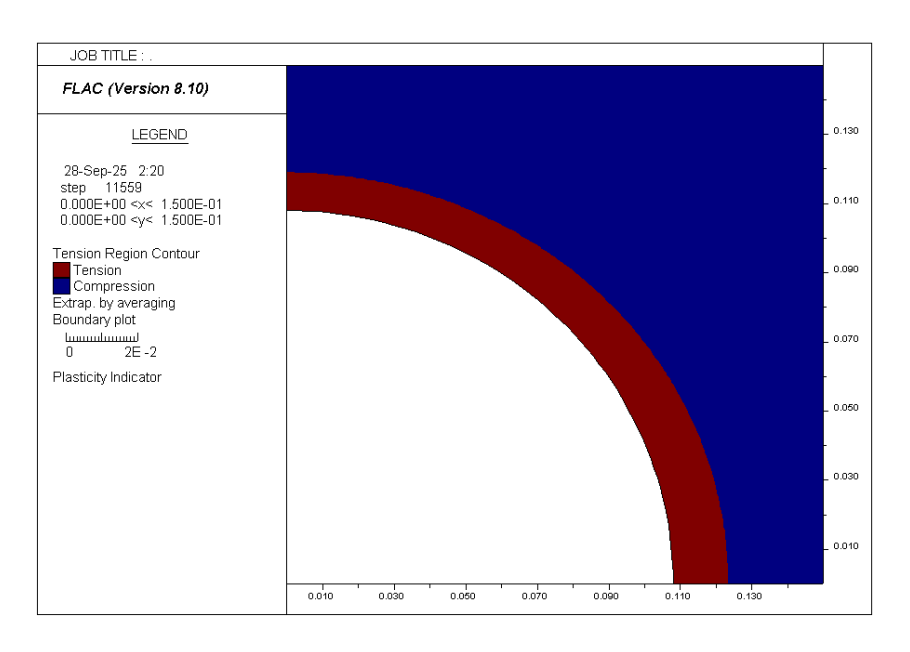


Figure 16 Tension/Compression Region (Elastic Drained Model), Pw = 15 Mpa

> Case C (Limit UBD): Pw = 0 MPa

• Effective radial stress:

$$\sigma'_r = (P_w - P_p) = (0 - 20) MPa = -20 MPa$$

Maximum effective hoop stress:

$$\sigma'_{\theta|\theta=90^{\circ}} = 69 MPa$$

• Minimum effective hoop stress:

$$\sigma'_{\theta|\theta=90^{\circ}} = 49 MPa$$

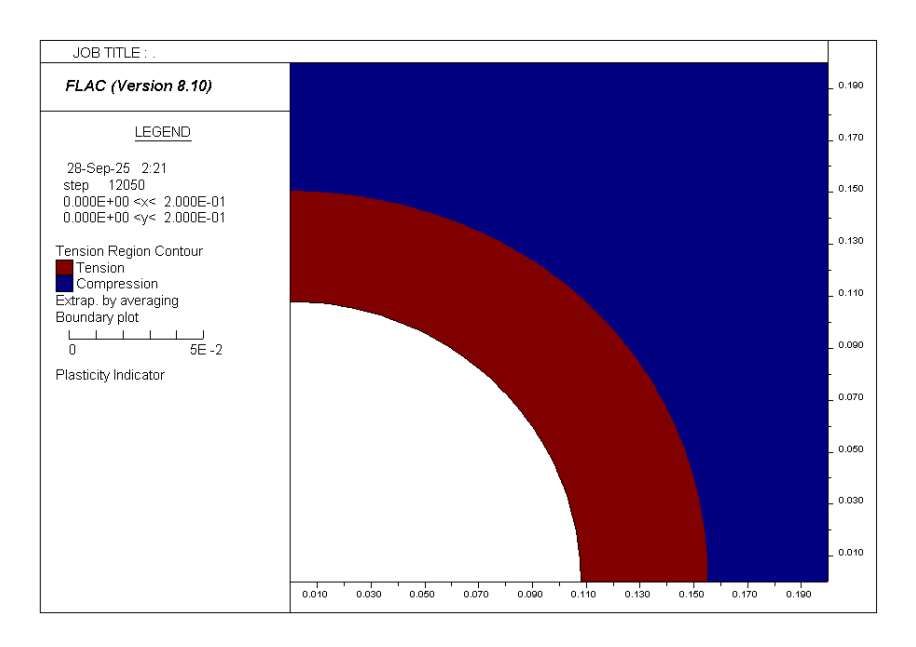


Figure 17 Tension/Compression Region (Elastic Drained Model), Pw=0 MPa (LIMIT CASE)

Figures 15, 16, and 17 present the simulation outputs, which show a "Tension Region" around the wellbore. The effective hoop stresses remain compressive in all cases, as shown by the calculations. Therefore, the tension region shown in the plots is primarily governed by the tensile effective radial stress, (σ'_r) . As the wellbore pressure is reduced which making the underbalance more severe, the two distinct and competing effects on the stress state occur simultaneously. First, as Pw decreases, the effective radial stress (σ'_r) becomes progressively more tensile, increasing from -2 MPa in the slight UBD case A to a significant -20 MPa in the limit UBD case C. This directly elevates the risk of tensile failure modes. The tensile stress acts to overcome the rock's intrinsic tensile strength, promoting the initiation and propagation of fractures originating at the wellbore wall.

Second, and concurrently, the reduction in supportive wellbore pressure transfers a greater load to the surrounding rock matrix. This causes the maximum effective hoop stress to

become significantly more compressive, rising from 51 MPa to 69 MPa (from Case A to Case C). This incereased stress concentration is localized at the azimuths aligned with the minimum horizontal stress, the typical location for compressive shear failure and borehole breakouts. This analysis demonstrates that increasing the degree of underbalance does not simply weaken the wellbore in a single manner. Instead, it makes the geomechanical environment more hostile by making both tensile failure (due to higher tensile radial stress) and compressive shear failure (due to higher compressive hoop stress and a much larger differential stress). This finding highlights a fundamental geomechanical trade-off inherent in the design and execution of UBD operations.

4.1.3. Elastic Model: Undrained Condition

This section investigates the immediate, short term geomechanical response following drilling by simulating an undrained condition, where pore fluids do not have time to dissipate. This condition is very important for analyzing the stability of a wellbore because it represents the state of the rock as the drill bit passes. The simulation maintains the same far-field stresses and rock properties as the previous cases, with an initial formation pressure (Pp) of 20 MPa and a wellbore pressure (Pw) of 15 MPa.

Figure 18 and figure 19 show the pore pressure distribution as a function of radial distance from the wellbore wall at the two critical azimuths. The initial far field pore pressure before drilling is uniform at 20 MPa. At the wellbore wall (r=0.108 m), the simulation shows a clear difference. At the azimuth aligned with the minimum horizontal stress ($\theta=90^{\circ}$), the pore pressure increases to almost 22.5 MPa, which is a positive induced pressure of +2.5 MPa. This increase of pore pressure reduces the effective stress, weakening the rock and making it more susceptible to compressive shear failure at $\theta=90^{\circ}$. On the other hand, at the azimuth aligned with the maximum horizontal stress ($\theta=0^{\circ}$), the pore pressure decreases to approximately 17.5 MPa, a negative induced pressure of -2.5 MP, increases the effective stress, which more convenient situation immediately after drilling.

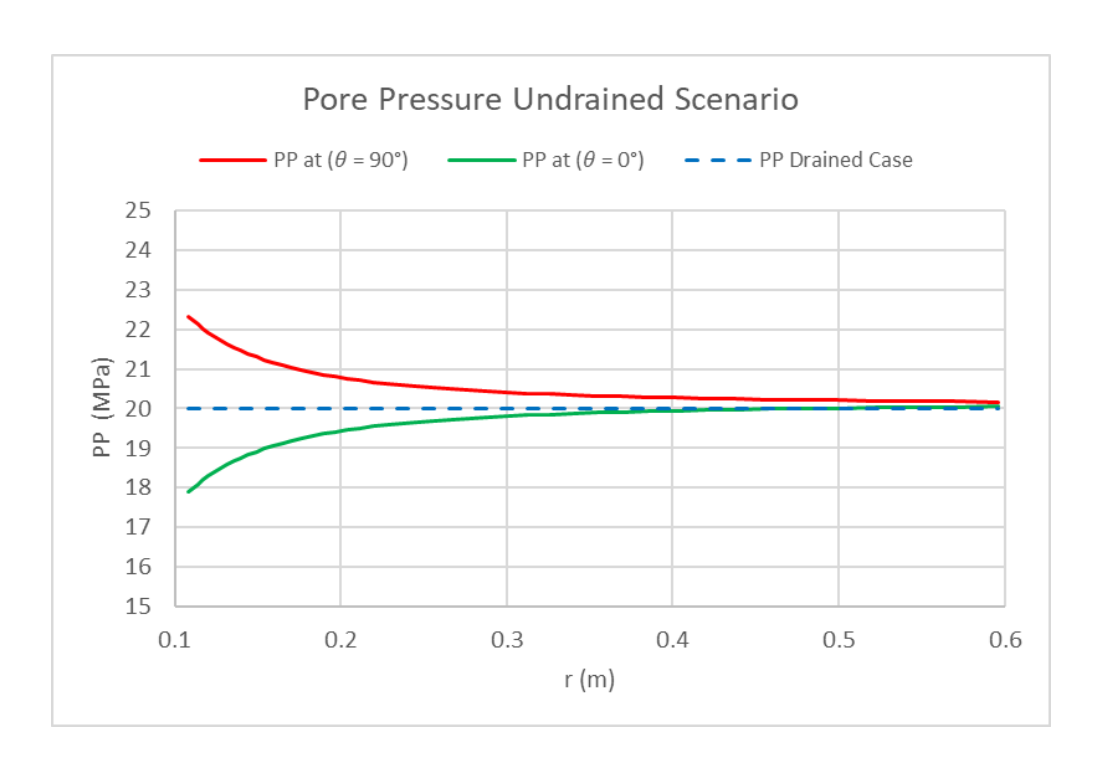


Figure 18 Pore Pressure Undrained Scenario (Elastic Model)

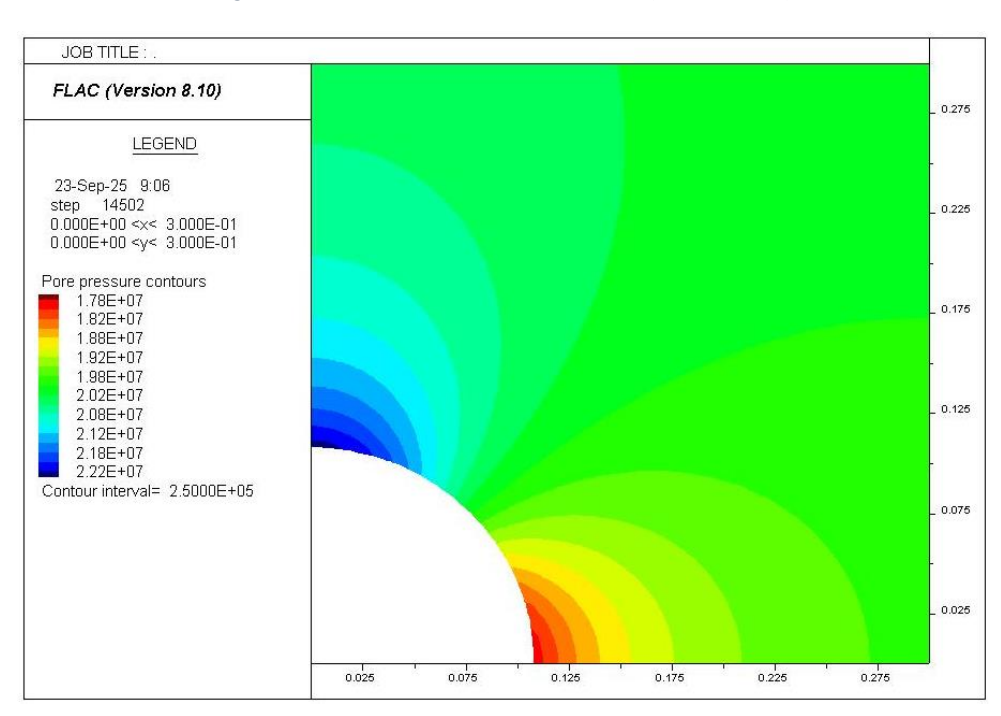


Figure 19 Pore Pressure Undrained Scenario (Elastic Model) FLAC2D

The plot also shows that this induced pressure effect is a near wellbore phenomenon. The pressure change is strongest at the wellbore wall and fades away with increasing radial distance, returning to a pressure of 20 MPa in the far field within about 0.4 m.

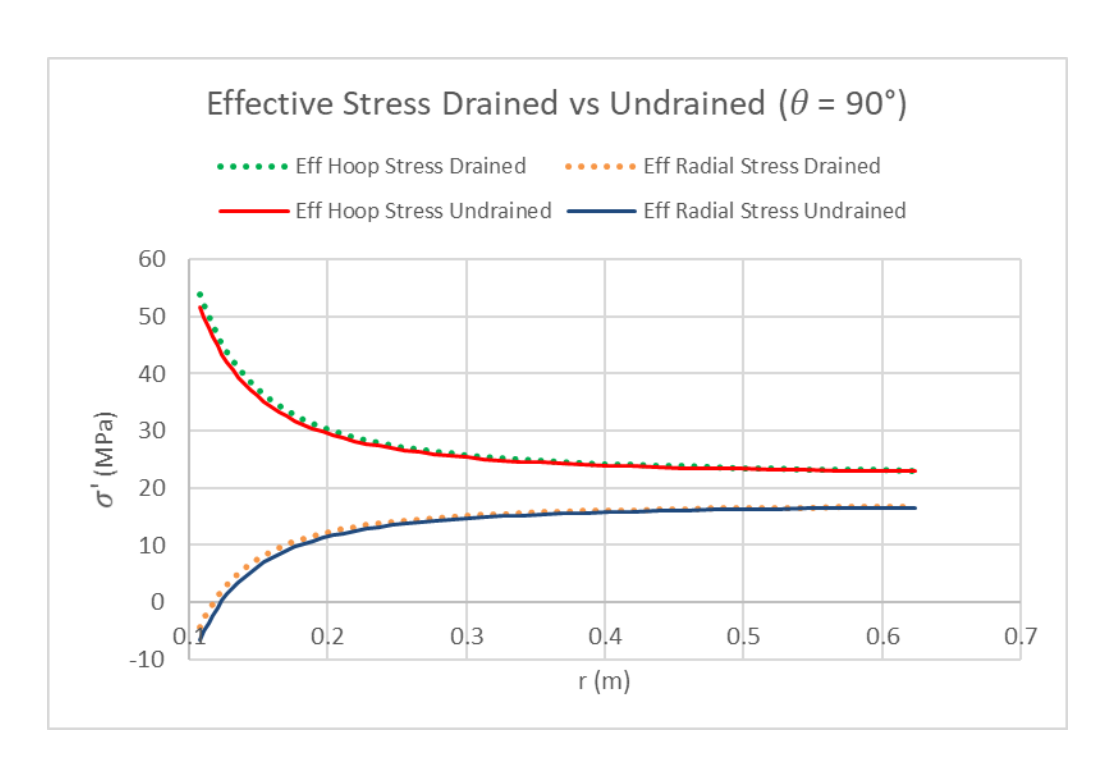


Figure 20 Effective Stress Drained vs Undrained Condition at $\theta=90^\circ$ (Elastic Model), Pw=15MPa

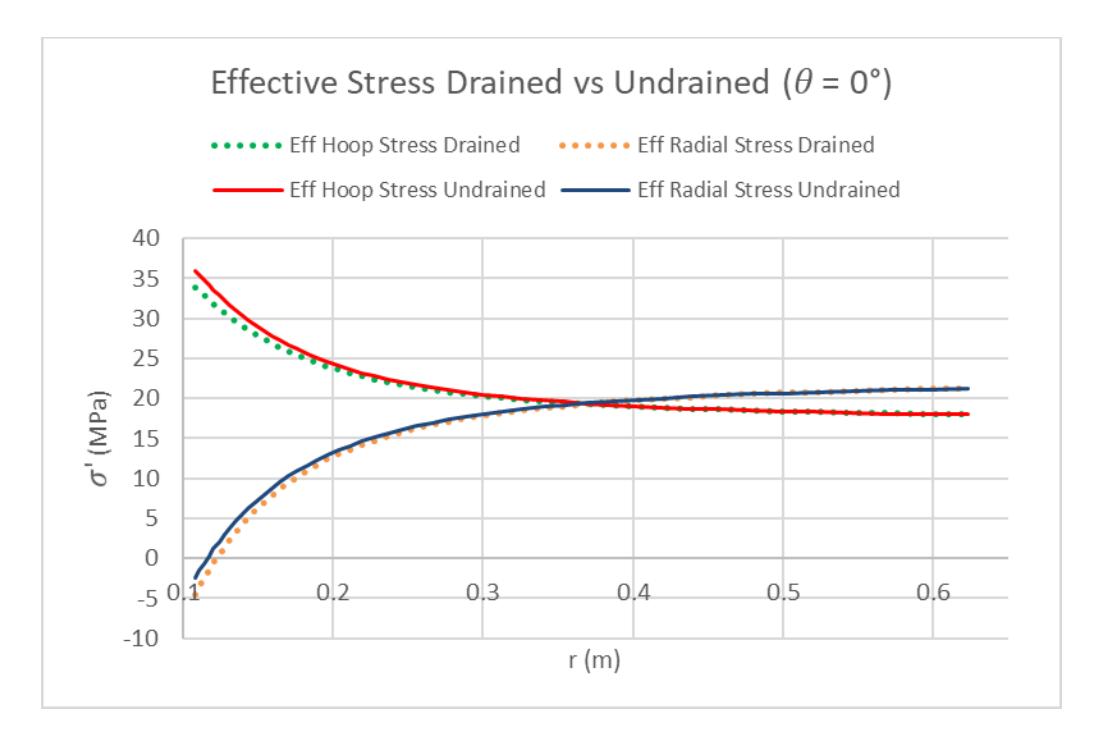


Figure 21 Effective Stress Drained vs Undrained Condition at $\theta=0^\circ$ (Elastic Model), Pw=15MPa

Figure 20 and figure 21 show a direct, quantitative comparison between the drained and undrained scenarios for the case of Pw = 15MPa. It shows that due to the increase of pore pressure at the azimuth aligned with the minimum horizontal stress ($\theta = 90^{\circ}$), the effective

stresses are reduced and becomes lower compare to the drained case. Vice versa, the reduction of pore pressure at the azimuth aligned with the maximum horizontal stress ($\theta = 0^{\circ}$), the effective stress is reduced and becomes higher compare to the drained case.

It is also expected that from figure 10, the ΔP is increase at $\theta=90^\circ$ and decreases at $\theta=0^\circ$. To prove this, below calculation at borehole wall has been done:

for $\theta = 90^{\circ}$:

- Pore pressure = 22.57 MPa
- Effective Maximum Horizontal Stress:

$$\sigma'_{H} = \sigma_{H} - P_{p} = 42MPa - 22.57 MPa = 19.42 MPa$$

• Effective Minimum Horizontal Stress:

$$\sigma'_{h} = \sigma_{h} - P_{p} = 37MPa - 22.57 MPa = 14.42 MPa$$

• Effective Vertical Stress:

$$\sigma'_{v} = \sigma_{v} - P_{p} = 63MPa - 22.57 MPa = 40.42 MPa$$

• Maximum effective hoop stress:

$$\sigma'_{\theta|\theta=90^{\circ}} = 3\sigma'_{H} - \sigma'_{h} - (P_{w} - P_{p})$$

$$\sigma'_{\theta|\theta=90^{\circ}} = 3(19.42)MPa - 14.42MPa - (15 - 22.57)MPa = 51.42MPa$$

• Effective radial stress :

$$\sigma'_{r|} = (P_w - P_p) = (15 - 22.57) MPa = -7.57 MPa$$

Effective axial stress:

$$\sigma'_z = \sigma'_v + 2v (\sigma'_H - \sigma'_h) = 40.42 + 2(0.33) * (19.42 - 14.42) = 43.72 MPa$$

• Effective initial mean stress (Pp = 20MPa) :

$$P'_{Initial} = \frac{1}{3}(\sigma'_{H} + \sigma'_{h} + \sigma'_{v}) = \frac{1}{3}(22 + 17 + 43) = 27.33 \text{ MPa}$$

• Effective final mean stress:

$$P'_{Final} = \frac{1}{3}(\sigma'_r + \sigma'_\theta + \sigma'_z) = \frac{1}{3}(-7.58 + 51.42 + 43.72) = 29.19 MPa$$

• Effective delta pressure :

$$\Delta P' = P'_{Final} - P'_{Initial} = 29.19 - 27.33 = 1.86 MPa$$

for $\theta = 0^{\circ}$:

The same equation but now the pore pressure is different

- Pore pressure = 17.66 MPa
- Effective Maximum Horizontal Stress:

$$\sigma'_{H} = \sigma_{H} - P_{p} = 42MPa - 17.66MPa = 24.34MPa$$

• Effective Minimum Horizontal Stress:

$$\sigma'_{h} = \sigma_{h} - P_{p} = 37MPa - 17.66 MPa = 19.34 MPa$$

• Effective Vertical Stress:

$$\sigma'_{v} = \sigma_{v} - P_{p} = 63MPa - 17.66MPa = 45.34MPa$$

• Minimum effective hoop stress:

$$\sigma'_{\theta|\theta=0^{\circ}} = 3\sigma'_{H} - \sigma'_{h} - (P_{w} - P_{p}) = 36.34 MPa$$

• Effective radial stress :

$$\sigma'_r = (P_w - P_p) = -2.66 MPa$$

• Effective axial stress:

$$\sigma'_{z} = \sigma'_{v} + 2v (\sigma'_{H} - \sigma'_{h}) = 42.04 MPa$$

• Effective initial mean stress (Pp = 20MPa) :

$$P'_{Initial} = \frac{1}{3}(\sigma'_{H} + \sigma'_{h} + \sigma'_{v}) = 27.33 \text{ MPa}$$

• Effective final mean stress :

$$P'_{Final} = \frac{1}{3} (\sigma'_r + \sigma'_{\theta} + \sigma'_z) = 25.24 MPa$$

• Effective delta pressure :

$$\Delta P' = P'_{Final} - P'_{Initial} = 25.24 - 27.33 = -2.10 MPa$$

The calculations prove that at $\theta=90^\circ$ not only does the pore pressure increases, but the effective delta pressure (ΔP) also increases. And vice versa at $\theta=0^\circ$ not only does the pore pressure decreases, but the effective delta pressure (ΔP) also decreases.

The interpretation of these results may indicate that the undrained condition is more stable at the critical azimuth $\theta=90^\circ$, as the maximum effective hoop stress (51.42 MPa) is lower than that in the drained case (54 MPa). This conclusion is fundamentally inaccurate since the wellbore stability is not governed by the absolute magnitude of the effective hoop stress alone, but by the proximity of the complete stress state to the rock's failure criterion. According to fundamental rock mechanics principles like the Mohr-Coulomb criterion, the shear strength ($\tau_s=c'+\sigma n'\,\tan\phi'$) of a material is directly proportional to the effective normal stress acting on the potential failure plane. In the undrained case at θ =90 \circ , the induced pore pressure of +2.5 MPa directly reduces the effective normal stress across any potential shear plane within the rock. This drop in $\sigma' n$ means that the rock's shear strength is also going down. Therefore, the rock is significantly weaker and closer to failure in the undrained condition because its intrinsic capacity to resist shear has been compromised by the excess pore pressure.

To parallel the previous analysis in drained condition, the sensitivity study was repeated under undrained conditions. This assessment again examines how modifying the wellbore pressure (Pw) impacts the near wellbore effective stress field and failure tendency, now accounting for induced pore pressure changes. Table 2 summarizes the calculated effective stresses and changes of pore pressures at the critical azimuths, and Figures 22-24 visualize the resulting tension regions.

Table 2 Comparison of Effective Stresses and Pore Pressure at θ =90° and θ =0° for Varying Wellbore Pressures (Pw) under Undrained Conditions

Pressure (Mpa)	θ=90°			θ=0°				
Pw	17.50	18.00	19.00	21.00	17.50	18.00	19.00	21.00
Рр	21.79	22.08	22.28	22.27	17.90	17.90	17.90	17.89
σ'Η	20.21	19.92	19.72	19.73	24.10	24.10	24.10	24.11
σ'h	15.21	14.92	14.72	14.73	19.10	19.10	19.10	19.11
σ'ν	41.21	40.92	40.72	40.73	45.10	45.10	45.10	45.11
σ'z	44.51	44.22	44.02	44.03	41.80	41.80	41.80	41.81
σ'θ	49.71	48.92	47.72	45.73	33.60	33.10	32.10	30.12
σ'r	-4.29	-4.08	-3.28	-1.27	-0.40	0.10	1.10	3.11
P'initial	27.33	27.33	27.33	27.33	27.33	27.33	27.33	27.33
P'final	29.98	29.68	29.48	29.50	25.00	25.00	25.00	25.02

> Case A : Pw = 18 MPa

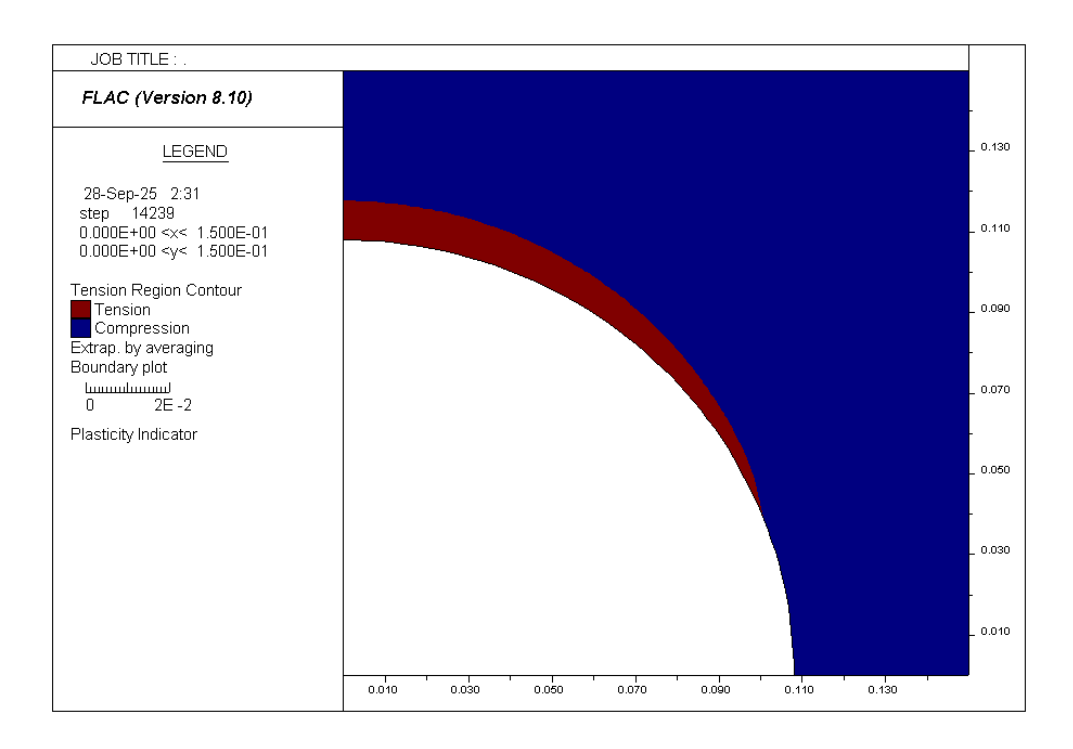


Figure 22 Tension/Compression Region (Elastic Undrained Model), Pw = 18 MPa

> Case B : Pw = 15 MPa

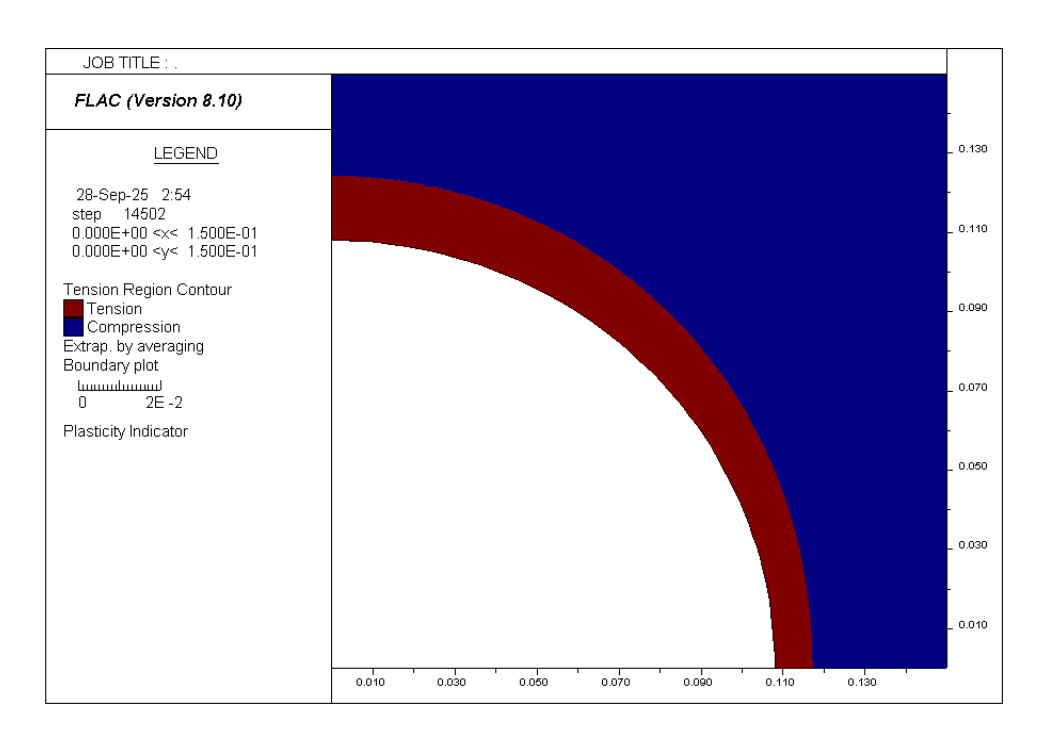


Figure 23 Tension/Compression Region (Elastic Undrained Model), Pw=15 MPa

> Case C : Pw = 0 MPa

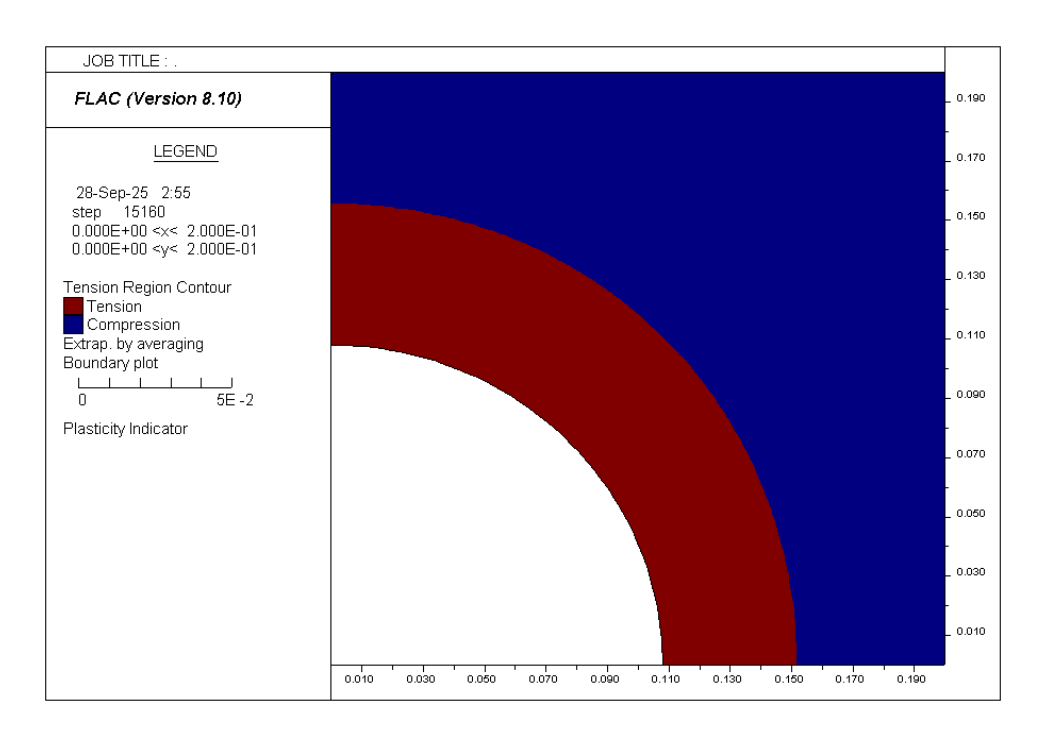


Figure 24 Tension/Compression Region (Elastic Undrained Model), Pw=0 MPa

The results confirm a consistent and critical trend which is as the wellbore pressure (Pw) is reduced, the effective hoop stress increases and the effective radial stress becomes progressively more tensile. From figure 22 we can see that by implementing Pw = 18MPa, at $\theta=0^\circ$ we don't see any tensile region because based on the calculation the effective radial stress (σ 'r) at this point is positive 0.35. On the other hand, with Pw = 15 MPa, we observe that the tensile region is built near wellbore wall at both of the angles even though it gets thinner as it goes to the azimuth aligned with the maximum horizontal stress. This phenomenon is influenced by the changes of pore pressure due to the undrained state condition.

4.2. Wellbore Stability Analysis with Mohr-Coulomb Model

The previous analysis, which used the Linear Elastic model, provided a basic understanding of how stress is redistributed and concentrated around the wellbore. It accurately measured the magnitude of the effective radial and hoop stresses, confirming the numerical model against the analytical Kirsch solution. The main problem with an elastic model, though, is that it can't predict when a material will fail. It assumes that the rock can handle any amount of stress without breaking or yielding. To overcome this constraint and perform a realistic stability analysis, it is important to apply an elasto-plastic constitutive model. This section presents the Mohr-Coulomb (M-C) model to simulate the initiation and propagation of rock mass failure around the wellbore.

Within the framework of an elasto-plastic analysis, the most direct and meaningful indicator of wellbore instability is the development of a "plastic zone" which is also referred to as a yielded zone. This zone represents the volume of rock around the wellbore where the effective stresses that have been applied have exceeded the strength set by the M-C failure criterion. The analysis of this plastic zone provides a far more nuanced and realistic assessment of wellbore damage than the calculation of a single critical collapse pressure. A critical pressure can show when something is about to fail, but the shape and size of the plastic zone can tell us how bad the damage is, which can be more useful for the analysis. The shape and size of the plastic zone are direct consequences of the in-situ stress field and the rock's strength properties. In an anisotropic horizontal stress field, the stress concentration is

not uniform around the wellbore circumference which already been discussed in previous section.

4.2.1. Mohr-Coulomb Model: Drained Condition

The simulations were performed using the Mohr-Coulomb model in FLAC 2D, with the sandstone formation's strength properties defined by the parameters in Table 3. The failure envelope is thus defined by a cohesion of 14.5 MPa and a friction angle of 41.5 degrees. A tensile strength limit of 5.0 MPa is also specified, meaning the rock will fail in tension if the effective stress becomes tensile and exceeds this value. The dilation angle is set to zero, indicating that the rock does not expand in volume upon shearing (non-associated flow rule).

Parameter	Symbol	Value	Unit
Cohesion	c'	14.50	MPa
Tension	σt	6.40	MPa
Friction Angle	φ′	41.50	Degrees
Dilation Angle	ψ	0.00	Degrees

Table 3 Mohr-Coulomb Parameters for Sandstone Formation

Based on the equation in section 2.2. Mud weight window, we obtained the mud window as below:

$$P_{w|min} < P_w < P_{w|max} = 17.47 MPa < P_w < 55.4 MPa$$

But in order to meet underbalance condition, the $P_{w|max}$ should be lower than the pore pressure, so the window will be:

$$P_{w|min} < P_w < P_{w|max} = 17.47MPa < P_w < 20MPa$$

To establish a clear threshold for the onset of instability, the analysis is anchored using a baseline case representing a marginally stable condition which utilizes a wellbore pressure (Pw) of 17.5 MPa. A detailed analytical verification is performed to demonstrate the concept of the stability margin and to validate the numerical model's output. The steps are as follows:

• Effective Maximum Horizontal Stress:

$$\sigma'_H = \sigma_H - P_p = 42MPa - 20 MPa = 22 MPa$$

• Effective Minimum Horizontal Stress:

$$\sigma'_h = \sigma_h - P_p = 37MPa - 20 MPa = 17 MPa$$

Effective Radial Stress

$$\sigma'_r = Pw - Pp = 17.5 - 20 = -2.5 MPa$$

• (o'1s) The compressive stress that causes the rock to fail in shear under a specific confining pressure (σ'_3)

$$\sigma_{1s}' = \frac{2c'\cos\phi'}{(1-\sin\phi')} + \sigma_{3}'\frac{(1+\sin\phi')}{(1-\sin\phi')} = \frac{2*14.5MPa*\cos(41.5)}{(1-\sin(41.5))} - 2.5MPa\frac{(1+\sin(41.5))}{(1-\sin(41.5))}$$

$$= 52.06 MPa$$

Tensile Strength

$$\sigma_t = \frac{1}{10} * \sigma_c = \frac{1}{10} * \frac{2c \cdot cos \phi'}{(1 - sin \phi')} = 6.4 MPa$$

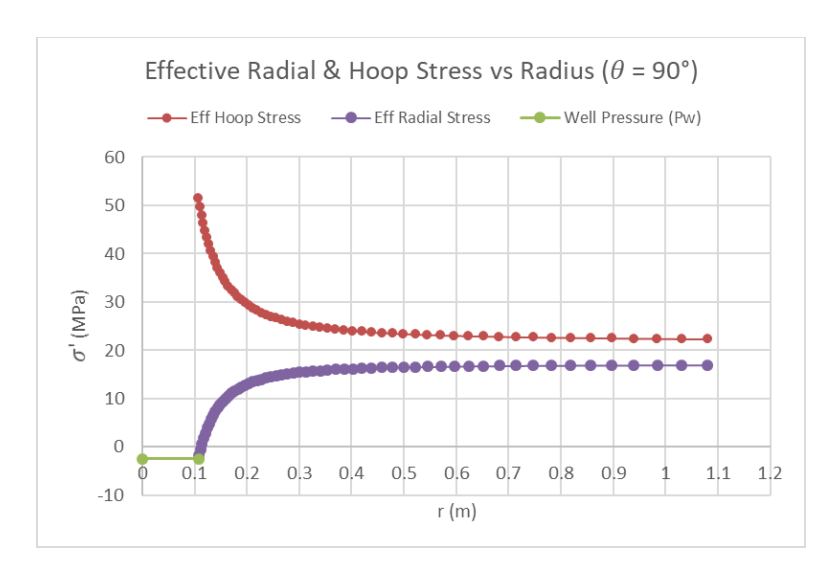


Figure 25 Eff. Hoop and Eff. Radial Stresses at $\theta = 90^{\circ}$ MC Model Drained Condition

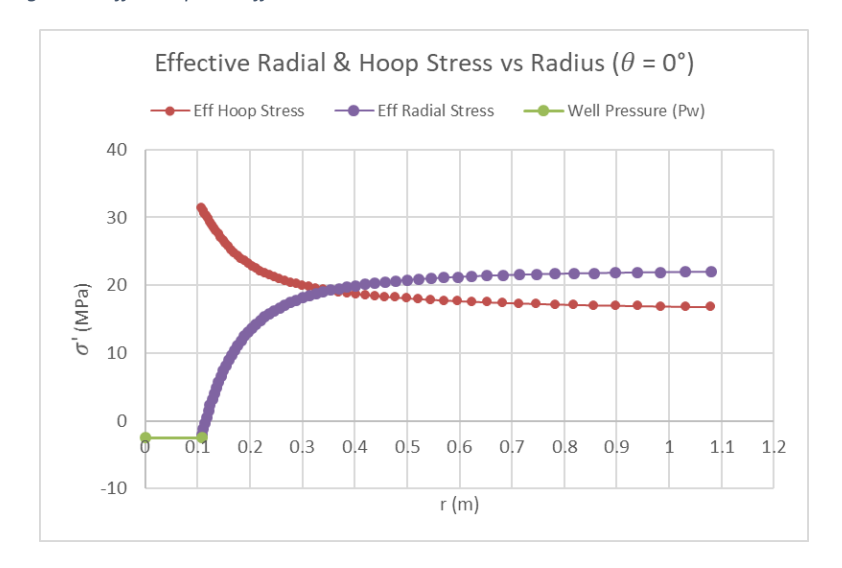


Figure 26 Eff. Hoop and Eff. Radial Stresses at $\theta=0^\circ$ MC Model Drained Condition

To maintain consistency and validate the model under these new conditions, the analytical Kirsch solution is once again employed. The maximum and minimum effective hoop stresses at the wellbore wall are calculated as follows:

Maximum effective hoop stress:

$$\sigma'_{\theta|\theta=90^{\circ}} = 3\sigma'_{H} - \sigma'_{h} - (P_{w} - P_{p}) = 3(22)MPa - 17MPa - (17.5 - 20)MPa$$

$$\sigma'_{\theta|\theta=90^{\circ}} = 51.5MPa$$

• Minimum effective hoop stress:

$$\sigma'_{\theta|\theta=0^{\circ}} = 3\sigma'_{h} - \sigma'_{H} - (P_{w} - P_{p}) = 3(17)MPa - 22 MPa - (17.5 - 20) MPa$$

$$\sigma'_{\theta|\theta=0^{\circ}} = 31.5 MPa$$

Determine stability margin:

Margin =
$$\sigma'_{1s} - \sigma'_{\theta \mid \theta = 90^{\circ}} = 52.06MPa - 51.5MPa = 0.56 MPa$$

To investigate the onset of instability, a sensitivity analysis was performed by incrementally reducing the wellbore pressure (Pw), thereby increasing the degree of underbalance. We will compare the applied maximum effective hoop stress ($\sigma'_{\theta|\theta=90^{\circ}}$) calculated from the Kirsch solution with σ' 1s calculated from the M-C failure criterion under the confining stress (σ' 3 = σ' r). Failure is predicted when the applied stress meets or exceeds the value of σ'_{1s} .

The results for three distinct wellbore pressure scenarios are summarized in Table 4.

 $\sigma'r = Pw - Pp$ σ'θ|max (σ'1s) Pw Margin Case (Mpa) (Mpa) (Mpa) (Mpa) (Mpa) 17.50 -2.50 51.5 52.06 0.56 Α 16.00 -3.00 53 44.67 -8.33 C 15.00 -5.00 54 39.74 -14.26

Table 4 Wellbore stability analysis with different well pressure (Pw) (MC Drained model)

> Case A (Pw = 17.5 MPa)

The analytical check in table 5 shows a positive stress-strength margin of +0.56 MPa. The applied hoop stress (51.5 MPa) is slightly less than the rock strength σ'_{1s} (52.1 MPa) under this confining pressure and the model therefore predicts that the wellbore wall will remain stable.

The FLAC simulation result, shown in the figure above, validates this prediction. The plot shows that the rock remains in an elastic state, with no plastic (yielded) zone forming around the wellbore, confirming its stability.

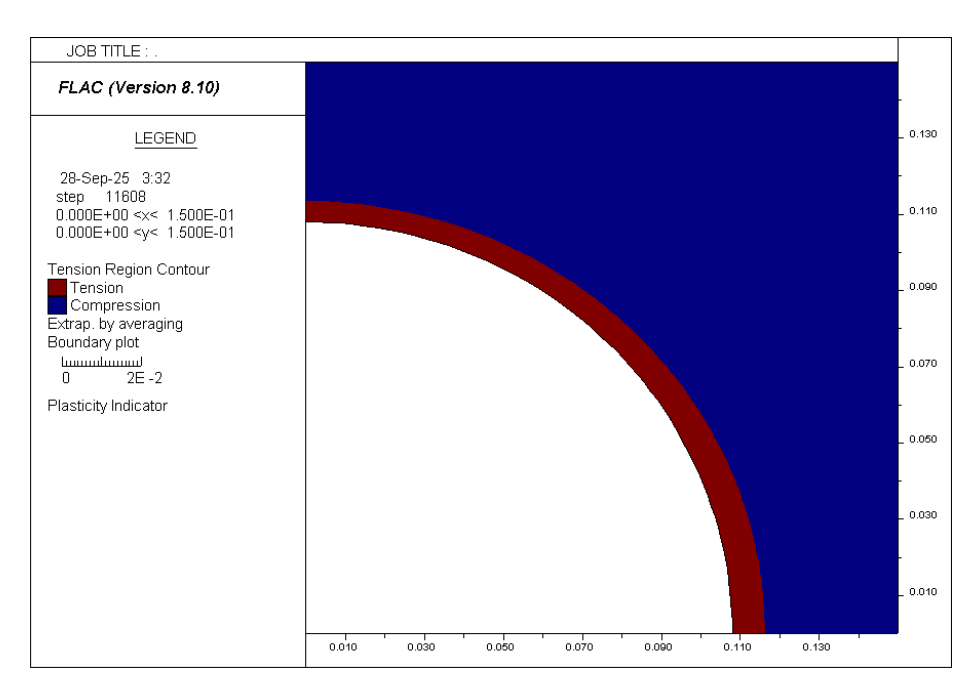


Figure 27 Tension/Compression Region (MC Drained Model), Pw=17.5 MPa

> Case B (Pw = 16 MPa)

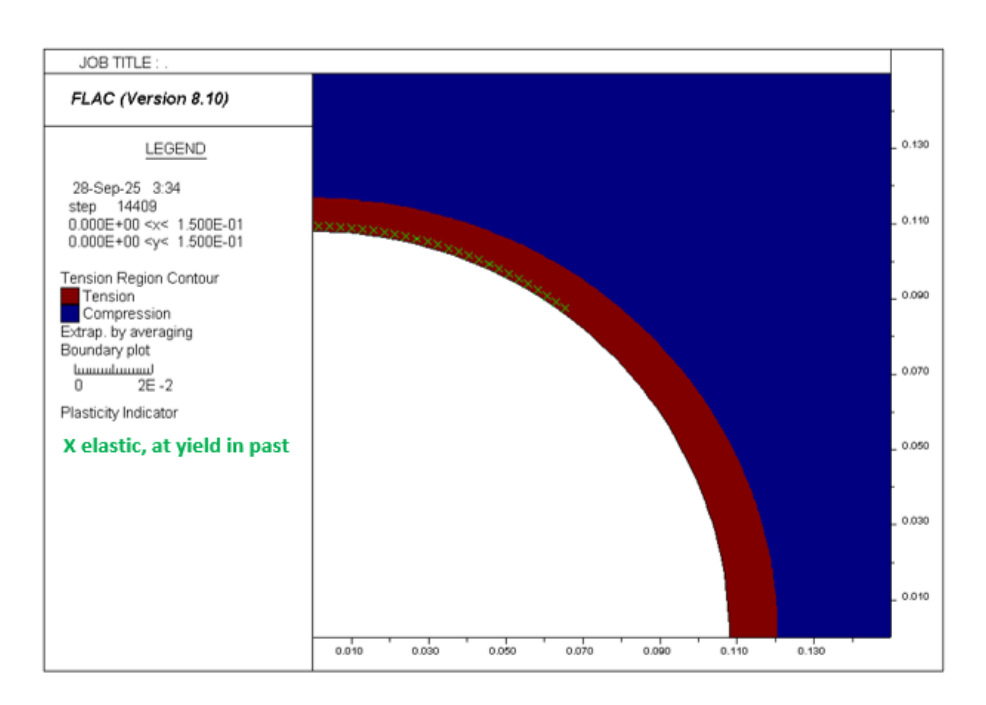


Figure 28 Tension/Compression Region (MC Drained Model), Pw=16MPa

By decreasing the wellbore pressure to 16.0 MPa, the o'r increases to -4.0 MPa. Table 4 shows that this change, which seems small, has an effect on stability. The rock's strength σ_{1s}' decreases to 44.67 MPa, while the maximum hoop stress rises to 53.0 MPa. The stability margin drops to -8.33 MPa, which means that the stress being applied is now stronger than the rock's ability to resist it. The numerical simulation result for this case on figure 28 confirms this prediction, showing the development of a small but distinct plastic zone, labelled by FLAC as "at yield in past" which represents a stable breakout. The term signifies that the rock within this zone has failed, deformed plastically, and redistributed its excess stress to the surrounding rock mass, reaching a new, stable equilibrium. The failure is contained and is not propagating uncontrollably.

Case C (Pw = 15 MPa)

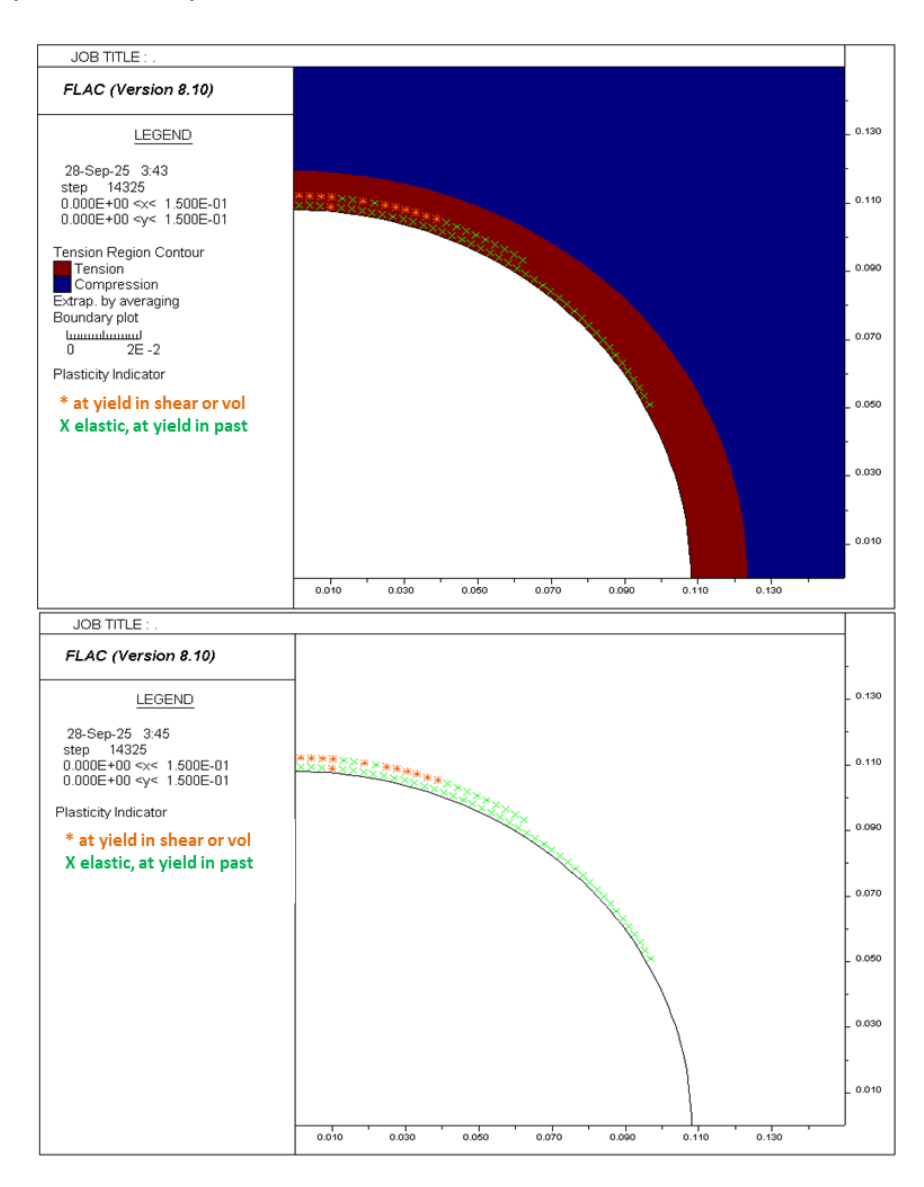


Figure 29 Tension/Compression Region (MC Drained Model), Pw=15MPa

Lowering the wellbore pressure even more, to 15.0 MPa, makes the instability worse and puts the well in a bad underbalance state. The effective radial stress becomes even more tensile at -5.0 MPa, but still below the tensile strength (σ_t) = 6.4 MPa, so it can be expected there is no tensile failure. However, as detailed in Table 4, the rock's shear strength drops to only 39.74 MPa, while the hoop stress increases to 54.0 MPa. This creates a large negative stability margin of -14.26 MPa, predicting shear failure.

Figure 29 shows the FLAC simulation, which graphically proves that this failure by showing a plastic zone that is bigger and deeper than in the previous case. This plastic zone has two different states that show how the failure process works. The outer boundary is made up of elements "at yield in shear or vol" (*), which show the active failure front where stable rock is being pushed to its limit. The majority of the zone behind this front is made up of "elastic, at yield in past" (X) elements, which are pieces of rock that have already failed and settled into a new equilibrium.

4.2.2. Mohr-Coulomb Model: Undrained Condition

This section investigates the immediate, short-term stability of the wellbore by integrating the Mohr-Coulomb failure criterion with the undrained pore pressure response. As established in the elastic analysis (Section 4.1.3), the act of drilling induces immediate, non-uniform changes in the near wellbore pore pressure. The increased pore pressure at the azimuth of $(\theta=90\circ)$ will weaken the rock mass by reducing the effective stress, thereby lowering its intrinsic shear strength and making the wellbore more susceptible to compressive failure.

This section follows the methodology established in Section 4.2.1 but incorporates the critical effect of induced pore pressure. To test this, the sensitivity analysis started with a wellbore pressure of 17.5 MPa, which was found to be a stable condition in the drained analysis. However, it was quickly observed that this pressure was insufficient to maintain stability under the more critical short term undrained conditions, resulting failure. This discovery led to the analysis moving forward by gradually raising the wellbore pressure, first to 18.0 MPa and then to 19.0 MPa to identify the new, higher critical pressure at which the wellbore first achieves stability in the undrained state. The stability analysis is performed by comparing the maximum effective hoop stress with the rock's shear strength at the critical azimuth of θ =90°

also by comparing the effective radial stress with the tensile strength. The shear strength is calculated using the Mohr-Coulomb criterion, but now the confining stress and the resulting pore pressure are specific to the undrained response at each level of wellbore pressure (Pw).

Table 5 below summarize the calculation of the sensitivity analysis by varying the well pressure (Pw). In this section we also analyse when drilling condition is slightly overbalanced (Pw > Pp), to see if by using Pw=21MPa really gives full overbalanced condition or not based on the numerical simulation.

Table 5 Wellbore Stress Distribution and Stability Analysis for Different Scenarios MC Undrained Model

Case	Pw (MPa)	σ'r (θ=90°) (MPa)	σ'r (θ=0°) (MPa)	σ'θ (θ=90°) (MPa)	σ'θ (θ=0°) (MPa)	(σ'1s) (MPa)	(σ'1s) - Max Hoop Stress (MPa)
Α	17.50	-4.29	-0.40	46.42	33.46	43.25	-3.16
В	18.00	-4.08	0.10	47.48	32.97	44.26	-3.22
С	19.00	-3.28	1.10	47.62	31.98	48.20	0.58
D	21.00	-1.27	3.11	45.64	30.00	58.10	12.46

> Case A (Pw = 17.5 MPa)

At a wellbore pressure of 17.5 MPa, which was perfectly stable in the drained analysis, the wellbore experiences significant failure under undrained conditions. The increase pore pressure is increased from 20MPa in drained condition to 21.79 MPa. Table 5 also shows that the effective maximum hoop stress, 46.42MPa is higher than the rock strength of 43.25MPa. We can see from figure 30, there is a development of plastic zone which some of zones were yield in past but now is stable (stable breakout), but some of the zone are active failure which the rock is currently yielding.

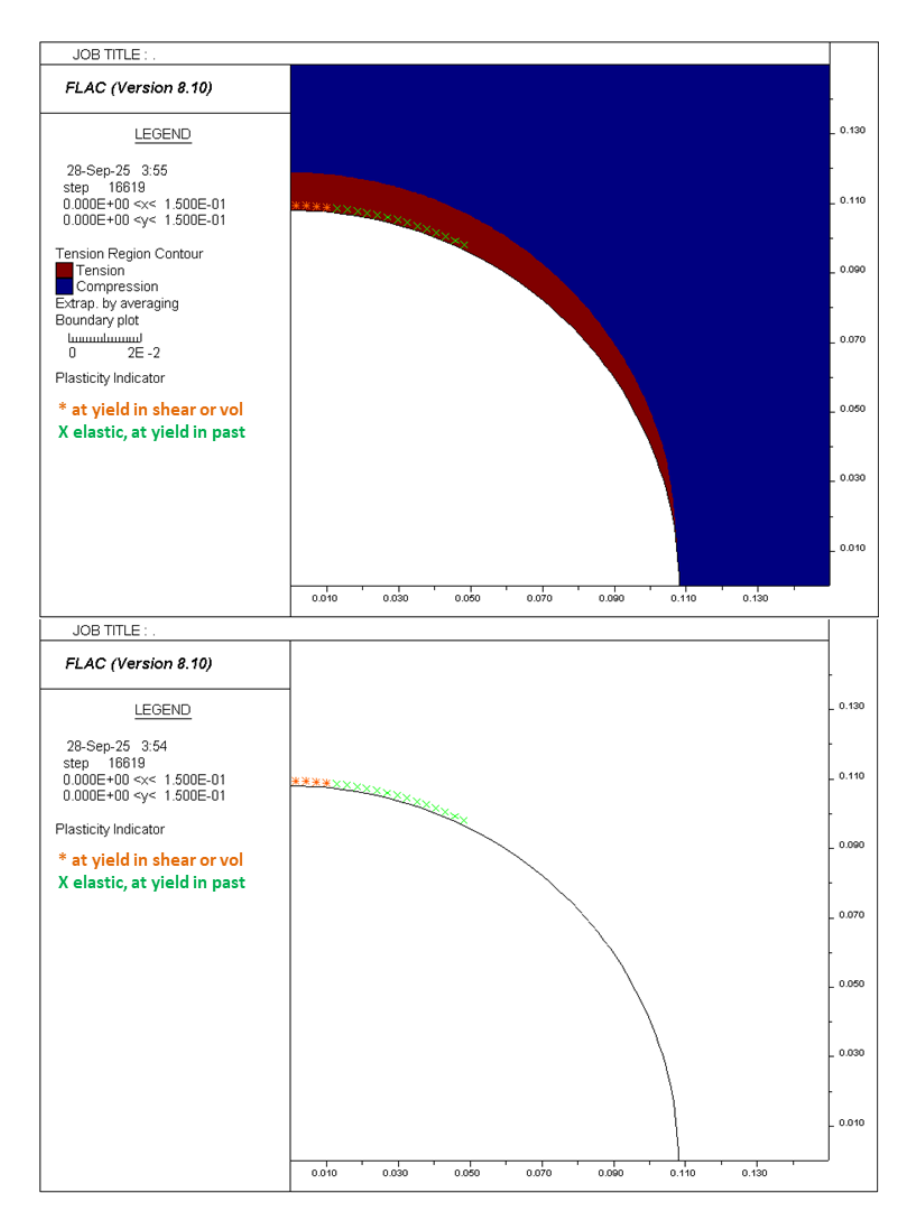


Figure 30 Tension/Compression Region (MC Undrained Model), Pw=17.5MPa

> Case B (Pw = 18 MPa)

Observing the shear failure at 17.5 MPa, the wellbore pressure then was increased to 18.0 MPa in the next simulation to search for a stable condition. This decreased the negative stability margin to -3.22 MPa, indicating that the applied stress still exceeds the rock's strength. The numerical simulation for this case in figure 31 confirms this still showing both distinct plastic zone localized near the azimuth corresponding to θ =90°.

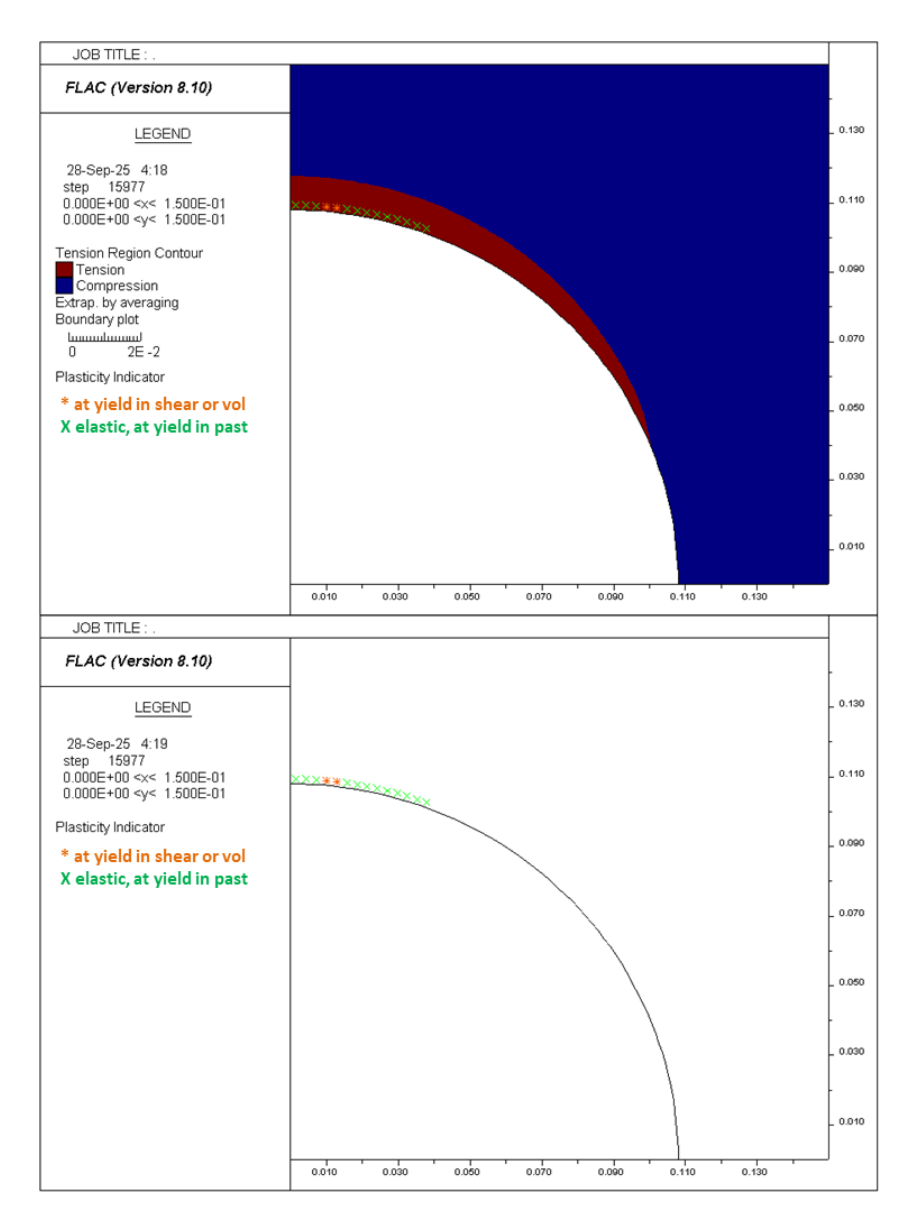


Figure 31 Tension/Compression Region (MC Undrained Model), Pw=18MPa

> Case C (Pw = 19 MPa)

With failure still predicted at 18.0 MPa, the wellbore pressure was increased further to 19.0 MPa. The analytical check in Table 5 now predicts a marginal but positive stability margin of +0.58 MPa, suggesting the wellbore now is stable. The FLAC simulation result for this case, shown in Figure 31, validates this prediction. The plot shows a complete absence of plasticity indicators around the wellbore circumference, confirming that the rock mass remains entirely within its elastic domain. This numerical result provides a perfect validation of the analytical prediction. A wellbore pressure of 19.0 MPa represents the minimum pressure required to maintain wellbore stability under undrained conditions.

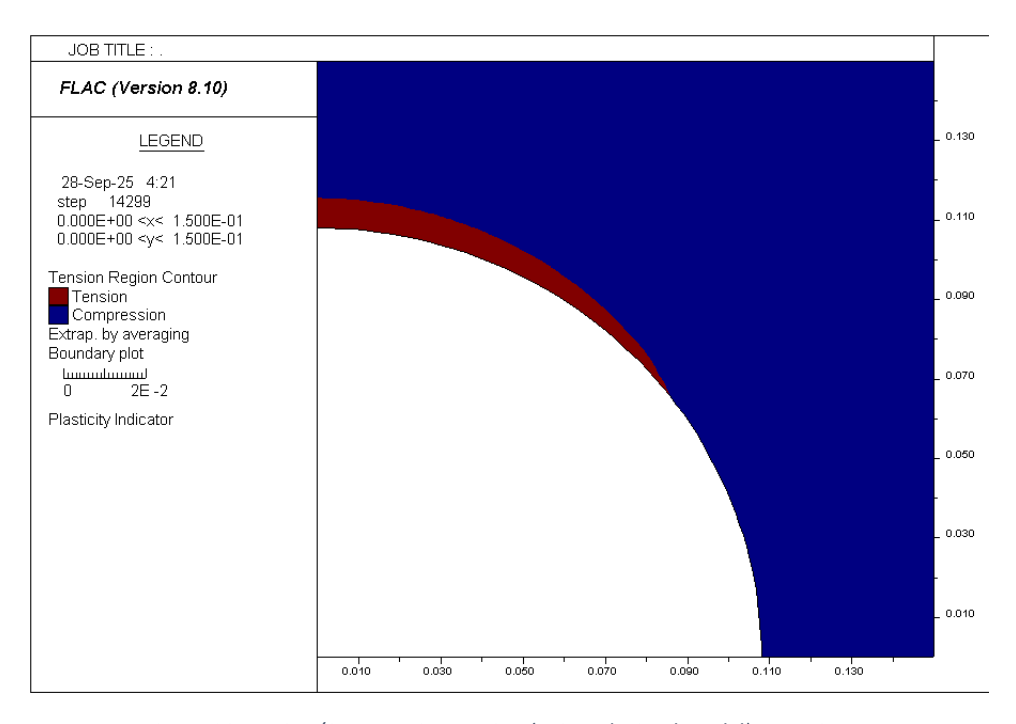


Figure 32 Tension/Compression Region (MC Undrained Model), Pw=19MPa

A direct comparison of the stability thresholds established in the drained (Section 4.2.1) and undrained analyses demonstrates the significant influence of transient pore pressure effects on wellbore stability. The critical finding is a significant shift in the stability threshold. The drained analysis established that the wellbore was stable at Pw=17.5 MPa with failure initiating only when the pressure was lowered to below 17.5 MPa. The undrained analysis, on the other hand, shows that the wellbore is stable only when Pw is 19MPa or higher. The minimum required wellbore pressure to ensure stability is therefore substantially higher in the undrained state (19.0 MPa) than in drained state (~17.5 MPa). This proves that the wellbore is demonstrably weaker and more prone to collapse immediately after drilling.

Case D (Pw = 21 MPa)

Another simulation was run with Pw=21MPa, respresenting a conventional overbalanced drilling condition where the wellbore pressure is greater than the pore pressure (Pp) = 20MPa. From table 5, it can be seen that the pore pressure increases from 20MPa to 22.27 MPa at θ =90°. This means that while the well is intended to be overbalanced, instead, it is locally underbalanced condition because now the effective radial stress at θ =90° becomes negative (-1.27MPa). The FLAC simulation, shown in Figure 33, visually confirms this analytical result, displaying a distinct tensile region localized at the azimuths aligned with the minimum horizontal stress. This phenomenon proves that simply maintaining a mud pressure above the

formation pressure does not guarantee a compressive stress state at the wellbore wall in undrained condition.

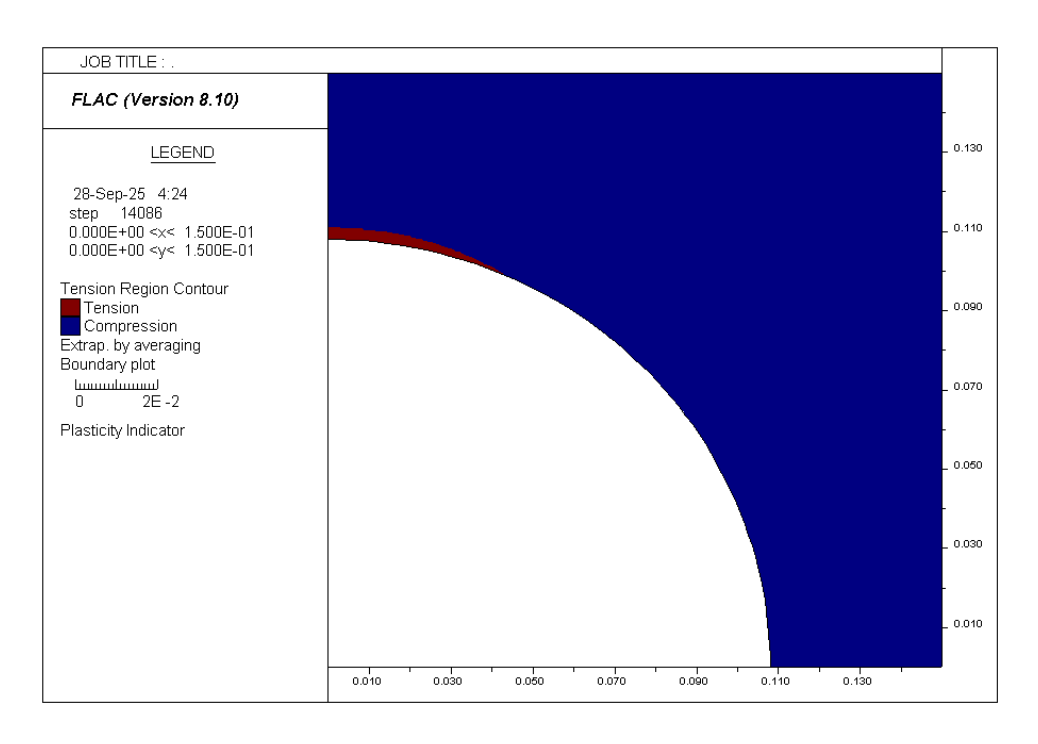


Figure 33 Tension/Compression Region (MC Undrained Model), Pw=21MPa

Changing the tensile strength cut-off

As mentioned before in section 2.1.2. Model 2: Mohr-Coulomb Criterion, it is important to mention that the estimation of rock tensile strength as 10% of the uniaxial compressive strength only gives a rough estimation. Figure 8 (distribution of the compressive to tensile strength ratio in sandstone) shows that this ratio varies. Thus, to analyse the effect of different tensile strength estimation, the result below was obtained by changing the ratio to $(\frac{\sigma_c}{\sigma_r}) = 22$, with Pw of 17.5MPa

$$\sigma_t = \frac{1}{22} \ \sigma_c = \frac{1}{22} * 64MPa = 2.91MPa$$

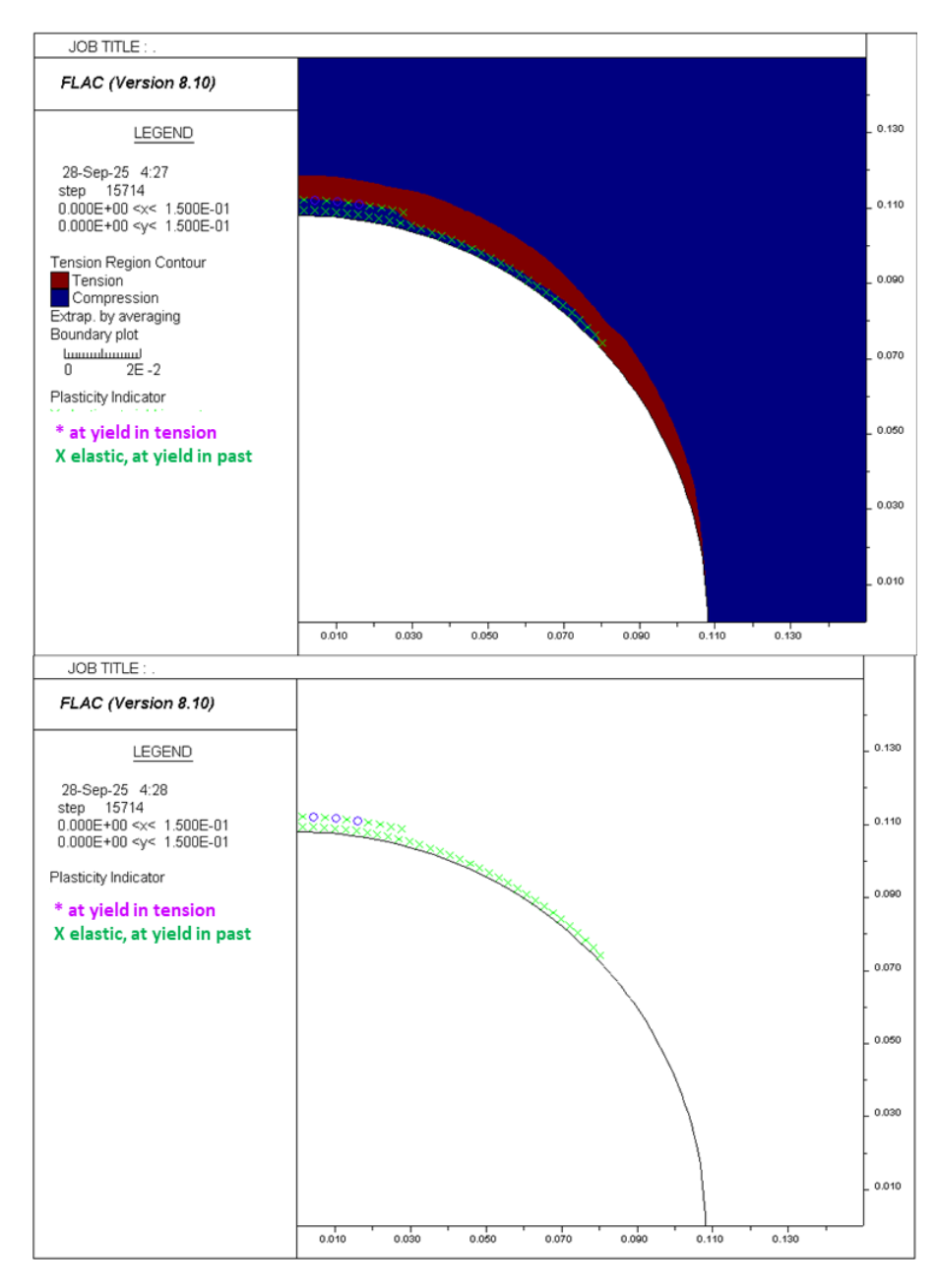


Figure 34 Tension/Compression Region (MC Undrained Model), Pw=17.5MPa, $\sigma_t=2.91$ MPa

Comparing the result in Figure 34 to the simulation in Figure 30 reveals a critical shift in the predicted failure mechanism. By lowering the tensile strength, σ t = 2.91MPa, the model now shows some points indicate yield in tension. This occurs because the effective radial stress at the wellbore wall, which is σ 'r =-4.29 MPa now exceeds the rock's reduced tensile strength. This results highlights a limitation of the Mohr-Coulomb model that the model has high sensitivity to the tensile strength cut-off, which is often an uncertain parameter based on rough estimations. An inaccurate assumption can lead to a completely incorrect diagnosis of the failure type.

4.3. Wellbore Stability Analysis with Hoek-Brown Model

This section presents the analysis of the empirically derived, non-linear Generalized Hoek-Brown (HB) model. As established in Chapter 2, The H&B model was selected for its non-linear envelope, which is generally considered an improvement over the linear M-C criterion. However, its predictions in this UBD scenario, where the effective radial stresses are tensile, it must be interpreted with caution. According to Cai (Cai, M., 2010), the H&B model performs well for strong rock at high confining pressures, it is less accurate in low confining pressure and tension zones, which are characteristic of underbalanced drilling, which could impact the accuracy of the predicted failure mechanism. Therefore, the lower strength forecasted by the H&B model is regarded as a conservative estimate, although its exact precision is depends upon the model's intrinsic limitations.

The H-B parameters used in the simulation, corresponding to different GSI values for the sandstone formation, from the excellent quality rock mass (GSI=100) and a slightly lower, good quality rock mass (GSI=96), are detailed in Table 6. From the equation 2.8 to equation 2.13, it can be observed that the parameters mb, s, and a are not independent material constants but are derived from fundamental rock properties. For this study, D is assumed to be 0, representing an undisturbed rock mass post drilling. The Generalized Hoek-Brown criterion is defined by the relationship between the major (σ'_1 and minor σ'_3) effective principal stresses at failure: $(\sigma'_1 - \sigma'_3) = (mb\sigma_c\sigma'_3 + s\sigma_c^2)^a$

From table 6 we can see that as the GSI decreases from 100 to 96, the parameters s, mb, and the tensile strength also decrease, resulting a reduction in the overall strength.

HB Parameter	Case A (GSI = 100)	Case B (GSI = 96)	Unit
mi	21.00	21.00	
S	1.00	0.64	
mb	21.00	18.20	-
a	0.50	0.50	-
σ_c	64.00	64.00	MPa
σ.	3.04	2 25	MPa

Table 6 HB Parameters for Each GSI

4.3.1. Hoek-Brown Model: Drained Condition

The initial investigation focuses on an excellent quality rock mass (GSI=100), representing an upper-bound strength scenario. A systematic, quantitative evaluation of wellbore stability is performed by incrementally reducing the wellbore pressure (Pw) from 17.5 MPa up to 19 MPa, thereby reducing the the underbalance state.

> Case A (GSI=100)

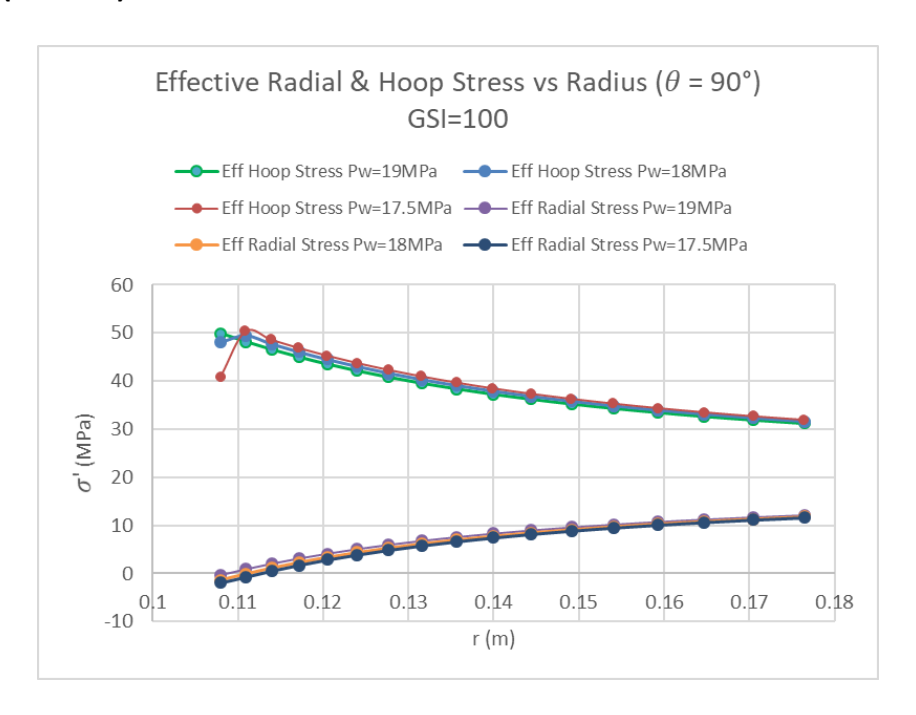


Figure 35 Eff. Hoop and Eff. Radial Stresses at $\theta = 90^{\circ}$ HB Model Drained ConditionGSI=100

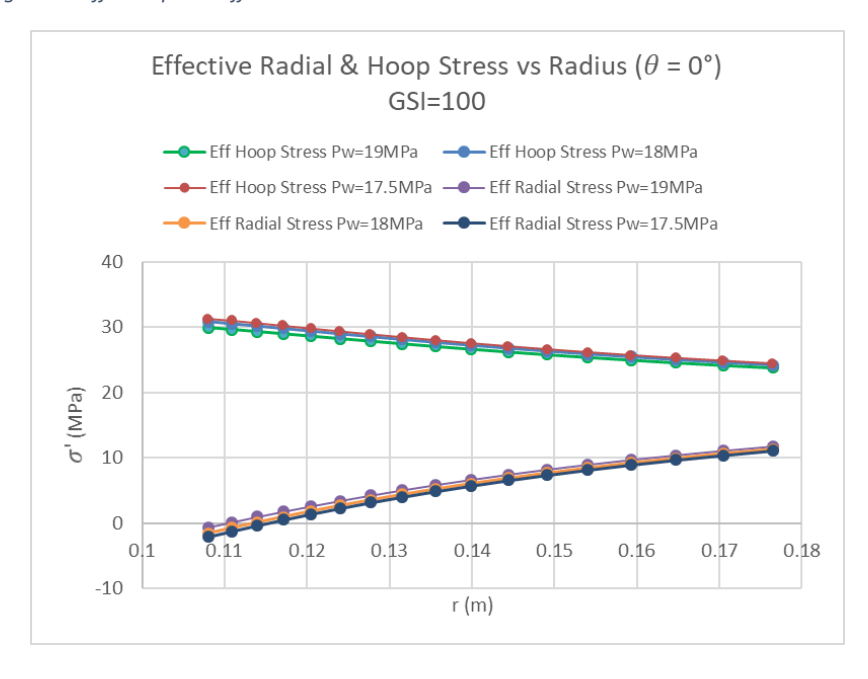


Figure 36 Eff. Hoop and Eff. Radial Stresses at $\theta=0^\circ$ HB Model Drained Condition, GSI=100

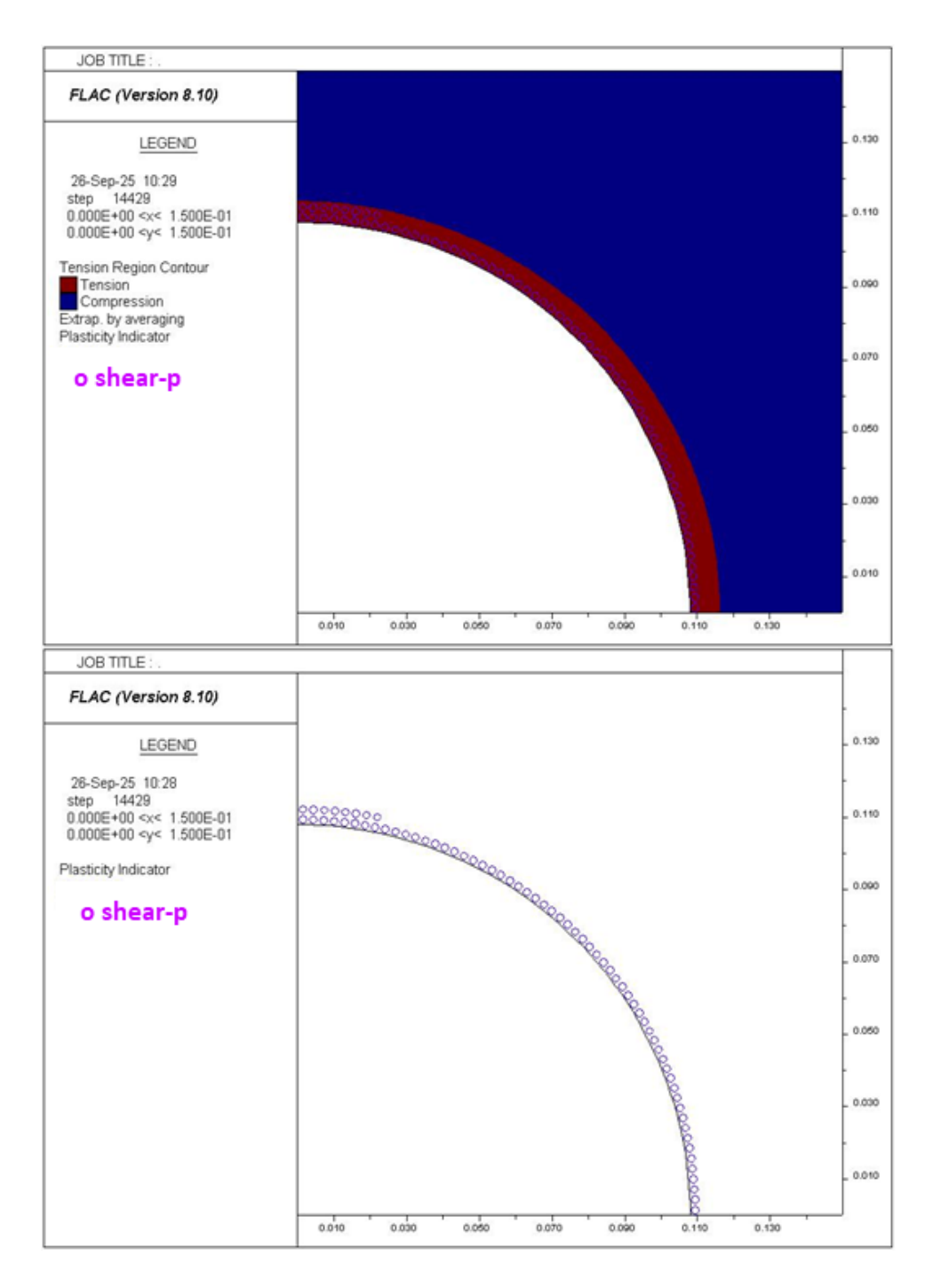


Figure 37 Tension/Compression Region (HB Drained Model) Pw=17.5MPa, GSI=100MPa

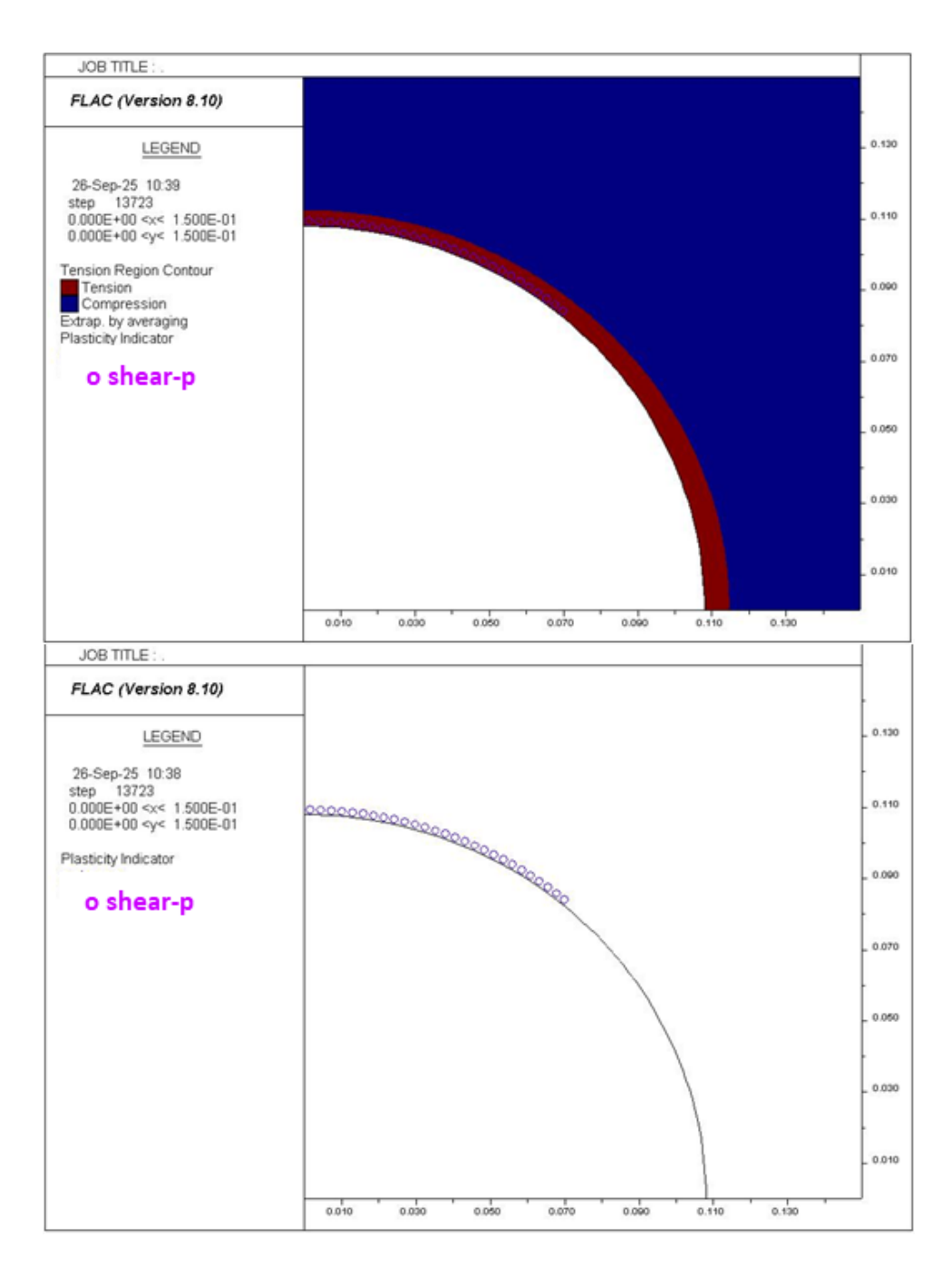


Figure 38 Tension/Compression Region (HB Drained Model) Pw=18MPa, GSI=100MPa

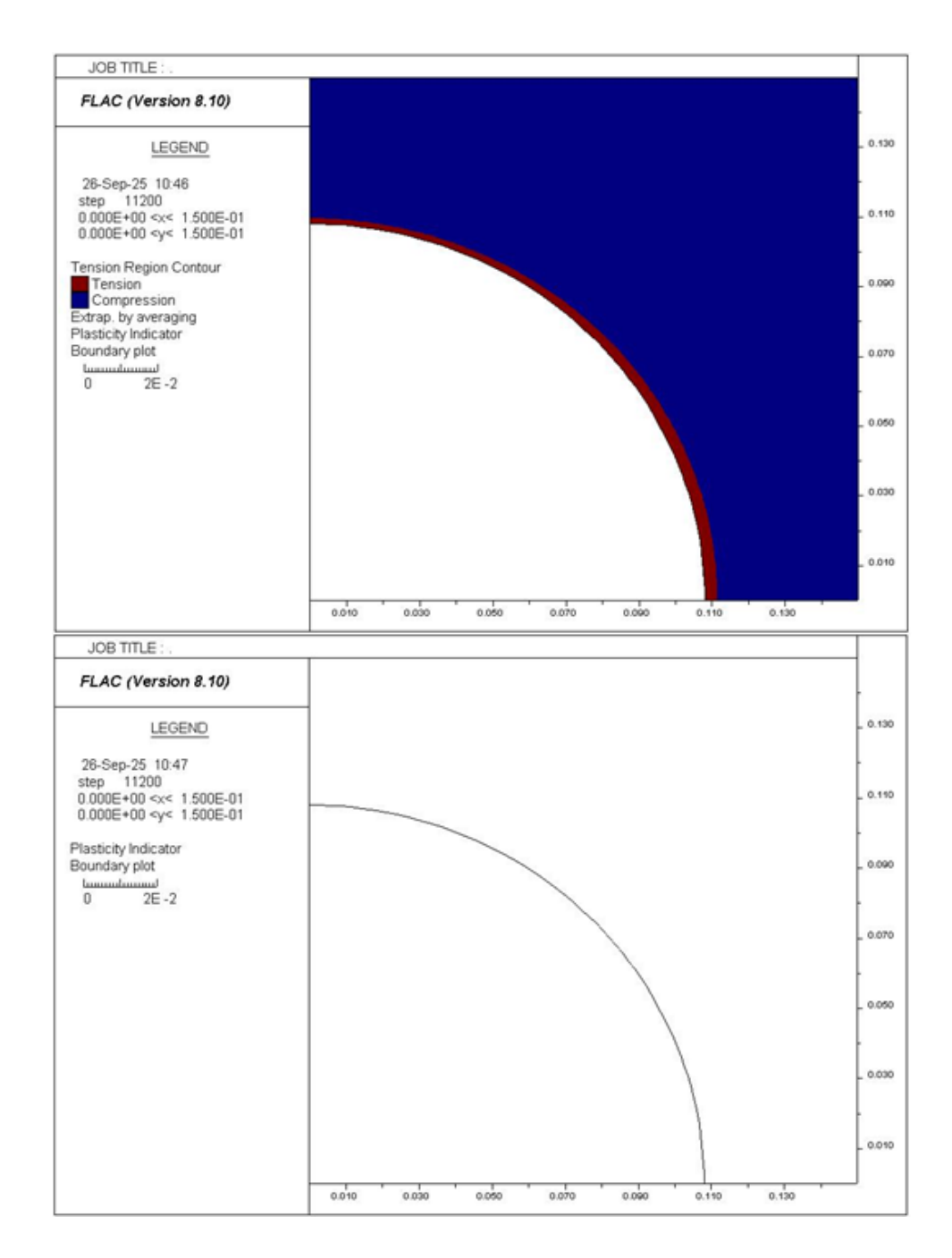


Figure 39 Tension/Compression Region (HB Drained Model) Pw=19MPa, GSI=100MPa

By applying the equation 2.12, the rock strength with HB criterion was obtained equals to 24.6MPa which is much lower compare to the rock strength calculated with MC model (52MPa). This is because the two models use fundamentally different failure envelopes to define rock strength. The Mohr-Coulomb model uses a linear failure envelope, which could make the rock strength seem stronger than it really is at the very low (and in this case, tensile) confining pressure found at the wellbore wall. The Hoek-Brown model, on the other hand, uses a non-linear (curved) envelope. However, it must be noted that its application to the UBD scenario places the analysis in a low confining pressure and tension zone, a regime where

the model's accuracy has been questioned (Cai, M., 2010). With Pw=17MPa, in figure 35 the effective hoop stress at $\theta=90^\circ$ which obtained from FLAC is ~41MPa which is higher than the rock strength (24.6MPa). Figure 37 shows that there is plasticity indicator 'o shear-p' signifies that the rock has yielded in the past and has now reached a new, stable equilibrium. This represents a stable breakout. While failure has occurred, it is contained and not actively propagating. Compare to MC model drained condition in figure 27, it was not observed any yield in past.

As the wellbore pressure is increased to 18 MPa and 19 MPa, the simulation in figure 36 and figure 37 show that the breakout zone diminishing and then disappearing entirely. The wellbore is confirmed to be fully stable at Pw=19.

> Case B (GSI=96)

By reducing the GSI to 96, the rock mass is weakened. Critically, the tensile strength now drops to 2.25MPa.

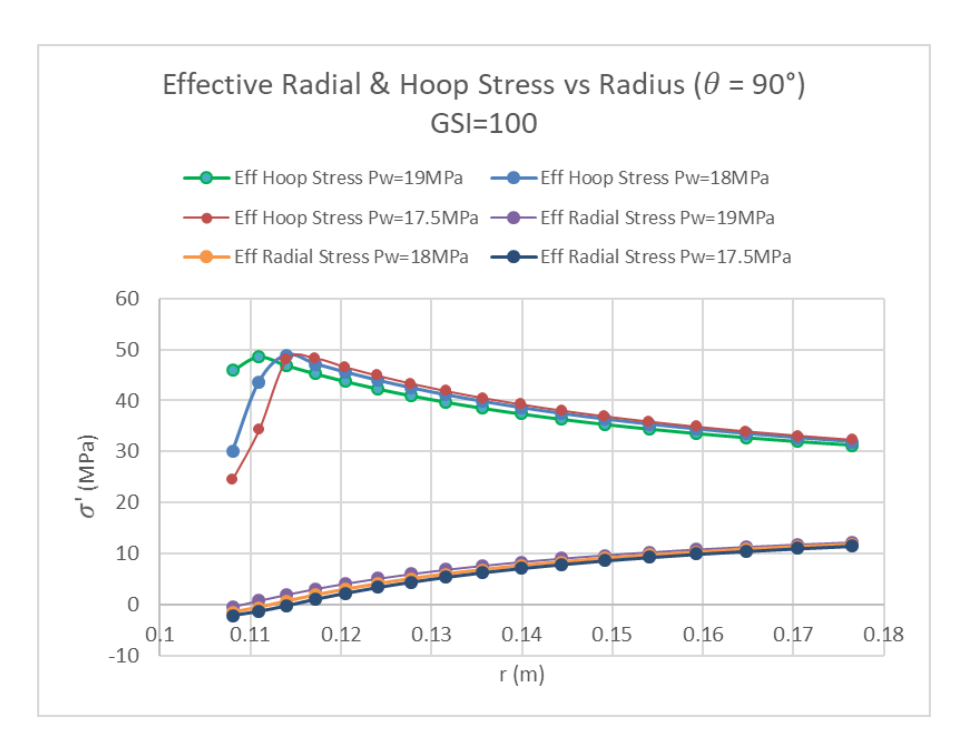


Figure 40 Eff. Hoop and Eff. Radial Stresses at $\theta=90^\circ$ HB Model Drained Condition, GSI=96

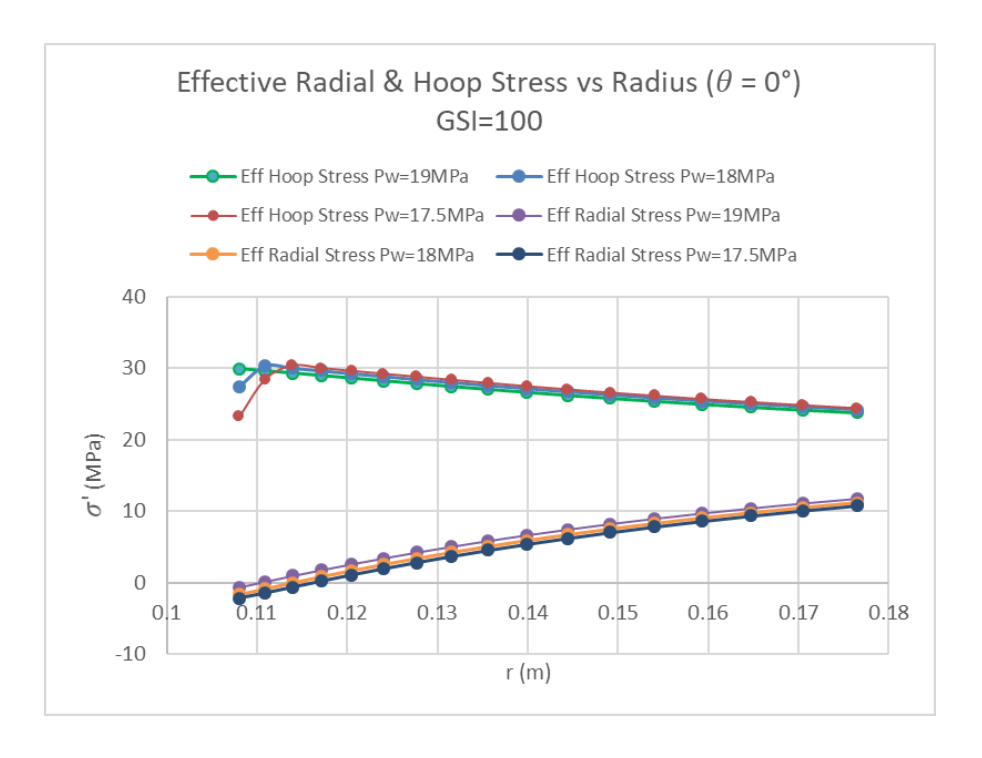


Figure 41 Eff. Hoop and Eff. Radial Stresses at $\theta=0^\circ$ HB Model Drained Condition, GSI=96

With Pw=17.5MPa, the effective radial stress, $\sigma'_r = Pw - PP = 17.5MPa - 20MPa = -2.5MPa$ now exceeds the tensile strength of rock GSI=96 which equals to 2.25MPa. As shown in figure 42, the plastic zone is significantly larger and deeper than that observed in the GSI=100 case. Critically, this figure also reveals the development of a mixed two different failure mechanism. In addition to the current shear failure in some points, it also shows indicators "tension-p" around the entire wellbore circumference. This implies that the rock has also yielded in tension in the past. This finding demonstrates that UBD in slightly weaker formations can create dual risk of both compressive breakouts and tensile fracturing originating at the wellbore wall.

Increasing the wellbore pressure to 18MPa provides additional support and, as expected, eliminates the tensile failure. This is because the magnitude of the effective radial stress (-2MPa) is higher than then tensile strength. However, in figure 43 still shows a plastic zone that, while smaller than the 17.5 MPa case, remains indicates current shear failure at some points with yield in past around the entire wellbore circumference. While in figure 44 by appling Pw=19MPa shows that the active shear failure indicators disappear, leaving only a small, contained zone of past yield.

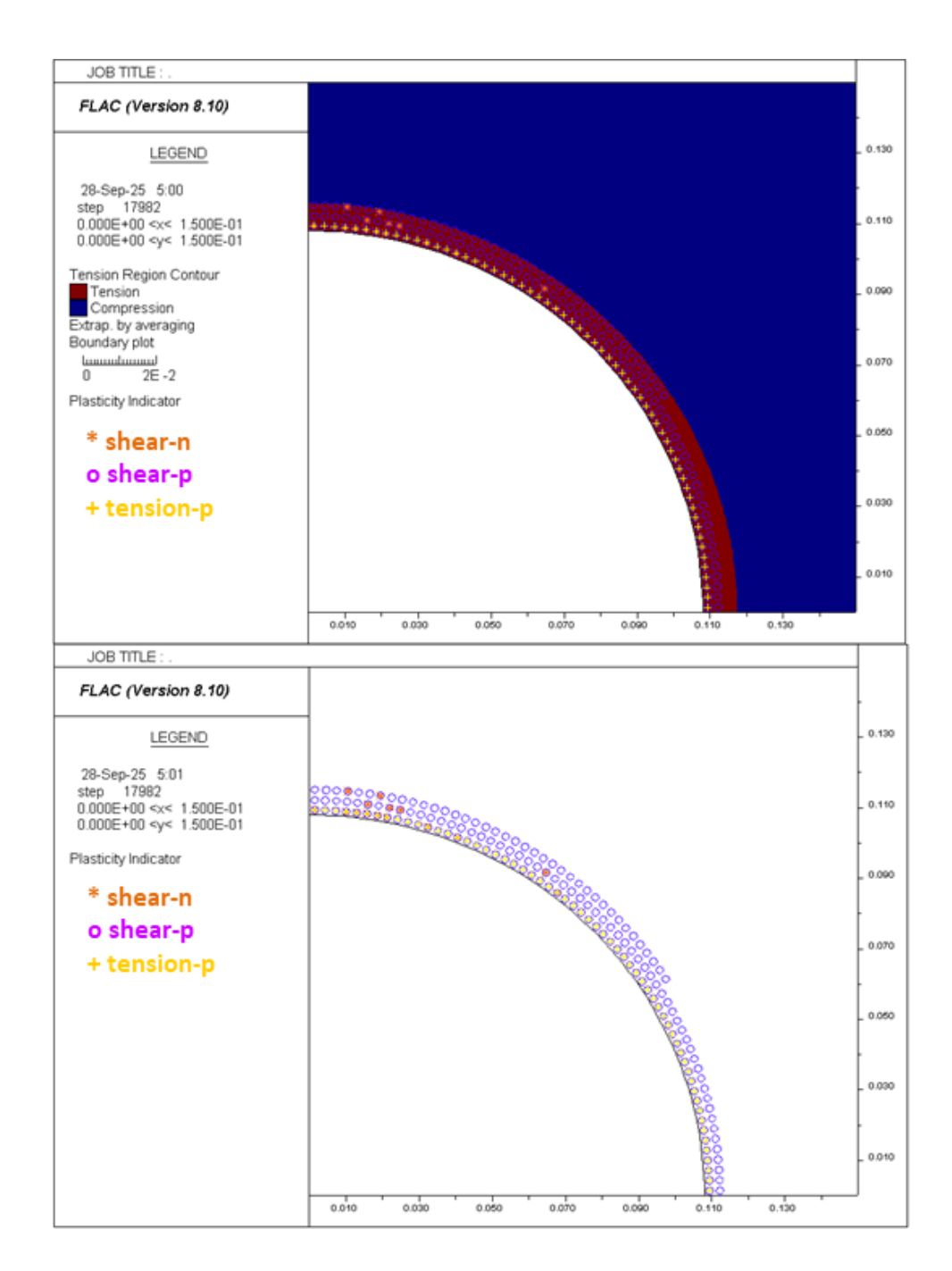


Figure 42 Tension/Compression Region (HB Drained Model) Pw=17.5MPa, GSI=96MPa

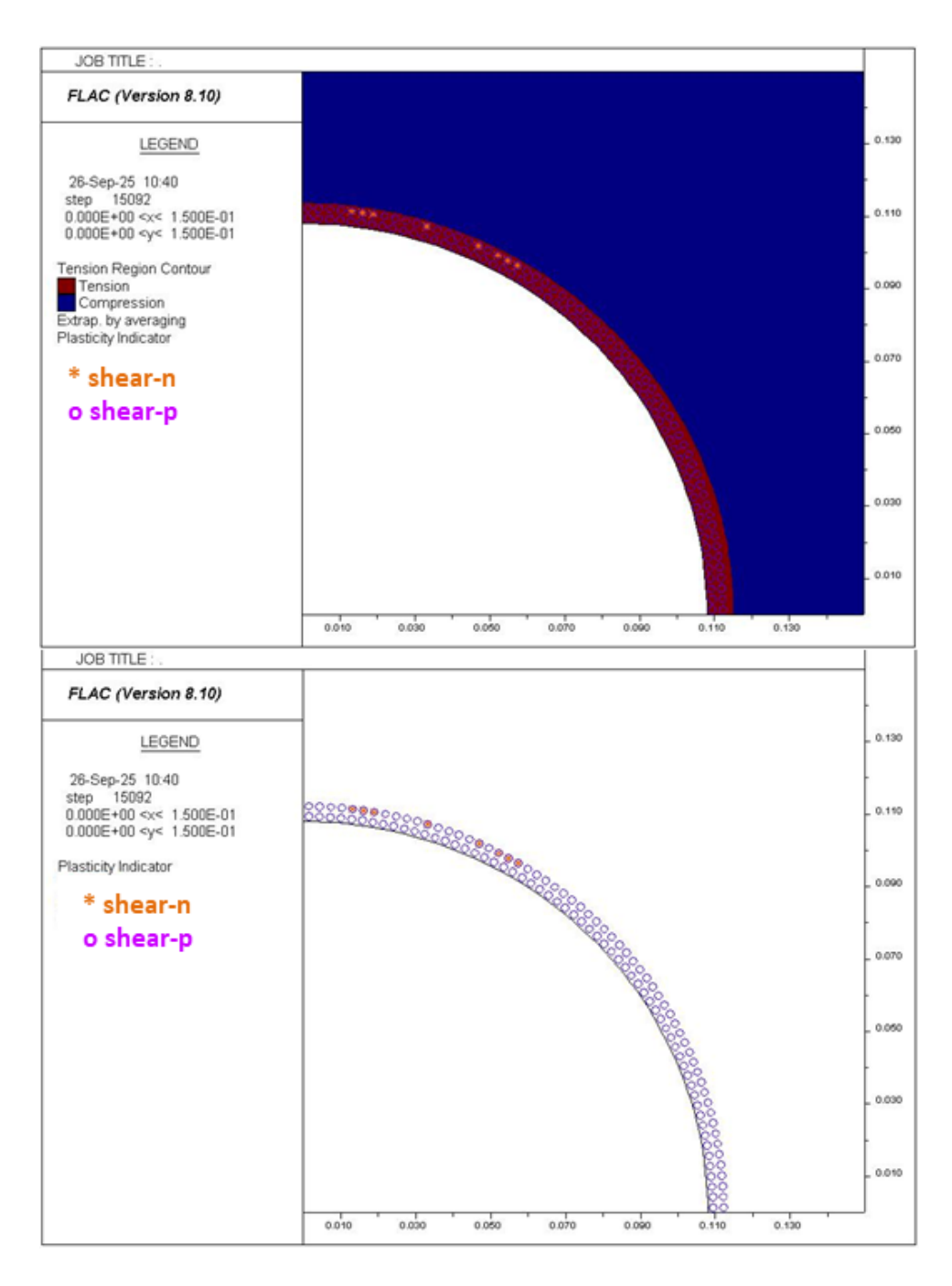


Figure 43 Tension/Compression Region (HB Drained Model) Pw=18MPa, GSI=96MPa

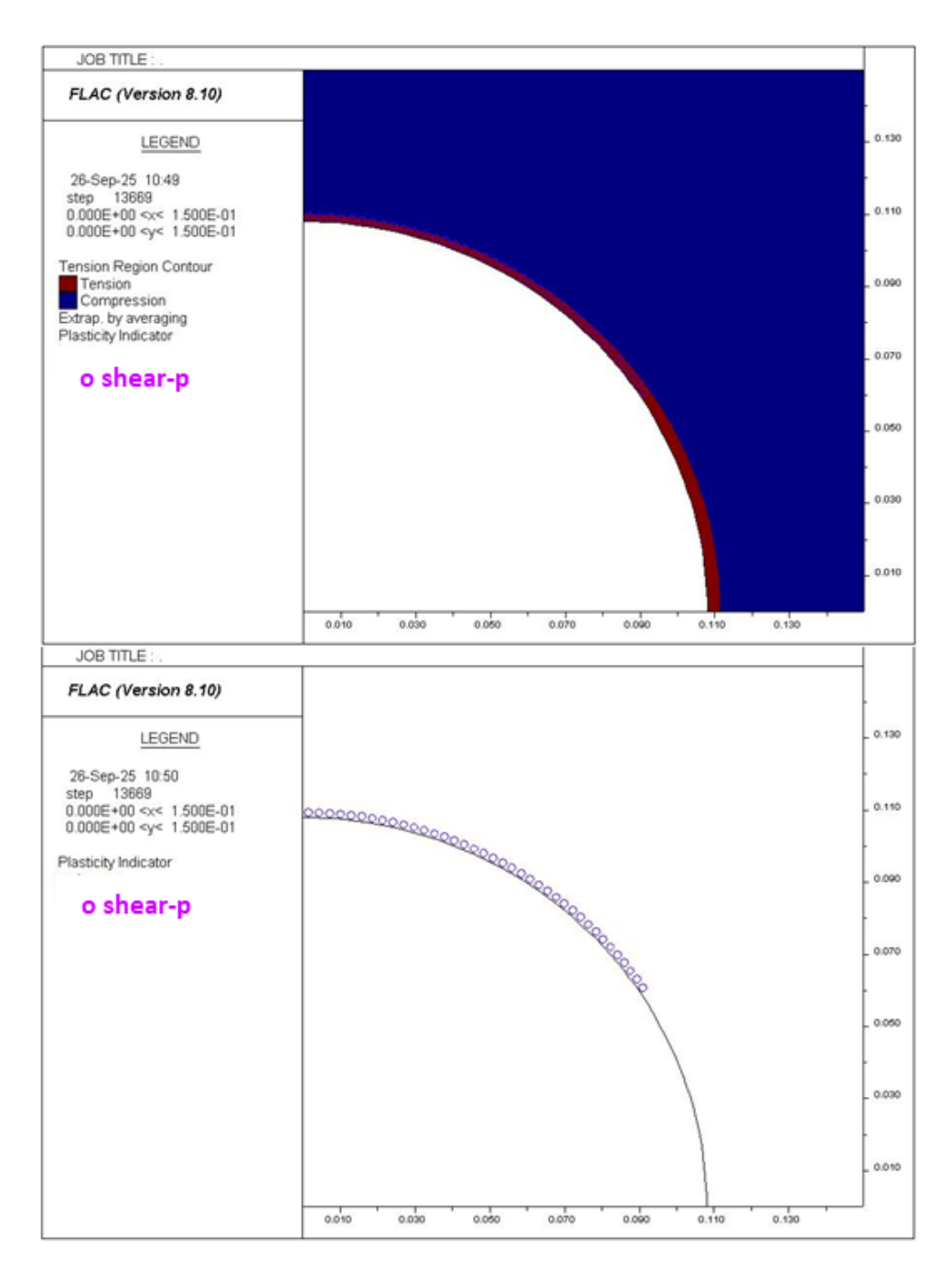


Figure 44 Tension/Compression Region (HB Drained Model) Pw=19MPa, GSI=96MPa

4.3.2. Hoek-Brown Model: Undrained Condition

This final section of the comparative analysis integrates the non-linear, empirically derived Hoek-Brown failure criterion in undrained condition. The methodology mirrors the previous sections, conducting a sensitivity analysis by varying the wellbore pressure for different rock mass qualities (GSI =100, 96).

Case A (GSI=100)

Comparing figure 45-46 with figure 35-36 in the drained condition, the simulation reveals the influence of induced pore pressures. At the critical azimuth for compressive failure, the undrained response leads to a significant increase in local pore pressure, resulting a reduction of effective hoop stress and at the same time also reduction of the effective radial stress which now make them are lower than in the drained case for any given wellbore pressure. This reduction in confinement is the primary mechanism that compromises the rock mass's strength. According to the Hoek-Brown criterion, the failure envelope is steepest at low confining stresse. So even with a small decrease in the confining pressure can still lead to a significant reduction in the rock's strength to withstand the applied hoop stress.

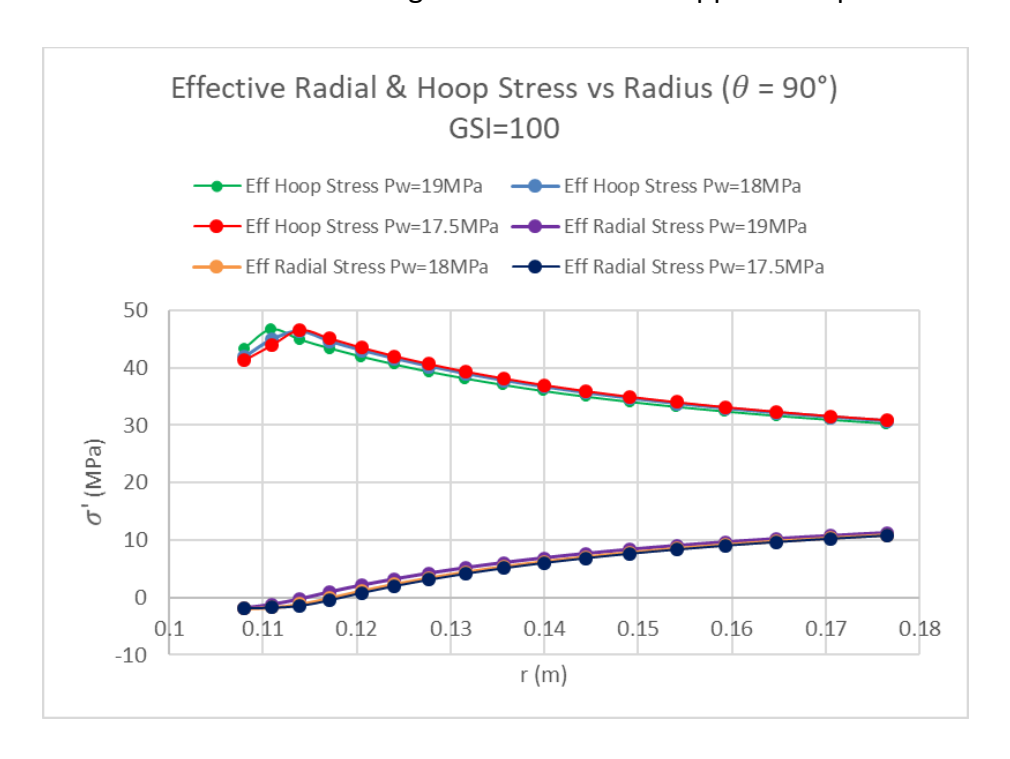


Figure 45 Eff. Hoop and Eff. Radial Stresses at $\theta=90^\circ$ HB Model Undrained Condition, GSI=100

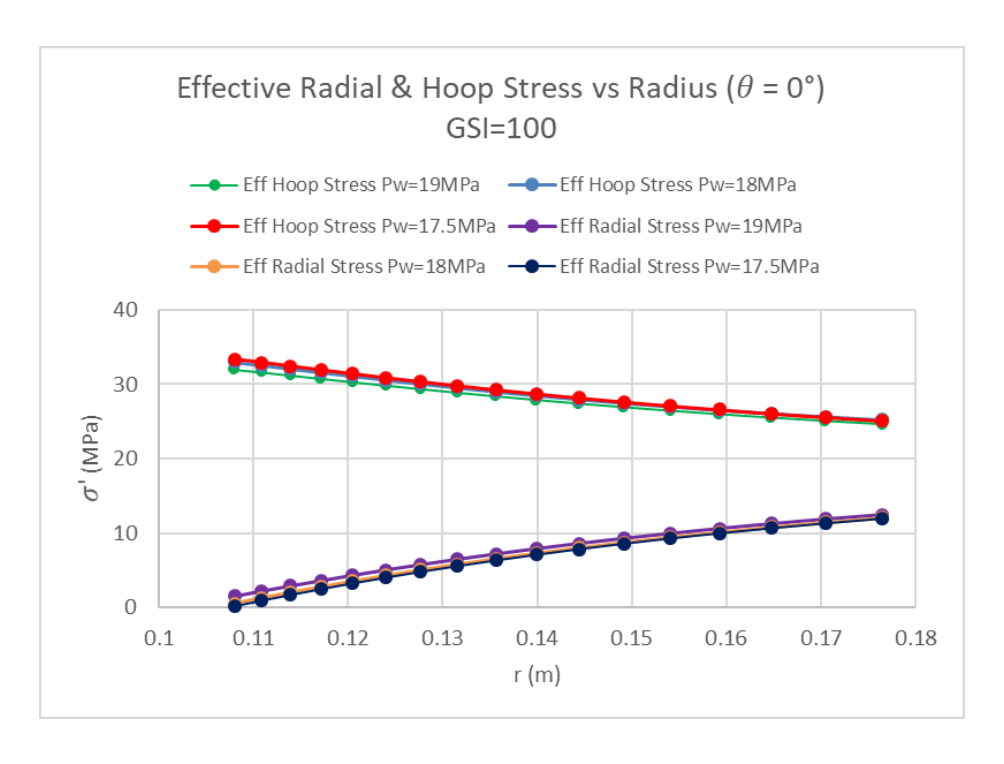


Figure 46 Eff. Hoop and Eff. Radial Stresses at $\theta=0^\circ$ HB Model Undrained Condition, GSI=100

For an excellent quality rock mass (GSI=100), the simulations demonstrate the significant weakening effect of undrained conditions. First, from all applied well pressure there is no indication of tensile failure. At wellbore pressure of Pw =17.5 MPa, a condition that was relatively stable in the drained analysis, the model now predicts active and propagating shear failure (Figure 47). The presence of active yield indicators ('shear-n') signifies that the failure is not contained. Increasing the pressure to Pw =18 MPa provides additional support to the wellbore wall, partially counteracting the high hoop stress. As a result, the size of the plastic zone is reduced, but this pressure is still insufficient to fully overcome the weakening effect of the undrained response (Figure 48). The continued presence of active failure indicators shows that the system is approaching, but has not yet reached, a stable equilibrium. A relatively stable state, which characterized by a small, contained breakout, is only achieved when the pressure is increased 19 MPa (Figure 49).

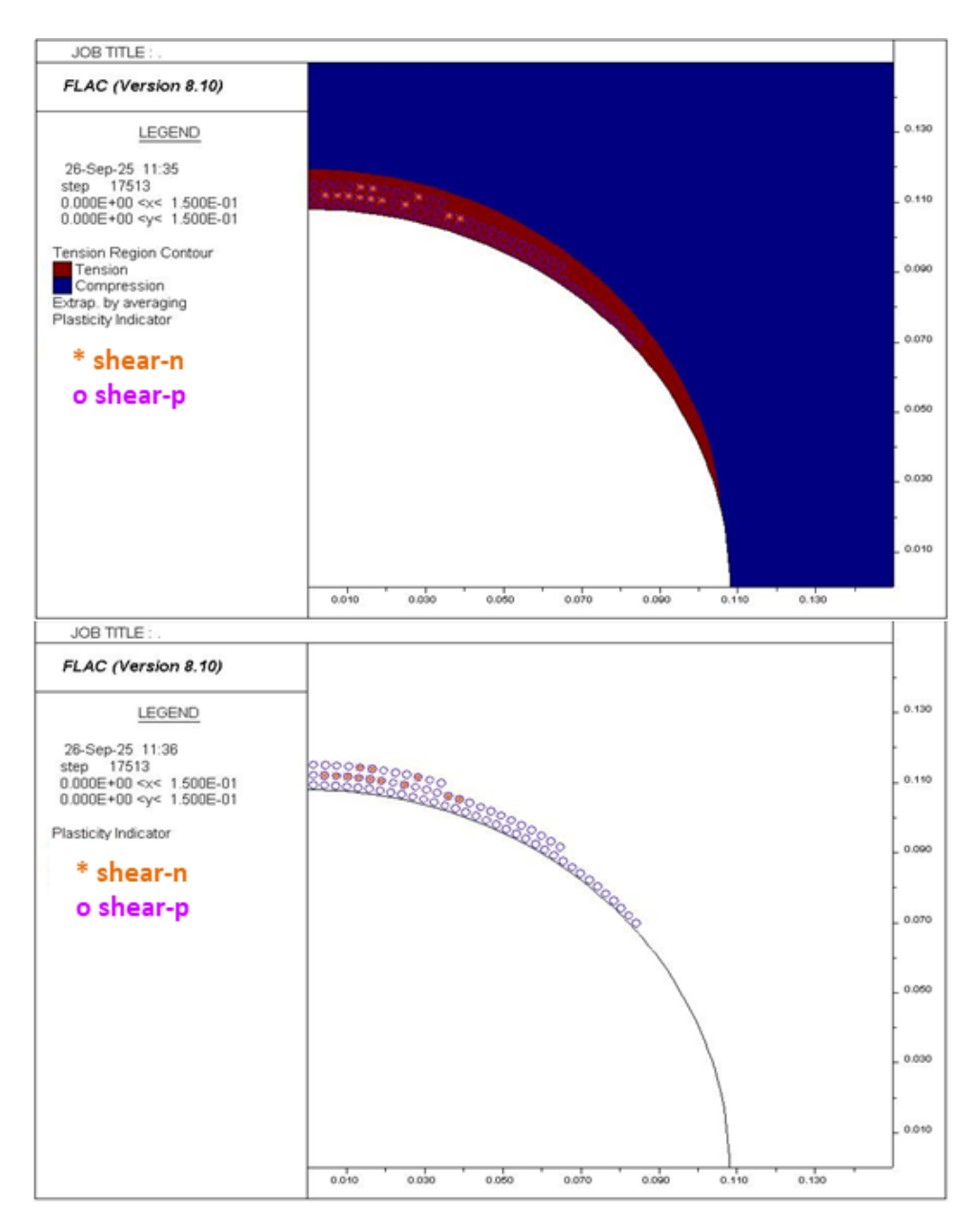


Figure 47 Tension/Compression Region (HB Undrained Model) Pw=17.5MPa, GSI=100MPa

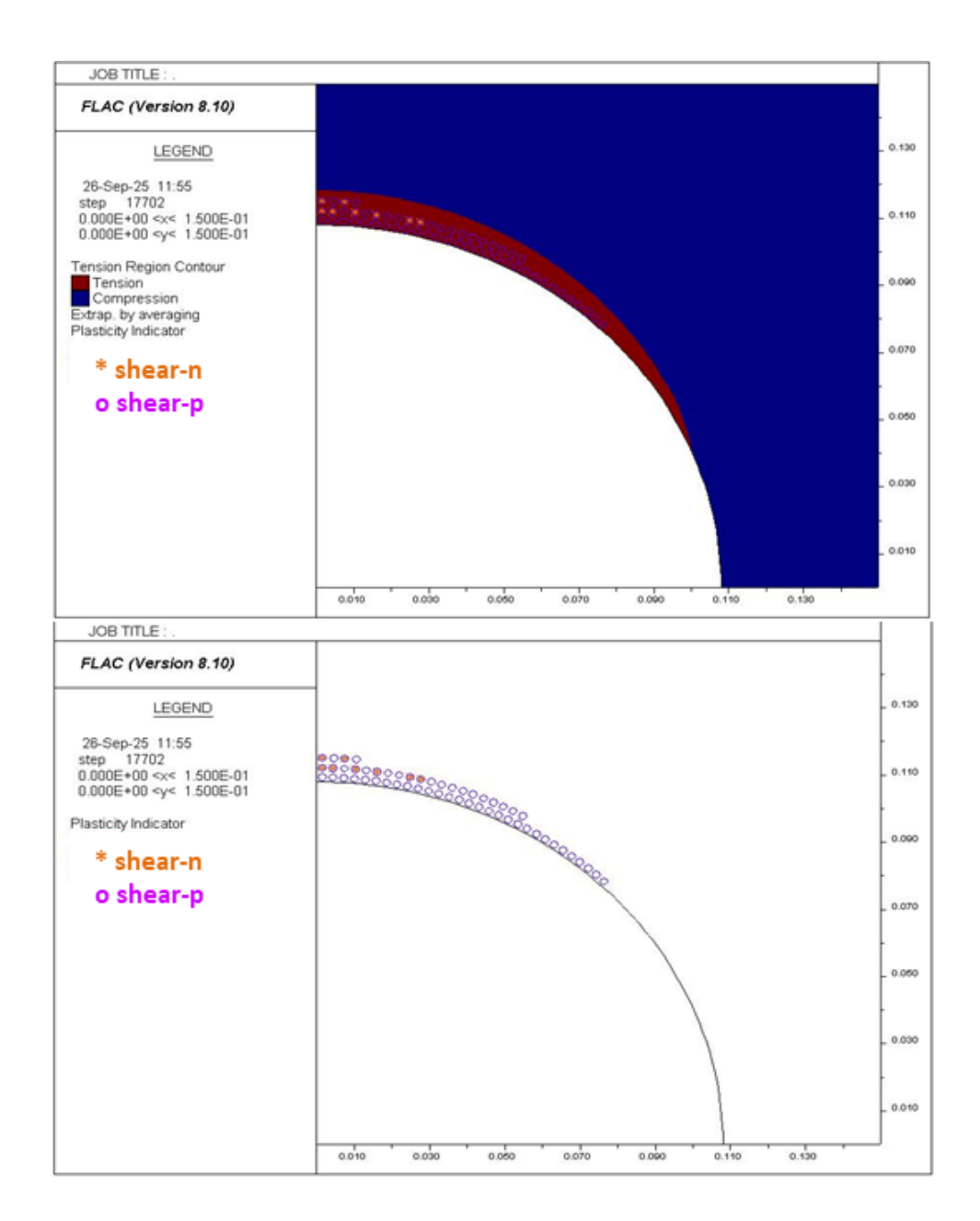


Figure 48 Tension/Compression Region (HB Undrained Model) Pw=18MPa, GSI=100MPa

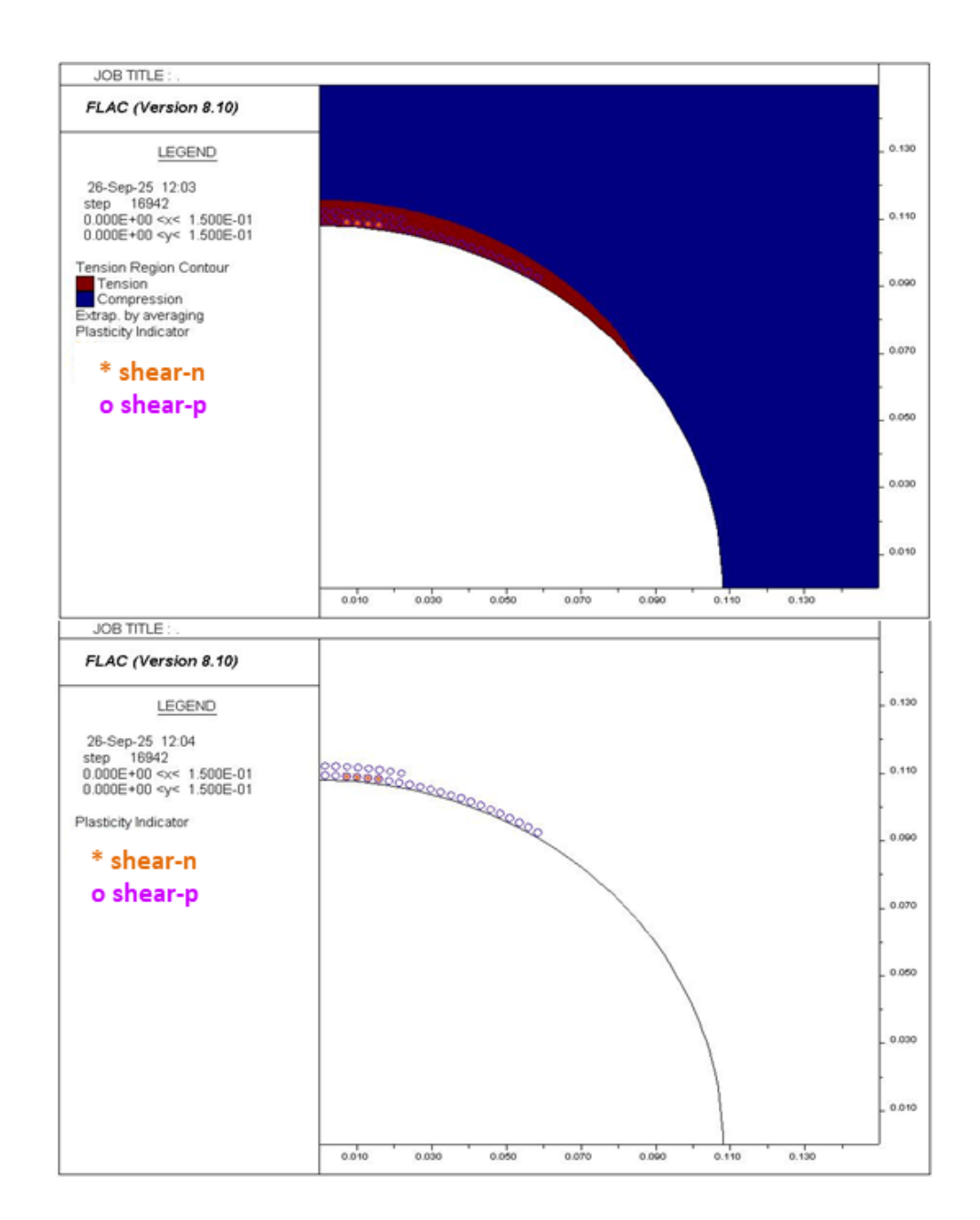


Figure 49 Tension/Compression Region (HB Undrained Model) Pw=19MPa, GSI=100MPa

> Case B (GSI=96)

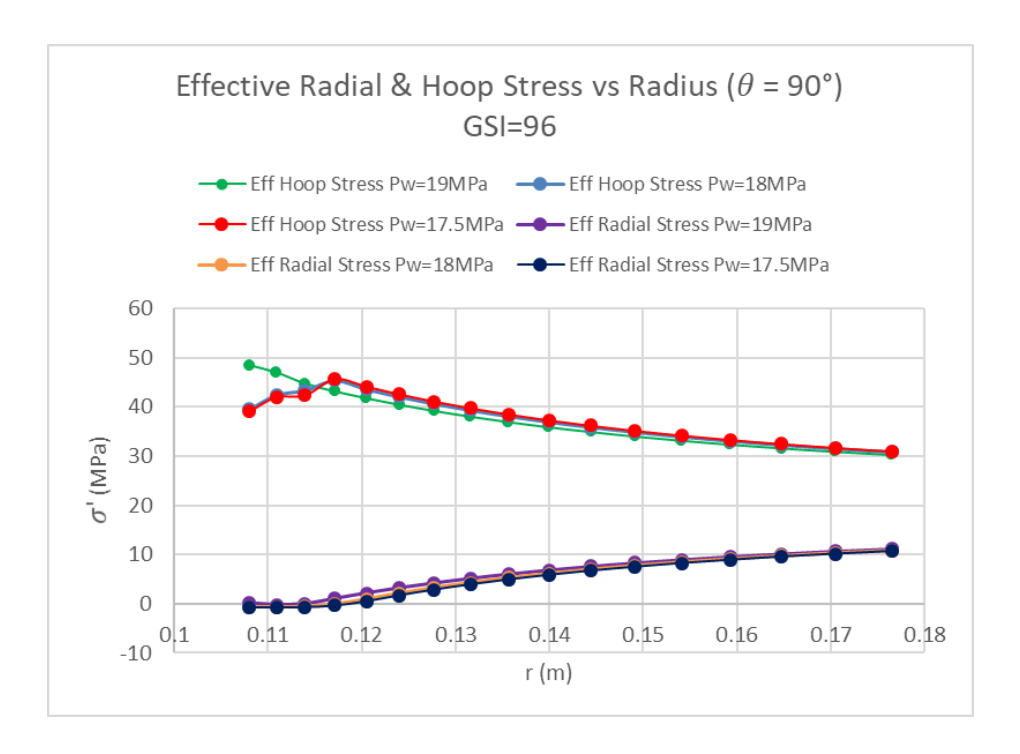


Figure 50 Eff. Hoop and Eff. Radial Stresses at $\theta=90^\circ$ HB Model Undrained Condition, GSI=96

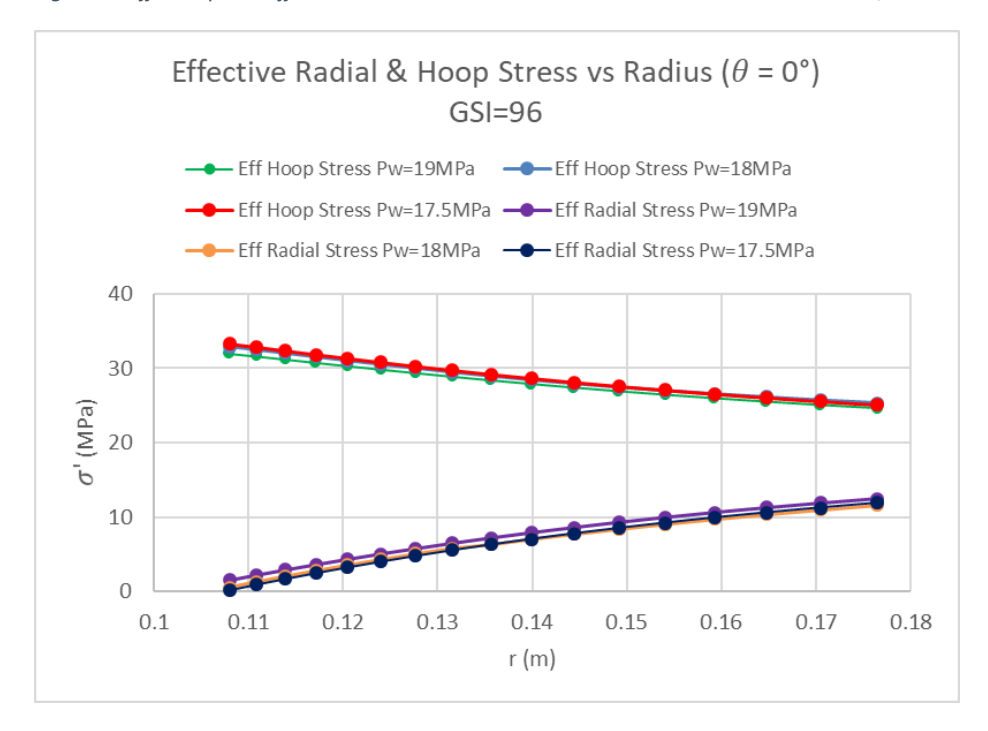


Figure 51 Eff. Hoop and Eff. Radial Stresses at $\theta=90^\circ$ HB Model Undrained Condition, GSI=96

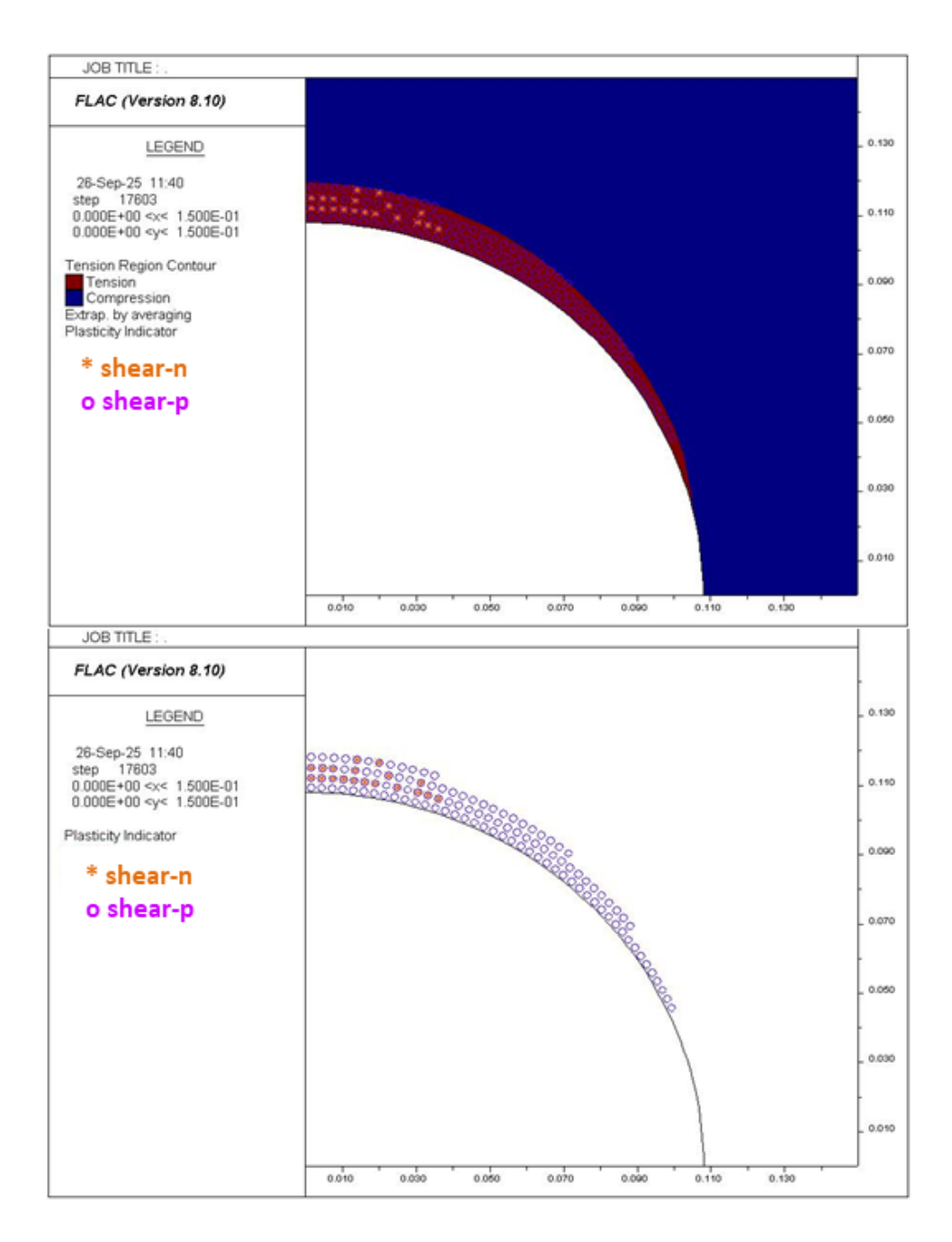


Figure 52 Tension/Compression Region (HB Undrained Model) Pw=17.5MPa, GSI=96MPa

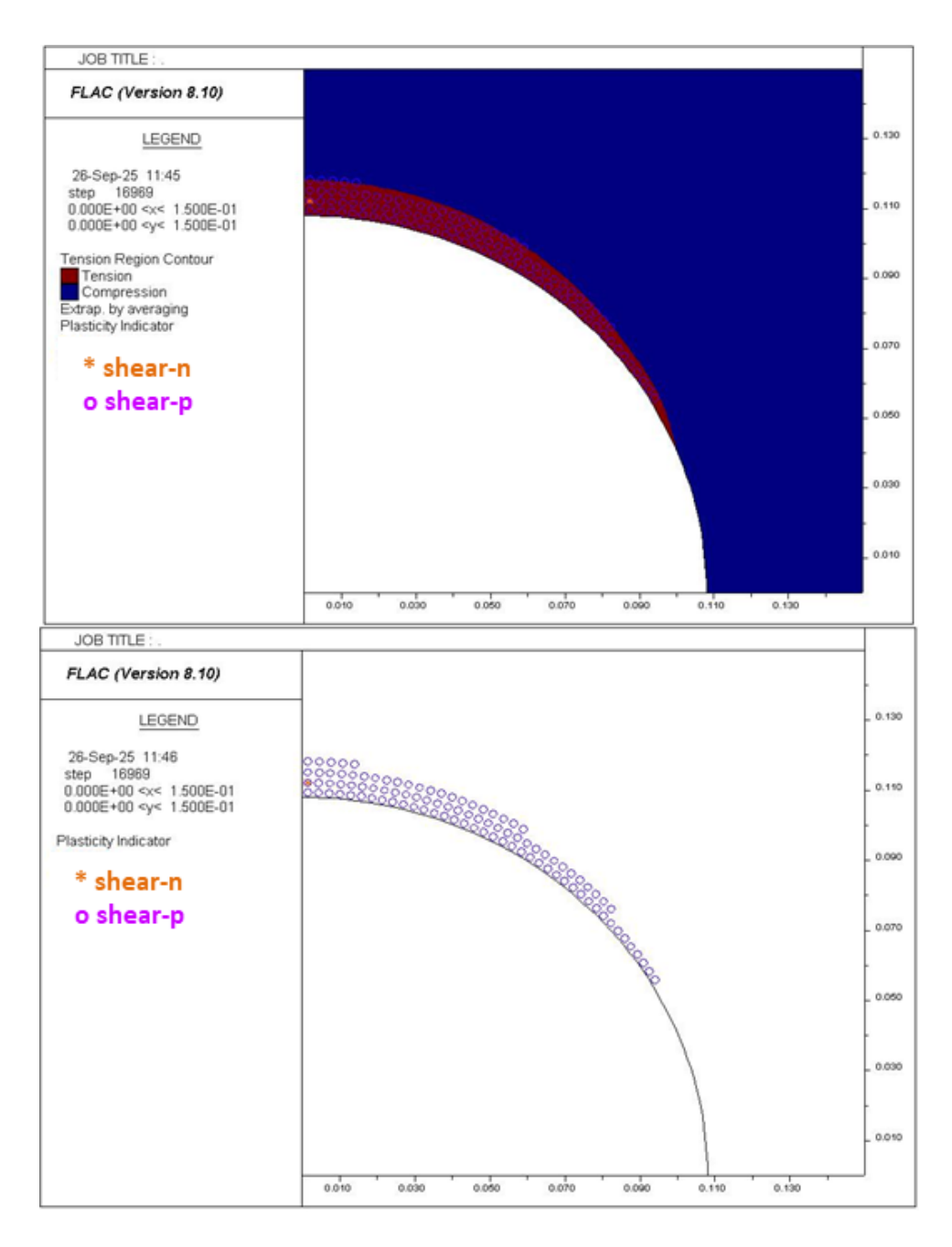


Figure 53 Tension/Compression Region (HB Undrained Model) Pw=18MPa, GSI=96MPa

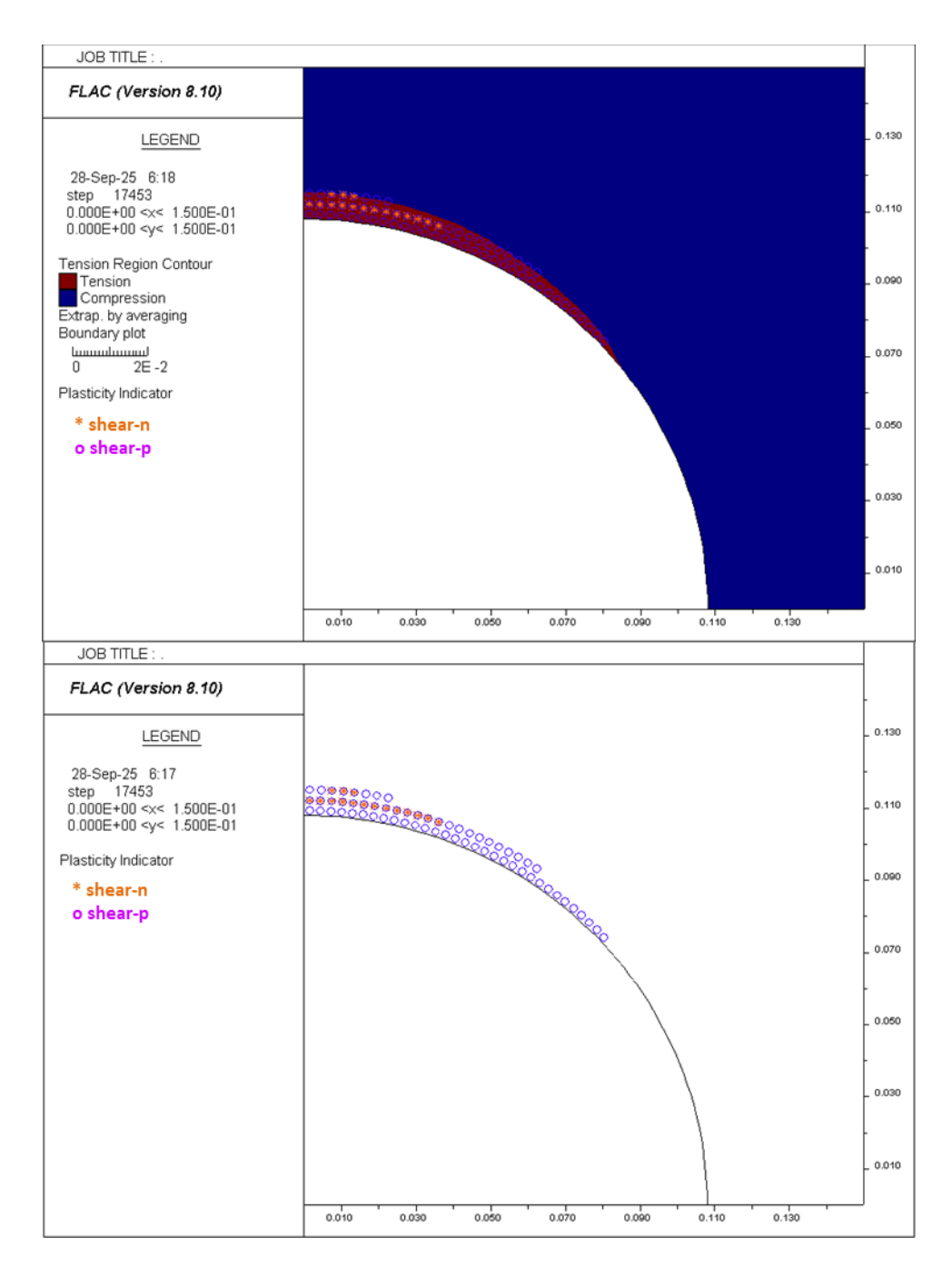


Figure 54 Tension/Compression Region (HB Undrained Model) Pw=19MPa, GSI=96MPa

The analysis of the slightly weaker quality rock (GSI=96) reveals a significantly more severe instability response under undrained conditions. This is primarily because the rock mass has a lower overall strength and, critically, a reduced tensile strength which makes the wellbore far more vulnerable to the tensile effective radial stresses generated during underbalanced drilling. With Pw = 17.5MPa, the induced negative effective radial stress exceeds the rock's low tensile strength. However, despite this condition being met for tensile failure, the

simulation's failure mechanism is expressed entirely as shear, with no tensile failure indicators detected. This is because the massive differential stress between the compressive hoop stress and tensile radial stress makes shear the dominant mode of yielding. This triggers a widespread failure, as shown in Figure 52, which is characterized by a deeper plastic zone of both active shear failure ('shear-n') and a large region of past yield ('shear-p'), indicating the instability. Even when the well pressure is increased to 18MPa, the wellbore remains unstable. While the plastic zone is visibly smaller (Figure 53), the continued presence of active failure indicators confirms that the failure process has not been arrested. Then, even with PW= 19MPa, rock mass remains unstable, with active shear failure indicators still present very near the wellbore wall (Figure 54). This result demonstrates again the high sensitivity of wellbore stability to rock mass quality. A small reduction in GSI from 100 to 96 is enough to shift the wellbore from a stable to an unstable state at the same mud weight.

Pw = 21MPa

Another analysis was conducted by conditioning the wellbore pressure to Pw = 21 MPa, representing an overbalanced condition. The purpose of this simulation was to investigate if this intended overbalance is maintained under short-term, undrained conditions.

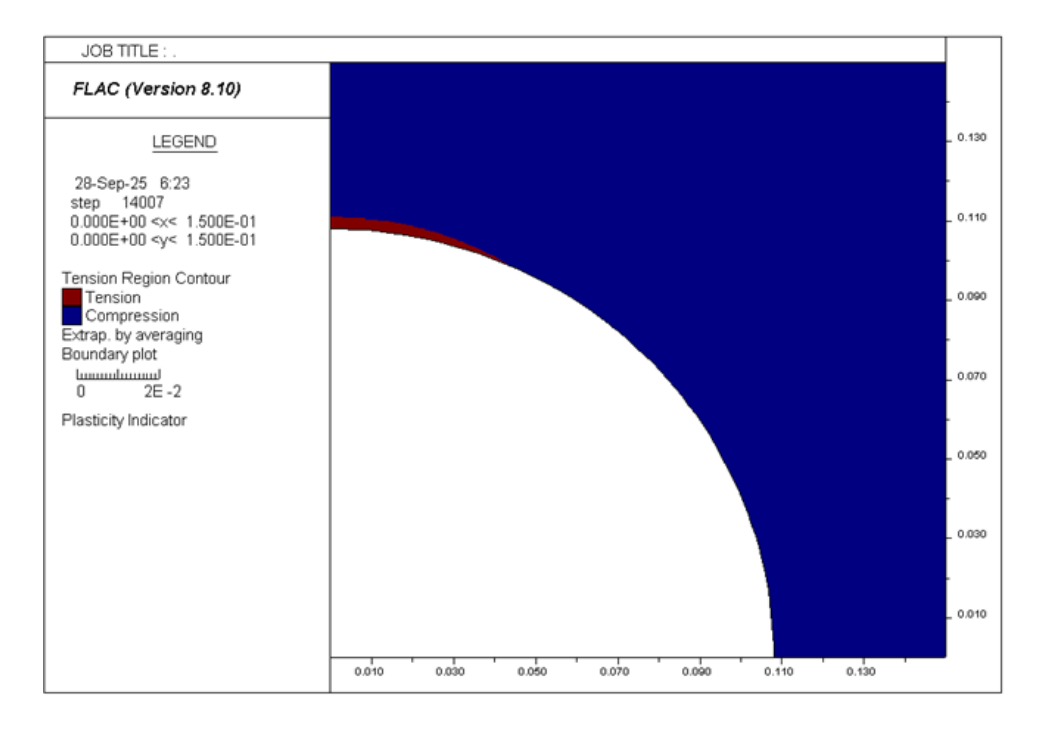


Figure 55 Tension/Compression Region (HB Undrained Model) Pw=21MPa, GSI=100MPa

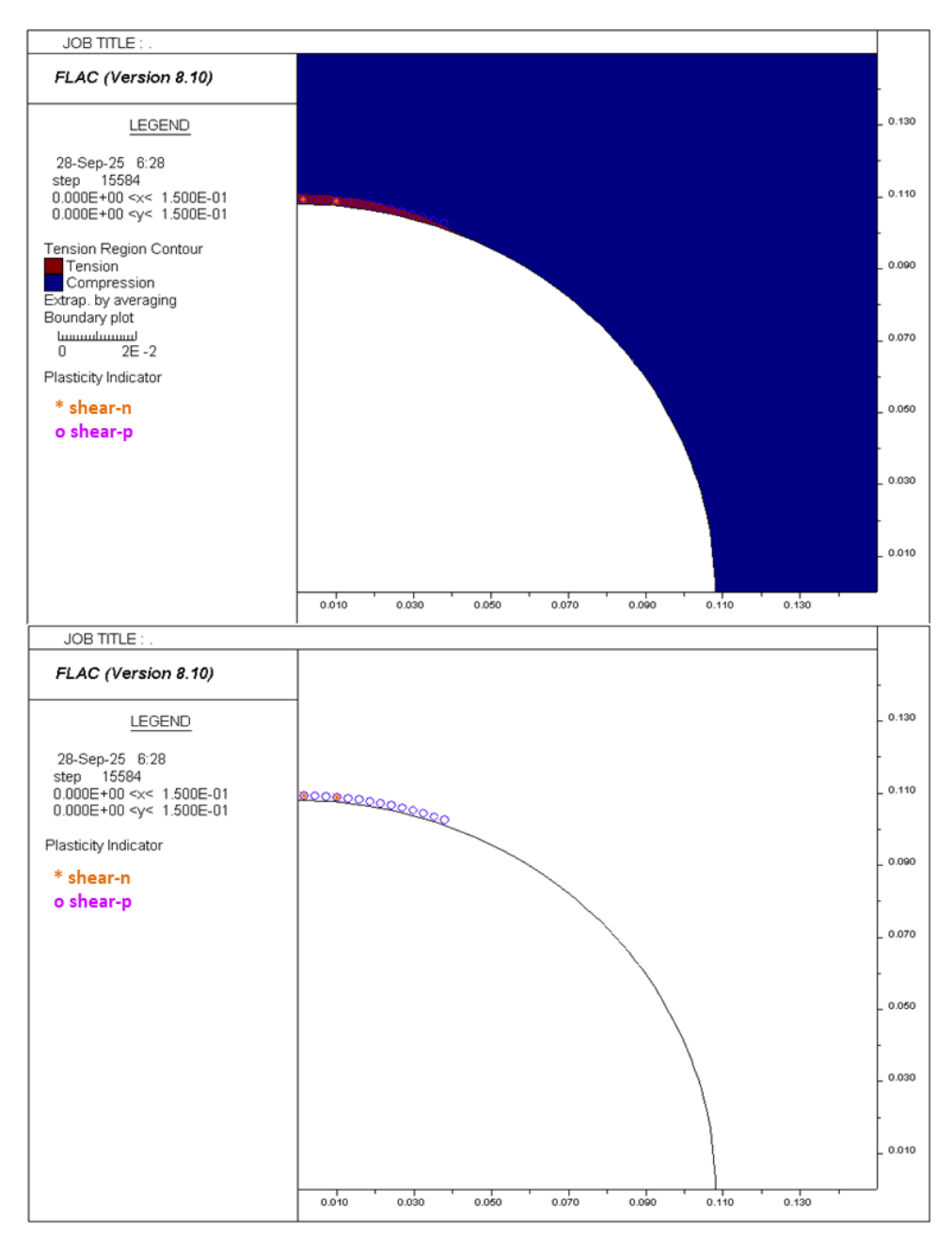


Figure 56 Tension/Compression Region (HB Undrained Model) Pw=21MPa, GSI=96MPa

The results reveal show that the stress concentration at the azimuth of the minimum horizontal stress (θ =90°) causes the local pore pressure to increase instantaneously. In this case, it rises above the applied wellbore pressure of 21 MPa. As a result, the effective radial stress becomes tensile (negative), creating a distinct "tension region" near the wellbore wall, even though the overall system is overbalanced. This demonstrates that simply maintaining a mud pressure above the formation pressure does not guarantee a fully compressive stress state at the wellbore wall in the short term. In figure 55 we dont see any plastic development with GSI=100 but we still see a minor shear failure with the GSI=96 at (θ =90°)

5. Conclusion

The main objective of this study is to analyse the rock failure in underbalanced drilling condition assuming a vertical well in normal fault scenario (vertical stress is the highest principal stress). The analysis then was conducted by applying three different constitutive models (Linear elastic, Mohr-Coulomb, and the generalized Hoek-Brown criterion) across three fundamental pore pressure scenarios: dry, drained, and undrained condition.

The analysis was performed using FLAC 2D (Fast Langrangian Analysis of Continua, ver. 8.1, Itasca) to illuminate the critical interplay between stress redistribution, the induced pore pressure, and the non-linear nature of rock behaviour. The principal conclusions drawn form the simulations are presented below:

5.1. Insights on Constitutive Model Performance

- The linear elastic model: Served as an essential baseline, perfectly matching the analytical Kirsch solution for stress distribution and validating the numerical model's setup. This perfect match proves that the basic setup of the numerical model, such as the grid, boundary conditions, and implementation of far-field stresses, is correct. So, Its purpose was not to predict failure but to establish a reliable "pre-failure" stress state for the more complex models.
- Mohr-Coulomb model: Provided a clear, quantitative prediction of failure initiation, successfully modeling the transition from a stable wellbore to a contained, stable breakout and finally to uncontrolled collapse. In the drained analysis, the wellbore was predicted to be stable with a wellbore pressure (Pw) = 17.5MPa by the manual calculation of the mud window. The simulation also shows that the wellbore is stable with no plastic deformation with Pw=17.5MPa. However, under undrained conditions, this pressure was insufficient, and stability was only achieved at a higher pressure of 19.0 MPa. This demonstrates the model's ability to quantify risk but also exposed its high sensitivity to the tensile strength cut-off because a simulation case where the tensile strength cut-off was reduced from 6.4 MPa to 2.91 MPa showed a complete shift in the failure mechanism from shear to tension, exposing how an uncertain estimate for this parameter can lead to a misinterpretation of the dominant failure mechanism.

• Hoek-Brown model: The model gives a more conservative failure prediction than the linear Mohr-Coulomb criterion based on all the result obtained, highlighting the importance of using non-linear models. This is especially true for UBD, where the effective radial stress becomes negative. However, the results must be interpreted with caution. As pointed out in research by Cai, the H&B criterion's reliability is reduced in the very low confinement and tensile stress regimes that are characteristic of UBD. This highlights a critical insight that is even advanced empirical models have limitations. Furthermore, the integration of the Geological Strength Index (GSI) effectively demonstrated that even a minor reduction in rock mass quality (from GSI=100 to GSI=96) can dramatically increase the depth of failure and shift the wellbore from a stable to an unstable condition at the same mud weight

5.2. Geomechanical Implications for Underbalanced Drilling

- A key insight is that UBD introduces a dual risk environment, generating both compressive and tensile failure. One simulation with HB model in drained condition really demonstrate this risk. It was revealed with GSI=96 the tensile strength is 2.25MPa, then by applying Pw=17.5MPa, the effective radial stress becomes higher than the tensile strength and the plots show the wellbore has experienced yielded in tension in the past around the entire wellbore circumference while also having some breakout points at ($\theta = 90^{\circ}$)
- The analysis uncovered that an intended overbalanced condition can still produce a localized underbalanced state and bring a risk of tensile failure. In undrained simulations with an applied wellbore pressure of Pw=21 MPa (above the 20 MPa formation pressure), a tension region still formed at ($\theta=90^{\circ}$). This occurs because the undrained response to stress concentration cause local pore pressure to rise above the applied wellbore pressure (e.g., to ~22.5 MPa). This inverts the pressure differential, making the effective radial stress (σ 'r =Pw -Pp) in tensile. This finding shows that maintaining a mud weight above formation pressure is not a guarantee against tensile failure in the undrained state, which can bring the unexpected risk.

References

- Aadnoy, B. S. (2019). Petroleum Rock Mechanics: Drilling Operations and Well Design (2e ed.). Gulf Professional Publishing. https://www.geokniga.org/bookfiles/geokniga-petroleumrockmechanicsdrillingoperationsandwelldesign.pdf
- Al-Ajmi, A. (2006). WELLBORE STABILITY ANALYSIS BASED ON A NEW TRUE-TRIAXIAL FAILURE CRITERION.
- Alawad, M. (2016). A Rock Mechanical Model for Overbalanced, Managed Pressure, and

 Underbalanced Drilling Applications. International Journal of Rock Mechanics and

 Geomechanics for Gas, Petroleum and Water., Vol. 1, 103.
- Alliance, S. (n.d.). The Art of Getting Stress Orientation from Borehole Image Logs.

 Subsurface Alliance. Retrieved September 28, 2025, from

 https://subsurfacealliance.com/technical-series/f/the-art-of-getting-stress-orientation-from-borehole-image-logs
- Bahrami, B., Sadatshojaie, A., & Wood, D. (2020). Assessing Wellbore Stability With a Modified Lade Failure Criterion. *Journal of Energy Resources Technology*, *142*. https://doi.org/10.1115/1.4046387
- Cai, M. (2010). Practical Estimates of Tensile Strength and Hoek–Brown Strength Parameter m i of Brittle Rocks | Rock Mechanics and Rock Engineering.

 https://link.springer.com/article/10.1007/s00603-009-0053-1
- Cai, M. (2010). Practical Estimates of Tensile Strength and Hoek–Brown Strength Parameter mi of Brittle Rocks. *Rock Mechanics and Rock Engineering*, *43*, 167–184. https://doi.org/10.1007/s00603-009-0053-1

- Davarpanah, S. M., Sharghi, M., Vasarhelyi, B., & Török, Á. (2021). Characterization of Hoek—

 Brown constant mi of quasi-isotropic intact rock using rigidity index approach. *Acta Geotechnica*, *17*. https://doi.org/10.1007/s11440-021-01229-2
- Deangeli, C. (2021). (PDF) Failure in the Tension Zone around a Circular Tunnel Excavated in Saturated Porous Rock.
 - https://www.researchgate.net/publication/354480628_Failure_in_the_Tension_Zone_around_a_Circular_Tunnel_Excavated_in_Saturated_Porous_Rock
- Eberhardt, E. (2012). The Hoek–Brown Failure Criterion. *Rock Mechanics and Rock Engineering*, 45(6), 981–988. https://doi.org/10.1007/s00603-012-0276-4
- Fjaer., E., R.M., H., P., H., A.M., R., & R., R. (2008). Petroleum Related Rock Mechanics.
- Hoek, E., Carranza-Torres, C., & Corkum, B. (2022). *Hoek-Brown failure criterion 2002 Edition*.
- Jaeger, J. C., Cook, N. G. W., & Zimmerman, R. (2009). *Fundamentals of Rock Mechanics*.

 John Wiley & Sons.
- Jaf, P. (2017). Introduction to Underbalanced Drilling Technology.
- Lake, L. W. (2006). Petroleum Engineering Handbook. Society Of Petroleum Engineers.
- Malloy, K. P. (2007). Managed Pressure Drilling—What is it anyway? World Oil.
- Nas, S. (2006). *Underbalanced Drilling*. https://doi.org/10.2118/9781555631147-ch12
- Qutob, H. (2004, October 10). *Underbalanced Drilling; Remedy for Formation Damage, Lost Circulation, & Other Related Conventional Drilling Problems*. Abu Dhabi International Conference and Exhibition. https://doi.org/10.2118/88698-MS
- Rehm, B., Haghshenas, A., Paknejad, A. S., Al-Yami, A., & Hughes, J. (2013). *Underbalanced Drilling: Limits and Extremes*. Elsevier.

- Salehi, S., Hareland, G., & Nygaard, R. (2010). Numerical simulations of wellbore stability in under-balanced-drilling wells. *Journal of Petroleum Science and Engineering*, 72, 229–235. https://doi.org/10.1016/j.petrol.2010.03.022
- Tingay, M., Reinecker, J., & Müller, B. (2008). *Borehole breakout and drilling-induced fracture analysis from image logs*.
- Wei, X., Gao, C., & Liu, K. (2020). A Review of Cracking Behavior and Mechanism in Clayey

 Soils Related to Desiccation. *Advances in Civil Engineering*, 2020, 1–12.

 https://doi.org/10.1155/2020/8880873
- Ye, Z., & Ghassemi, A. (2023). Reexamining In-situ Stress Interpretation Using Laboratory

 Hydraulic Fracturing Experiments. *Proceedings of the 11th Unconventional Resources Technology Conference*. Unconventional Resources Technology Conference,

 Colorado Convention Center, Denver, Colorado, US. https://doi.org/10.15530/urtec-2023-3862544
- Zoback, M. D. (2011). Reservoir geomechanics (5. print). Cambridge Univ. Press.